Effects of Realistic First-Stage Turbine Endwall Features

Nicholas D. Cardwell

Thesis submitted to the Faculty
of Virginia Polytechnic Institute and State University
in partial fulfillment of the requirements for the degree of

Master of Science
in
Mechanical Engineering

Dr. Karen Thole, Chair
Dr. Walter O'Brien
Dr. Brian Vick

December 9, 2005
Blacksburg, VA

Keywords: gas turbines, film-cooling,
vane endwalls, surface roughness

Effects Realistic First-Stage Turbine Endwall Features

Nicholas D. Cardwell

Abstract

The modern gas turbine engine requires innovative cooling techniques to protect its internal components from the harsh operating environment typically seen downstream of the combustor. Much research has been performed on the design of these cooling techniques thus allowing for combustion temperatures higher than the melting point of the parts within the turbine. As turbine inlet temperatures and efficiencies continue to increase, it becomes vitally important to correctly and realistically model all of the turbine's external cooling features so as to provide the most accurate representation of the associated heat transfer to the metal surfaces. This study examines the effect of several realistic endwall features for a turbine vane endwall. The first study addresses the effects of a mid-passage gap, endwall misalignment, and roughness on endwall film-cooling. The second study focuses on the effect of varying the combustor-to-turbine gap width. Both studies were performed in a large-scale low speed wind tunnel with the same vane geometry. Geometric and flow parameters were varied and the variation in endwall cooling effectiveness was evaluated.

Results from these studies show that realistic features, such as surface roughness, can reduce the effectiveness of endwall cooling designs while other realistic features, such as varying the combustor-to-turbine gap width, can significantly improve endwall cooling effectiveness. It was found that, for a given coolant mass flowrate, a narrow combustor-turbine gap width greatly increased the coverage area of the leaked coolant, even increasing adiabatic effectiveness upstream of the vane stagnation point. The turbine designer can also more efficiently utilize leaked coolant from the combustor-to-turbine gap by controlling endwall misalignment, thereby reducing the overall amount of film-cooling needed for the first stage.

Preface

Increasing turbine inlet temperatures necessitate new cooling techniques to maintain acceptable part life within the turbine. The first stage vane experiences the highest heat load, and therefore requires the greatest amount of cooling. Typically a combination of internal and external cooling is employed for both the vane itself and its accompanying endwall surface. A combination of experimentation and computational predictions are traditionally employed to analyze the effectiveness of a new cooling design before production of the actual part. It is the purpose of the following studies to extend current experimental models to include several realistic endwall features which have not been included in prior evaluations of endwall cooling effectiveness. It is hypothesized that these features can have a drastic effect on the amount of heat transferred to the metal surface. Included are two journal papers that analyze the effects of realistic endwall features on coolant effectiveness and supporting appendices with additional data which was not included in the papers.

The first paper, entitled "Effects of Mid-Passage Gap, Endwall Misalignment, and Roughness on Endwall Film-Cooling", was presented at the ASME 2005 International Gas Turbine Institute Conference in Reno, Nevada. Measurements of endwall and mid-passage gap adiabatic effectiveness levels were presented for a surface with realistic turbine endwall features such as a mid-passage gap, endwall misalignment, and roughness. It was reported that surface roughness decreases cooling effectiveness. This effect of roughness worsened as coolant blowing ratio was increased. The mid-passage gap impacted the progression of upstream slot coolant across the endwall due to the fact that the leading edge portion of the gap was ingesting, thereby decreasing total coolant coverage area. For endwall misalignment, a cascade design was found to be greatly superior to either the aligned or dam configurations. A cascade design consisted of two adjacent first-stage vanes with one vane's endwall surface lowered with respect to its adjacent vane and the combustor liner. A dam design was similar, except that the vane surface was raised with respect to its adjacent vane and the combustor liner.

The second paper, entitled "The Effects of Varying the Combustor-Turbine Gap", is to be presented at the 2006 IGTI conference. The effect of varying the combustor-to-

turbine slot width for a range of coolant flowrates through the slot was evaluated for this second study. When varying slot width while matching mass flow rate, it was observed that altering the slot width caused a dramatic change in coolant coverage area. Matching slot momentum flux ratio for varying slot width resulted in nominally the same coolant coverage area. Additional research performed for each of these studies is included in the appendices.

Acknowledgments

I would like to acknowledge all the support and help I have received in the pursuit of my dream. Coming to a prestigious college like Virginia Tech and finding success and my place has been a life changing experience that I could never have accomplished without the support of my family and friends. Above all I would like to thank the Lord, who has richly blessed my life by giving me the strength to do things beyond my normal capabilities and for being a light to guide my way through the winding path of life. I would also like to thank my family for all of their support and love. This could never have come to fruition without all of your help, especially you Mom and Wes! You have all helped me so much: sending me care packages when I got lonely, listening intently as I rattled on about Gas Turbines or research at any lull in conversation, buying a starving graduate student a plane ticket to come back home for Christmas, calling to include me in the Thanksgiving prayer (even though I am 20ft. up a tree tentatively hanging on to life), and instilling a great love for building and all things scientific and gadgety for as far back as I can remember (yes Pop, I'm talking about you here!)

And to my advisor, Karen, I would like to especially thank you for all of the guidance and opportunity that you have given me over the past two years. I have grown tremendously as a student and as a researcher under your leadership and I know this is because you care so much for the success of your students. I know truly that all of my accomplishments here would have been unattainable without you. Friend and colleague, it is truly my privilege to call you both. Thanks for everything, looking forward to the next chapter.

And of course, what would the lab be without all of the great people who work in it. I just couldn't ask for a better group of people to share the good times. One could fill a book with all the "evil" lab shenanigan stories. Seriously though, it has been my great pleasure to know all of you. The Toolbox will rise to national prominence in the realm of collegiate intramural co-recreational softball, I just know it!

Table of Contents

List of Tables

List of Figures

Paper 1:

EFFECTS OF MID-PASSAGE GAP, ENDWALL MISALIGNMENT AND ROUGHNESS ON ENDWALL FILM-COOLING

Presented at the *2005 IGTI Conference**
Accepted to the *Journal of Turbomachinery**

Abstract

To maintain acceptable turbine airfoil temperatures, film-cooling is typically used whereby coolant, extracted from the compressor, is injected through component surfaces. In manufacturing a turbine, the first stage vanes are cast in either single airfoils or double airfoils. As the engine is assembled, these singlets or doublets are placed in a turbine disk in which there are inherent gaps between the airfoils. The turbine is designed to allow outflow of high pressure coolant rather than hot gas ingestion. Moreover, it is quite possible that the singlets or doublets become misaligned during engine operation. It has also become of interest to the turbine community as to the effect of corrosion and deposition of particles on component heat transfer. This study uses a large-scale turbine vane in which the following two effects are investigated: the effect of a mid-passage gap on endwall film-cooling and the effect of roughness on endwall film-cooling. The results indicate that the mid-passage gap was found to have a significant effect on the coolant exiting from the combustor-turbine interface slot. When the gap is misaligned, the results indicate a severe reduction in the film-cooling effectiveness in the case where the pressure side endwall is below the endwall associated with the suction side of the adjacent vane.

*Co-authors: Narayan Sundaram, Mechanical Engineering Department, Virginia Tech
Dr. Karen A. Thole, Mechanical Engineering Department, Virginia Tech

Introduction

Traditional techniques to cool the hot section of a gas turbine engine involve the use of air from the compressor that has bypassed the combustion chamber and is used for impingement cooling, film-cooling, and convective cooling in the turbine airfoils. The coolant is generally high pressure air that has been routed to the turbine section through a secondary flow path. During the manufacturing of a turbine engine, the airfoils and their associated endwalls are typically cast as singlets or doublets that are then placed in the turbine disk. It is inherently difficult to seal interfaces between the singlets and doublets, particularly when considering the expansion and contraction of turbine components during engine operation. Given there is high-pressure coolant that must be routed to the turbine through a secondary flow path to cool the blades and vanes, this high pressure coolant can also leak through any gaps that may exist in the turbine. Moreover, since combustor profiles are not always uniform it would be expected that the thermal contraction and expansion of adjacent vanes would be significantly different. This difference can lead to turbine airfoils that are misaligned. The question then becomes, how should a turbine designer account for a potential misalignment in airfoil components in their calculations of airfoil temperatures?

Airfoil roughness is an important problem in today's operation of gas turbines. With the push to use fuels other than natural gas, such as coal-derived fuels for industrial turbines, erosion and deposition are issues that must be accounted for. Moreover, propulsive gas turbines are being used in harsh environments in which sand or other foreign debris is ingested and deposited on components in the hot section.

The work presented in this paper compares measured adiabatic effectiveness levels of a well-sealed mid-passage gap that is aligned and misaligned to determine the effect on endwall film-cooling and slot cooling. Also compared in this paper is the effect that roughness can have on endwall film-cooling.

Past Relevant Studies

There have been turbine endwall studies in the literature that have documented the effects of an upstream slot, discrete film-cooling holes, and combined upstream slot and film-cooling. Only a few studies exist on the effect of a mid-passage gap. There have been no studies documenting what happens in the case of having a misaligned mid-passage gap in an actual

airfoil passage. In addition, there have been no studies on the effect of roughness on endwall film-cooling.

Most of the studies evaluating leakage flows have been concerned with an upstream slot that represents the leakage flow that might occur between the combustor and turbine. Some of the earliest work related to a leakage flow was performed by Blair [1] who used a two-dimensional aligned slot upstream of vane geometry. Enhancements in film-cooling effectiveness along the endwall were observed as the flow through the slot was increased. In a similar study of coolant upstream of a vane passage, Burd et al. [2] studied the effects of an upstream aligned, 45° slot. By using coolant flows as high as 6% of the total passage flow, better cooling was observed over the endwall and on both sides of the vanes relative to lower coolant flows. A study by Colban and Thole [3, 4] measured the effects of changing the combustor liner film-cooling and upstream slot flows on the effectiveness levels along the endwall of a first stage turbine vane. Their results showed that the coolant from the slot was not uniform across the exit with coolant accumulating along the endwall near the suction side of the vane. Coolant injection from the upstream combustor liner caused a different total pressure profile entering the vane passage, relative to a turbulent boundary layer, that in turn changed the secondary flow field.

Detailed endwall film-cooling results have been conducted by Friedrichs et al. [5, 6, and 7]. The results of their first study [5], which were all surface measurements or visualization, indicated a strong influence of the secondary flows on the film-cooling and an influence of the film-cooling on the secondary flows. Their data showed that the angle at which the coolant leaves the hole did not dictate the coolant trajectory except near the hole exit. Furthermore, the endwall cross-flow was altered so that the cross-flow was turned toward the inviscid streamlines, which was due to the film-cooling injection.

The only studies to have combined an upstream slot with film-cooling holes in the passage of the vane were those of Zhang and Jaiswal [8], Kost and Nicklas [9], Nicklas [10] and Knost and Thole [11, 12]. One of the most interesting results from the Kost and Nicklas [9] and Nicklas [10] studies was that they found for the slot flow alone, which was 1.3% of the passage mass flow, the horseshoe vortex became more intense. This increase in intensity resulted in the slot coolant being moved off of the endwall surface and heat transfer coefficients that were over three times that measured for no slot flow injection. They attributed the strengthening of the horseshoe vortex to the fact that for no slot injection the boundary layer was already separated

with fluid being turned away from the endwall at the injection location. Given that the slot had a normal component of velocity, injection at this location promoted the separation and enhanced the vortex. Their adiabatic effectiveness measurements indicated higher values near the suction side of the vane due to the slot coolant migration. Knost and Thole reported a significant change in the streamlines in the near endwall region resulting from the upstream slot flow. Their results also indicated that the momentum flux ratio was an important parameter in predicting the cooling jet behavior.

Using a flat plate geometry with no turbine airfoils, Yu and Chyu [13] studied the influence of gap leakage downstream of injection cooling holes. They observed that for a moderate level of film-cooling upstream of a coolant slot, the combined presence with the gap promoted better coolant film protection. However, as the film-cooling flow was increased the coolant from the gap appeared to lift the slot flow coolant from the wall resulting in decreased adiabatic effectiveness.

The only known studies of flow from a slot within the mid-passage of adjacent airfoils were performed by Aunapu et al. [14], Ranson and Thole [15], and Yamao et al. [16]. Aunapu et al. used blowing through a passage gap in an attempt to reduce the effects of a passage vortex. They hypothesized endwall blowing in the blade passage could reduce the effects of the passage vortex. Aunapu et al. [14] observed that endwall jets in the center of the blade passage effectively altered the path of the pressure side leg of the vortex. Unfortunately, the increased blowing caused higher turbulence and higher aerodynamic losses. Ranson and Thole used an aligned mid-passage gap between two adjacent blades for their combined experimental and computational studies. Their results indicated that the flow leaving the gap was directed toward the blade pressure side, as a result of the incoming velocity vector, and then traversed towards the suction side of the adjacent airfoil. Yamao et al. [16] investigated the distribution of film-cooling effectiveness due to sealing air injected from combustor-vane interface and vane-to-vane interface on annular cascade test equipment. Their study indicated that the film-cooling effectiveness was enhanced with an increase in the sealing air flowrate between the vanes. Also, the increase in sealing air flowrate between the combustor-vane interfaces resulted in significant increase in film-cooling effectiveness near the leading edge but a slight increase along the trailing edge.

In summary, it is important to understand the effect of coolant flow from leakage points in the endwall region under realistic surface conditions to further the technology of turbine blade cooling. To date, there have been only a few studies that have addressed roughness effects on an actual turbine airfoil but none of these studies have addressed the effect of roughness with adiabatic effectiveness levels on a film-cooled endwall.

Mid-Passage Gap Geometry

The flat endwall in the linear cascade used for these studies was comprised of five realistic features: a combustor to turbine (upstream) gap, endwall film-cooling, a mid-passage gap with accompanying strip seal, the capability of simulating an endwall misalignment, and surface roughness representative of that found in an engine. The first stage vane endwall film-cooling pattern, which was originally designed and tested by Knost and Thole [12], is shown in Figure 1.1, which also shows iso-velocity contours and hole injection angles. All film-cooling holes were at an angle of 30º with respect to the endwall surface.

Also included in the endwall pattern is a two-dimensional slot representing the interface between the combustor and first stage of the turbine. This slot is located 30% of the axial chord upstream of the vane stagnation location and is designed to be forward facing with an injection angle of 45º with respect to the endwall surface. This leakage interface will be referred to as the upstream slot. Table 1.1 provides a description of turbine vane geometry and operating conditions and Table 1.2 provides a summary of parameters relevant to film-cooling and upstream slot geometries.

The focus of this paper, as explained, is the interface between the surrounding coolant and mainstream flows. Also, the mid-passage gap does not open into the upstream slot and has its own supply plenum. The dimensions and arrangement of the mid-passage gap plenum is shown in Table 1.2 and Figure 1.2. The vane-to-vane interface has three distinct alignment modes: aligned, forward facing step (dam), and backward facing step (cascade). The aligned mode, which is shown in Figure 1.3a, represents no disparity in height between adjacent vanes and the combustor.

The offset that was considered for the misaligned endwall was 1.2% of vane height or 0.65 cm for the 9X scale geometry. The dam endwall refers to a condition where the suction surface of vane 1 (V1) is raised relative to the pressure side of vane 2 (V2) which is flush with

the combustor wall. This configuration is referred to as a dam because, as the secondary flows are driven from the pressure side of one vane towards the suction side of the adjacent vane, the flow faces an upward step. Figure 1.3b shows the dam configuration has a raised step for V1 at the upstream slot location.

The cascade endwall refers to a condition where the suction surface of V1 is lowered relative to the pressure side of the V2, which is flush with the combustor wall as shown in Figure 1.3c. This configuration is referred to as a cascade because the secondary flows from the pressure to the suction side experience a waterfall, or cascade, effect. For the cascade case, the upstream slot has a recessed step for the V1 portion of the platform.

Relative to the work that was done by Knost and Thole [12], endwall roughness was also investigated. For this simulation, the study completed by Bons et al. [17] was referenced to model realistic surface roughness on a first stage vane platform. Bons et al. lists measured values of endwall rms roughness height (Ra) as 28 μm. This rms value translates to a equivalent sand grain roughness of 0.227 mm for a 9X wind tunnel simulation scale (as described by Bogard et al. [18]), which is the scaling factor for the test vane.

To simulate a uniformly rough surface, wide-belt industrial sandpaper was used to cover the entire endwall. It has a closed-coat 36 grit surface and grade Y cloth backing. The 36 grit sandpaper corresponds to sand grain roughness of 0.55 mm microns (www.sizes.com/tools/sandpaper.htm), which is slightly above the corresponding values in the engine. A closed-coat surface has roughness elements arranged in a random array over 100% of the surface. Custom construction of the sandpaper was used to guarantee tight tolerances around each film-cooling hole. This ensured that the rough surface does not block the hole and that the interaction between the rough surface and coolant jets is uniform for the entire endwall.

Experimental Methodology

The experimental facility included a test section placed in a wind tunnel as shown in Figure 1.4. The test section consisted of a vane scaled up by a factor of nine with cooling holes and slot geometries. Adiabatic endwall temperature measurements were taken for different flowrates through film-cooling holes and through the slot representing the combustor turbine interface. For the present study, there was no flow through the mid-passage gap at the interface

of the vanes. This was primarily done to study the aerodynamic effect caused by the presence of the gap and to simulate a perfectly sealed interface.

The test section was placed inside the closed-loop wind tunnel facility shown in Figure 1.4 and a detailed account of its construction has been previously described by Knost and Thole [12]. The difference in this test section from the one used by Knost and Thole is the presence of a rough endwall surface and the presence of a mid-passage gap between the endwalls of the adjacent vanes. The flow in the wind tunnel is driven by a 50 hp axial vane fan, which is controlled by variable frequency inverter. Downstream of the fan, the flow encounters a 90° turn and passes through a primary finned-tube heat exchanger used to cool the bulk flow. After the heat exchanger, the flow encounters a three-way flow split. Note that only the bottom channel was used for this study. This split was done to create a primary core flow and a cooled secondary flow. The primary core flow was made to pass through a heater bank consisting of three heaters where the air temperature was increased to 55°C. The secondary flow, in the outer channel, was made to pass through a secondary heat exchanger where the flow temperature was lowered to about 15°C. The secondary flow path represented the coolant flow through the film-cooling holes and the slots.

The test section consisted of two full passages with one center vane and two half vanes. It is important to note that film-cooling effectiveness studies were done only in the passage where the mid-passage gap was simulated. The test section consisted of separate plenums for independent control of flow through the film-cooling holes and the upstream slot as shown in Figure 1.5. A temperature difference of about 40°C was maintained at all times between the mainstream and coolant flows under steady state conditions. Typical times to achieve steady state conditions were 3 hours.

The freestream turbulence effects were not taken into consideration as these studies were more focused on industrial gas turbines rather than on aero engines. Freestream turbulence levels are generally higher for aero engines when compared to industrial gas turbines. The inlet turbulence effects and length scales were however measured to be 1.3% and 4 cm respectively. The endwall of the vane, which was the main focus of study, was constructed of foam because of its low thermal conductivity (0.033 W/mK). The endwall foam was 1.9 cm thick and was mounted on a 1.2 cm thick Lexan® plate. The cooling hole pattern on the endwall was cut with

a five-axis water jet to ensure precision and integrity. The upstream slot was constructed with hard wood as it had a low conductivity and was stiffer.

Coolant Flow Settings

For every test condition the dimensionless pressure coefficient distribution was verified to ensure periodic flow through the passages. As stated earlier two separate plenums were used to control the flowrate through the film-cooling holes and through the upstream slot. Friedrichs et al. [5] suggested that a global blowing ratio based on the inlet flow conditions could be characterized by the blowing ratio of a loss-free hole injecting into inlet conditions calculated from:

$$M_{ideal} = \sqrt{\frac{\rho_c}{\rho_{in}} \frac{P_{o,c} \quad p_{s,in}}{P_{o,in} \quad p_{s,in}}} \tag{1}$$

A modification of this approach was done in this study and a global discharge coefficient, CD, was derived so that a cumulative flowrate through the film-cooling holes could be defined. These CD values were obtained from CFD studies done on a similar geometry and have been reported earlier by Knost and Thole [11]. Measurements of the inlet velocity, average inlet static pressure, and coolant total pressures were obtained which then allowed the fraction of coolant flow relative to the inlet core flow to be calculated from:

$$\frac{\dot{m}_c}{\dot{m}_{core}} = M_{ideal} . C_D . \frac{A_{hole}}{A_{in}} . \#holes \tag{2}$$

The upstream slot flow was assumed to have a discharge coefficient of 0.6 which is the assumed value for a flow through a sharp-edged orifice and the flowrate was calculated accordingly. Table 1.3 gives a description of the actual and ideal global blowing ratios used for the different film-cooling and upstream slot mass flowrate settings.

Instrumentation and Temperature Measurements

An Inframetrics P20 infrared camera was used to capture the spatially-resolved adiabatic wall temperatures on the endwall. Measurements were taken at seven different viewing locations to ensure that the entire endwall surface was mapped. The camera was placed perpendicular to the endwall surface at a distance of 55 cm. Each picture covers an area 24 cm by 18cm, with the area being divided into 320 by 240 pixel locations. The spatial integration of the camera was 0.715 mm (0.16 hole diameters). Thermocouples were also placed on the endwall surface at different locations to directly measure the temperature to post calibrate the infrared images. For

the post calibration the emissivity and background temperature were adjusted until the temperatures from the infrared camera images were within 1ºC of the corresponding thermocouple data. Typical emissivity values and background temperatures were 0.92 and 45ºC (note that the freestream temperature was 55ºC). Seven images were taken at each of the viewing locations to obtain an averaged picture using an in-house Matlab program. The same program was also used to assemble the averaged pictures at all locations to give a complete temperature distribution along the passage endwall.

Freestream temperatures were measured at multiple locations along the pitch and the average was determined by using a thermocouple rake consisting of three thermocouples along the span. It was found that the variations along the pitch were less than 0.2ºC and that along the span were less than 1.5ºC. Three thermocouples were attached in the upstream slot location at the combustor exit, and two thermocouples were attached in the film-cooling plenum. Eleven thermocouples were placed in the mid-passage gap to measure the temperature profile along the gap. The thermocouples in the mid-passage gap were placed six strip seal thicknesses beneath the surface, which was roughly one-third of the slot flow length beneath the surface (Table 1.2). Voltage outputs from the thermocouples were acquired by a 32 channel data acquisition module that was used with a 12-bit digitizing card. The temperature data was compiled after the system reached steady state.

An uncertainty analysis was performed on the measurements of adiabatic effectiveness using the partial derivative method described at length by Moffat [19]. The precision uncertainty was determined by taking the standard deviation of six measurement sets of IR camera images with each set consisting of five images. The precision uncertainty of the measurements was ±0.014°C. The bias uncertainty was ±1.0°C based on the calibration of the image. The bias uncertainty of the thermocouples was ±0.5°C. The total uncertainty was then calculated as ±1.0°C for the images and ±0.51°C for the thermocouples. Uncertainty in effectiveness, η, was found based on the partial derivative of η with respect to each temperature in the definition and the total uncertainty in the measurements. Uncertainties of $\delta\eta=\pm0.082$ at $\eta=0.2$ and $\delta\eta=\pm0.029$ at $\eta=0.9$ were calculated. A one-dimensional conduction analysis was performed at the entry and exit of the passage to calculate the conduction error. The resulting η correction was found to be 0.07 at the entrance and 0.02 at the exit region at a measured η value of 0.5.

Discussion of Results

As stated previously, all tests and data acquisition were completed for no flow through the mid-passage gap. First, the effect of the presence of the mid-passage gap and roughness will be discussed for an aligned endwall. The results from this test will be compared with an existing case having no mid-passage gap. Second, a comparison of results obtained for aligned and misaligned mid-passage gap will be discussed.

Film-Cooling Effectiveness with a Rough Endwall and a Mid-Passage Gap

The nominal film-cooling cases with and without a mid-passage slot for 0.75% upstream slot flow and 0.5% film-cooling flow are shown in Figure 1.6a-b. Note that the percentages refer to the coolant flow relative to the hot gas path flow. There are two noticeable effects that can be determined by comparing these two cases that include the effect of the mid-passage gap and the effect of roughness.

It can be seen from Figure 1.6a that there is no coolant flow from the upstream slot crossing over the mid-passage gap location. This condition becomes apparent when comparing the contours of Figure 1.6a with those of Figure 1.6b where, in the absence of the gap, the coolant from the upstream slot convects towards the suction side of the vane sweeping over a large area of the endwall. In the presence of the mid-passage gap, Figure 1.6a shows no coolant exiting the upstream slot on the pressure side of the mid-passage gap. The reason for this lack of coolant is that the coolant from the upstream slot is ingested until the end of the vane passage where it then exits the gap. This effect will be discussed further in a later section of the paper. As a result of this degradation of the coolant on the pressure side of the mid-passage gap, the hot streak through the center of the passage appears to be wider with the presence of a mid-passage gap relative to the no gap case.

In determining the effect of roughness on the endwall film-cooling, comparisons can also be made between Figures 1.6a and 1.6b. Observing the coolant exiting from the leading edge holes upstream of the stagnation location on the suction side, one can see that the coolant is dispersed more rapidly for the case with the rough endwall relative to the smooth endwall. Along the pressure side, the jets merge more evenly in the case of the rough endwall relative to the smooth endwall where in the case of the smooth endwall there are distinct jets.

To quantify the effects of roughness, a section of the endwall near the pressure side of the vane, as shown in Figure 1.7, was further analyzed. Figures 1.7a and 1.7b show the effect of

roughness on the laterally averaged effectiveness for 0.5% and 0.75% film-cooling flows, respectively. Also indicated in Figure 1.7 are the row-averaged local blowing ratios for each row of holes along the pressure side. Note that CFD results were used to quantify the local coolant flows from each cooling hole and the local static pressure was used to calculate the local freestream velocity that was used in the blowing ratio definition. For the 0.5% case, where the local blowing ratios ranged from 0.58 and 0.78, the laterally averaged effectiveness values indicate that there is essentially no effect of roughness of the film-cooling performance. In looking at the contours in Figure 1.6a and 1.6b, however, there are some local differences indicated particularly with the jet merging.

For the higher coolant flow condition in Figure 1.7b, where the local blowing ratio ranges from 0.68 to 1.28, there is a dramatic decrease in the average effectiveness along the pressure side with roughness. The decrease in the laterally averaged effectiveness due to roughness is on the order of 30% mid-way between film-cooling rows. One plausible reason that there is a larger decrease at the higher blowing ratio relative to the lower blowing ratio is because for a rough wall the boundary layer is thicker thereby allowing the jets to separate from the endwall. As the front jet separates from the wall, this effect is compounded as one progresses downstream along the pressure side. This reduction in film-cooling effectiveness may also be attributed to increased interaction with hot mainstream. The rough surface greatly increases boundary layer thickness and turbulence levels, causing enhanced mixing between the coolant and mainstream and thereby lowering area averaged values of adiabatic effectiveness.

In comparing Figures 1.7a and 1.7b, it is seen that there is a benefit in cooling when increasing the coolant flow from 0.5% to 0.75% for the smooth wall case. In contrast, when increasing the coolant flow for the rough wall case, the average adiabatic effectiveness levels actually decrease with an increase in blowing ratio. As such, Figure 1.8 compares the laterally averaged effectiveness values for the rough endwall case along the pressure side holes for three different coolant flowrates: 0.35%, 0.5% and 0.75%. The corresponding contours for these lateral averages just along the pressure side are shown in Figures 1.9a-1.9c. As expected, increasing the film-cooling flow from 0.35% to 0.5%, there is increased gas performance in the film-cooling effectiveness levels. In comparing the contours shown in Figures 1.9a and 1.9b, it is clear that the first row of holes in the averaging area defined in Figure 1.7 appears nearly the

same between the two cases, but that cooling appears to be much better at the second row for the higher blowing ratio case.

By increasing the coolant flow to 0.75%, the laterally averaged effectiveness significantly decreases relative to the 0.5% coolant flow case but is better than the 0.35% coolant flow case, as shown in Figure 1.8. The contours in Figure 1.9c indicate better penetration towards the pressure side of the endwall for the 0.75% coolant flow case, but that the overall levels of effectiveness downstream of the film-cooling holes are significantly lower than for the 0.5% coolant flow case. These contours indicate that as the jets penetrate closer to the pressure side surface, they are also lifted off the surface. Knost and Thole [11] observed a similar trend for the smooth wall case in that the pressure side film-cooling jets appeared to be lifted off the surface for the 0.75% coolant flow case, but as seen from Figure 1.7b this effect is worsened with roughness.

Outside of the averaging area, at the most upstream row of film-cooling holes, the contours in Figure 1.9a-1.9c indicate little change in effectiveness levels as a function of increased coolant levels. There was only slightly better performance for the 0.5% coolant flow condition relative to the 0.35% and 0.75% coolant flows. Just upstream of the stagnation location, the contours in Figures 1.9a-1.9c indicate that for the 0.5% and 0.75% coolant flow conditions, the leading edge film-cooling jets are impacting the vane and then being washed back down onto the surface indicating some coolant at the vane-endwall junction.

Effect of a Misaligned Mid-Passage Gap

One of the primary questions raised for this work was how to best design an endwall simulating the surface roughness and turbine vane misalignment. As discussed previously, there is a possibility for an aligned endwall configuration, a cascade endwall configuration, and a dam endwall configuration. The misalignment value was set to 1.2% of the vane span. For these comparisons, both the film-cooling and upstream slot flows remained constant at 0.5% and 0.75% of the core flow respectively. Figures 1.10a-1.10c corresponds to aligned, dam, and cascade endwall configurations respectively. Indicated on the vanes on these figures is the portion of the endwall that is raised (U) and lowered (D). For explanatory purposes, the section of endwall closest to the top vane picture is referred to as the suction side section and the section of the endwall closest to the bottom vane will be referred to as the pressure side section.

In comparing the aligned case to the dam case, it can be seen that in the case of the dam the overall platform cooling is much worse than in the case of the aligned endwall. It appears

that because of the front slot misalignment, the leakage coolant from the upstream slot is directed into the hot gas path rather than along the endwall. It is also interesting to look at the end of the mid-passage gap. Figure 1.10a for the aligned endwall indicates that at the mid-passage gap exit, coolant exits the slot. This coolant was the upstream slot coolant and film-coolant that was ingested into the slot and then exited at the lowest external static pressure location. In the case of the dam endwall, Figure 1.10b indicates that there is no coolant exiting the end of the mid-passage slot. It is also quite interesting to see the diminished effectiveness levels in the vicinity of the mid-passage slot at about 20% of the slot length measured from the upstream slot shown in Figure 1.10b. This warmer region was also shown for aligned endwall in Figure 1.10a, but it is not as dramatic. At this location, there is no upstream slot flow present, which was worsened for the dam configuration, nor is there any film-cooling flow present.

When the endwall surface is set to cascade configuration, coolant from the upstream slot can flow in an unobstructed manner onto the endwall. The effectiveness contours in Figure 1.10c indicate a much improved performance for the cascade case relative to both the aligned and the dam configurations. The lowered endwall in the case of the cascade acts like a trough in which the upstream slot flow does not mix out as quickly with the mainstream hot gas. As a result, higher effectiveness values occur on the suction side portion of the endwall. For the cascade configuration, the pressure side contours are very similar to the aligned endwall configuration, because there is no blockage for the secondary flows, as compared with the dam case. At 20% slot length downstream from the upstream slot the warm region previously discussed is diminished for the cascade condition relative to both the dam and aligned cases.

Figure 1.11a compares the pitchwise-averaged effectiveness along the suction side of the endwall for the three endwall configurations and Figure 1.11b compares the effectiveness distribution along the suction and pressure sides for the aligned case. Figure 1.11a clearly substantiates the previous results that the cascade configuration results in better cooling along the suction side and Figure 1.11b strengthens the conclusion that there is better cooling on the suction side than on the pressure side for any kind of endwall configuration. It was also found that the pitch-wise averaged effectiveness on the pressure side for the three endwall settings remained the same. The area-averaged effectiveness was higher for the cascade configuration when compared to the aligned or dam. The area-averaged effectiveness levels, which include

both the pressure and suction side portions of the endwall were 0.49 for cascade, 0.45 for the aligned and 0.42 for the dam, respectively.

As was previously discussed, the air temperature inside the gap was measured as indicated in Figure 1.2. Recall that for the study reported in this paper there was no flow exiting the mid-passage gap such that the temperatures measured were those of any flow that might ingest into the mid-passage slot. The measured non-dimensional gap temperatures for the aligned and misaligned cases are shown in Figure 1.12. The non-dimensionalization was based on the coolant temperature and hot gas freestream temperatures. Also shown in Figure 1.12 are the inviscid gap velocities that were calculated based on the local static pressure at the gap exit. Note that this inviscid analysis assumed a constant total pressure difference between the mainstream and the gap plenum. An iterative procedure was used to calculate the pressure difference which resulted in zero net mass flow from the slot (ingested flow balanced with exiting flow).

Figure 1.12 shows that for the aligned and dam cases, a large amount of coolant is ingested into the leading edge of the mid- passage gap region relative to the cascade case. In the location $0<x/L<0.2$ there is coolant ingestion from the upstream slot resulting in higher θ, with the amount of coolant being ingested decreasing with an increase in x/L. There is also increased ingestion of the mainstream flow causing a rapid rise in the gap air temperature and hence a decrease in θ. The non-dimensional temperatures in the gap decrease dramatically as hot mainstream flow is ingested near $x/L = 0.2$. For the mid- passage gap location between $0.3 < x/L < 0.5$, all of the endwall cases show a decrease in the air temperature (increase in θ) along the mid-passage gap, which results from a fresh influx of coolant from the two rows of film-cooling holes directly upstream of this region (see Figure 1.10a-c). The dam case benefits less because of the step, in conjunction with the cross-passage secondary flows that forces more hot flow into the gap. Figure 1.12 also shows that the temperatures inside the gap associated with the cascade endwall setting are cooler than that for the dam endwall setting, which is a result of the cooler fluid from the upstream slot. Up to $x/L = 0.5$, the inviscid velocity is indicated to be into the slot (static endwall pressure is higher than the plenum pressure), which is consistent with the fact that flow is ingesting into the slot.

Beyond $x/L = 0.5$, Figure 1.12 shows that flow exits the mid-passage gap. Between $0.5 < x/L < 0.7$, there is an increase in the temperature within the mid-passage gap, which is followed

by a decrease beyond x/L = 0.9. The slight increase at the exit results from any coolant that was channeled through the mid- passage gap from the upstream slot.

Effect of Slot Flow with a Cascade Endwall

Because the best configuration appeared to be the cascade endwall, more studies were completed with this configuration whereby flow from the upstream slot was varied. As previously discussed, the coolant flow from upstream slot has little effect on the pressure side of the mid-passage slot. Figure 1.13 compares adiabatic effectiveness contours for different slot flowrates (or different momentum flux ratios) with cascade endwall setting. The momentum flux ratios were calculated for all the flowrates through the slot using the relation,

$$I = \frac{\rho_s u_s^2}{\rho_\infty U_\infty^2} = \frac{\rho_s (\dot{m}/\rho_s A_s)^2}{\rho_\infty U_\infty^2} \tag{3}$$

It can be seen in Figure 1.13a that for 0.75% slot flow there is little cooling around the leading edge holes on the pressure side. With an increase in the slot flowrate, however, the adiabatic effectiveness near the upstream slot region increases, indicating some coolant exiting from the upstream slot onto the pressure side of the mid-passage gap as seen in Figure 1.13b and Figure 1.13c. It is also interesting that as the upstream slot flow is increased, the warmer region is no longer present that was shown at the 0.75% coolant flow condition about one-third of the way downstream of the mid-passage slot. It is also interesting to note that the film-cooling holes on the pressure side of the mid-passage gap showed better cooling as the slot flow was increased to 0.95% relative to 0.75%.

Conclusions

Measurements of endwall and mid-passage gap adiabatic effectiveness were presented for an endwall surface with realistic features, namely a combustor to turbine interface gap, endwall film-cooling, a vane to vane mid-passage gap, a platform misalignment, and surface roughness. When compared to a smooth surface, it was observed that the effect of roughness could vary. For the higher blowing ratio, there was a definite decrease in adiabatic effectiveness due to roughness but for the lower blowing ratio, there was essentially no difference in cooling. This difference was related to the boundary layer thickness whereby a thicker boundary layer had a significant impact on the jet separation from the endwall in the case of a high blowing ratio.

The mid-passage gap had a significant impact on the progression of the upstream coolant whereby the gap limited the area of coverage for the upstream slot coolant flow. The cooling from the upstream slot had a beneficial effect only along the suction side surface of the vane. Measurements along with an inviscid analysis indicated that fluid from the platform was ingested into the mid-passage gap. Near the start of the gap most of the flow ingested was coolant, which rapidly decayed because of the hot gas ingested.

Platform misalignment proved to also have a substantial effect on endwall adiabatic effectiveness levels. Clearly, from a heat transfer standpoint, a cascade configuration would be the most desirable endwall alignment mode. The cascade setting showed considerably better adiabatic effectiveness levels relative to an aligned or dam endwall configuration nearly removing the need for cooling holes on the suction side of the endwall. From a turbine design standpoint, the cascade setting is ideal relative to a dam configuration as the cascade acts like a trench where the coolant flow can reside.

This study has shown the drastic effects that realistic turbine features can have on first stage nozzle platform cooling. Upstream slot flow and a cascade misalignment provide for better cooling on the endwall. Quite the opposite is the case for a misaligned dam, mid-passage gap, and, in some cases, endwall surface roughness. These competing effects, when properly understood, can be used to better design endwall cooling arrangements.

Acknowledgments

This publication was prepared with the support of the US Department of Energy, Office of Fossil Fuel, and National Energy Technology Laboratory. However, any opinions, findings, conclusions, or recommendations expressed herein are solely those of the authors and do not necessarily reflect the views of the DOE. The authors would also like to thank Mike Blair (Pratt & Whitney), Ron Bunker (General Electric), and John Weaver (Rolls-Royce) for their input on the modeling of realistic turbine features.

Nomenclature

C	true chord of stator vane
C_a	axial chord of stator vane
D	diameter of film-cooling hole
I	momentum flux ratio

L length of mid-passage gap
$\dot{m}$ mass flowrate
M mass flux/ blowing ratio
P vane pitch; hole pitch
P_o or p total and static pressures
Re_{in} Reynolds number defined as $Re = CU_\infty / \nu$
s distance along vane from flow stagnation
S span of stator vane
T temperature
x,y,z local coordinates
u,v,w local velocity components
U velocity global

Greek

η adiabatic effectiveness, $\eta = (T_\infty - T_{aw})/(T_\infty - T_c)$
ρ density
ν kinematic viscosity
θ non-dimensionalized gap effectiveness, $\theta = (T_\infty - T_G)/(T_\infty - T_c)$

Subscripts

aw adiabatic wall
c coolant conditions
G gap
in inlet conditions
j coolant flow through film-cooling holes
s flow through upstream slot
∞ freestream conditions

References

[1] Blair, M.F., 1974, "An experimental Study of Heat Transfer and Film-cooling on Large-Scale Turbine Endwall," *ASME J of Heat Transfer*, vol. 96, pp. 524-529.

[2] Burd, S.W., Satterness, C.J., and Simon, T.W., 2000, "Effects of Slot Bleed Injection Over a Contoured Endwall On Nozzle Guide Vane Cooling Performance: Part II - Thermal Measurements," 2000-GT-200.

[3] Colban, W. F., Thole, K. A., and Zess, G., 2002, "Combustor-Turbine Interface Studies: Part 1: Endwall Measurements," *J of Turbomachinery*, vol. 125, pp. 193-202.

[4] Colban, W. F., Lethander, A. T., Thole, K. A., and Zess, G., 2002, "Combustor-Turbine Interface Studies: Part 2: Flow and Thermal Field Measurements," *J of Turbomachinery,* vol. 125, pp. 203-209.

[5] Friedrichs, S., Hodson, H. P. and Dawes, W. N., 1996, "Distribution of Film-Cooling Effectiveness on a Turbine Endwall Measured Using the Ammonia and Diazo Technique," *J of Turbomachinery*, vol. 118, pp. 613-621.

[6] Friedrichs, S., Hodson, H. P. and Dawes, W. N., 1997, "Aerodynamic Aspects of Endwall Film- Cooling," *J of Turbomachinery*, vol. 119, pp. 786-793.

[7] Friedrichs, S., Hodson, H. P. and Dawes, W. N., 1999, "The Design of an Improved Endwall Film- Cooling Configuration," *J of Turbomachinery*, vol. 121, pp. 772-780.

[8] Zhang, L.J., and Jaiswal, R.S., 2001, "Turbine Nozzle Endwall Film-cooling Study Using Pressure Sensitive Paint," *J of Turbomachinery*, vol**.** 123**,** pp. 730-738.

[9] Kost, F. and Nicklas, M., 2001, "Film-Cooled Turbine Endwall in a Transonic Flow Field: Part I – Aerodynamic Measurements," ASME Paper Number 2001-GT-0145.

[10] Nicklas, M., 2001, "Film-Cooled Turbine Endwall in a Transonic Flow Field: Part II – Heat Transfer and Film-Cooling Effectiveness," *J of Turbomachinery*, vol. 123, pp.720-729.

[11] Knost, D.G., and Thole, K.A., "Computational Predictions of Endwall Film-Cooling for a First Stage Vane," GT2003-38252.

[12] Knost, D. G., and Thole, K. A., "Adiabatic Effectiveness Measurements of Endwall Film-Cooling for a First Stage Vane," *J of Turbomachinery*, GT2004-52236.

[13] Yu, Y., and Chyu, M.K., 1998, "Influence of Gap Leakage Downstream of the Injection Holes on Film-cooling Performance," *J of Turbomachinery*, vol. 120, pp. 541-548.

[14] Aunapu, N.V., Volino, R.J., Flack, K.A., and Stoddard, R.M., 2000, "Secondary Flow Measurements in a Turbine Passage with Endwall Flow Modification," *J of Turbomachinery*, vol. 122, pp. 651-658.

[15] Ranson, W., Thole, K. A., and Cunha, F., "Adiabatic Effectiveness Measurements and Predictions of Leakage Flows Along a Blade Endwall" IMECE2004-62021.

[16] Yamao, H., Aoki, K., Takeishi, K., and Takeda, K., 1987, "An Experimental Study for endwall Cooling Design of Turbine Vanes," IGTC-1987, Tokyo, Japan.

[17] Bons, J.P., Taylor, R.P., McClain, S.T., and Rivir, R.B., 2001, "The Many Faces of Turbine Surface Roughness," 2001-GT-0163.

[18] Bogard, D. G., Schmidt, D. L., Tabbita, M., 1998, "Characterization and Laboratory Simulation of Turbine Airfoil Surface Roughness and Associated Heat Transfer," *J of Turbomachinery*, vol. 120, pp. 337-342.

[19] Moffat, R. J., "Describing the Uncertainties in Experimental Results," *Experimental Thermal and Fluid Science*, vol.1, pp. 3-17.

Table 1.1 Geometric and Flow conditions

Scaled up chord length (C)	59.4 cm
Scaled up axial chord length (C_a)	29.3 cm
Pitch / chord (P/C)	0.77
Span / chord (S/C)	0.93
Re_{in}	2.1×10^5
Inlet and exit angles	0° & 72°
Inlet, exit Mach number	0.017,0.085
Inlet mainstream velocity	6.3 m/s

Table 1.2 Summary of Endwall Geometry

	Parameter	Experimental
Mid-Passage Gap	W - Passage gap width	0.01C
	H - Seal strip thickness	0.5W
	A - Thermocouple location	6H
	B - Passage gap depth	10H
	C - Seal strip gap	2H
	D - Seal strip width	16.8H
	E - Passage gap plenum width	28H
Up-stream Slot	Upstream Slot width	0.024*C*
	Slot flow length to width	1.88
Film Cooling	FC hole diameter (cm)	0.46
	FC Hole L/D	8.3

Table 1.3 Summary of Coolant Settings

%mass flow	C_D	M_{ideal}	M_{actual}
0.35 Film Cooling	0.85	1.24	1.06
0.50 Film-Cooling	0.8	1.88	1.51
0.75 Film-Cooling	0.71	3.2	2.26
0.75 Upstream Slot	0.6	0.48	0.29
0.95 Upstream Slot	0.6	0.69	0.414
1.10 Upstream Slot	0.6	0.72	0.43

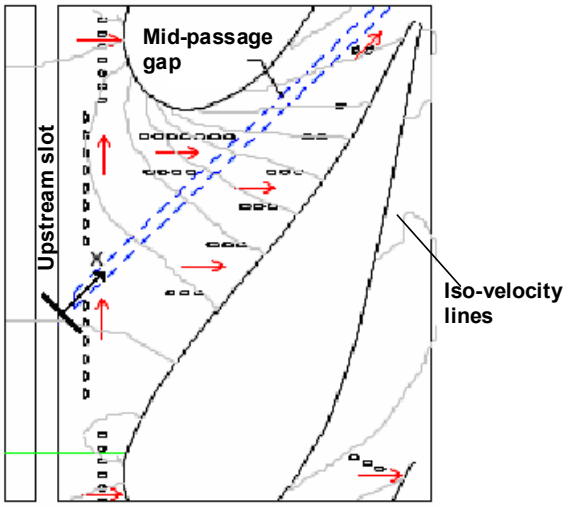

Figure 1.1 **Directions of the coolant hole injection along with iso–velocity contours and the mid-passage gap location for mating two turbine vane platforms.**

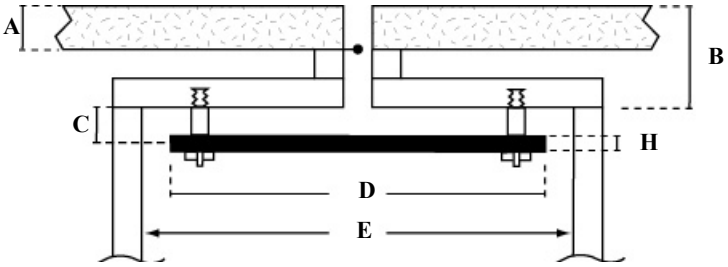

Figure 1.2 **Cross section view (section AA, Figure 1.1) of the mid-passage gap plenum and accompanying seal strip (see Table 1.2).**

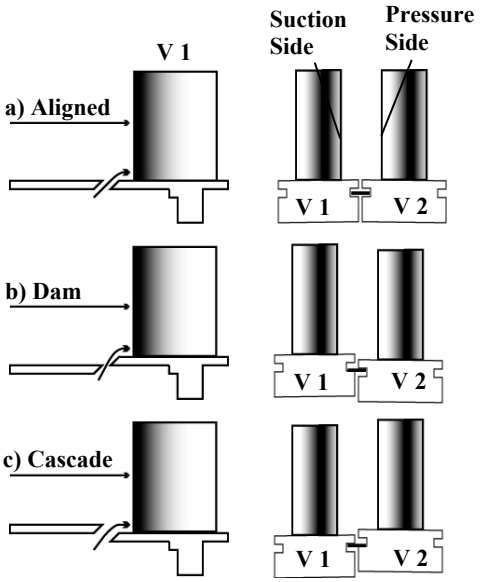

Figure 1.3 **Side and upstream views of the three alignment modes for two adjacent vane platforms.**

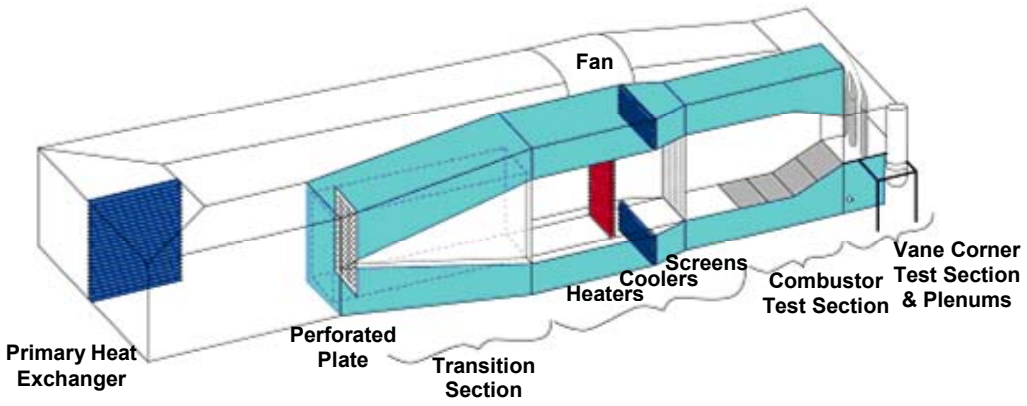

Figure 1.4 Illustration of the wind tunnel facility

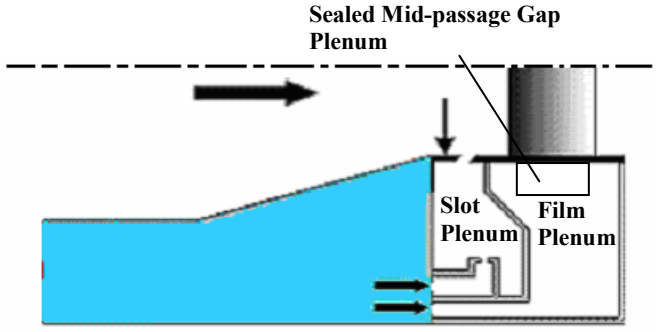

Figure 1.5 Separate plenums for film-cooling and upstream slot provided independent control of the flow through each of them.

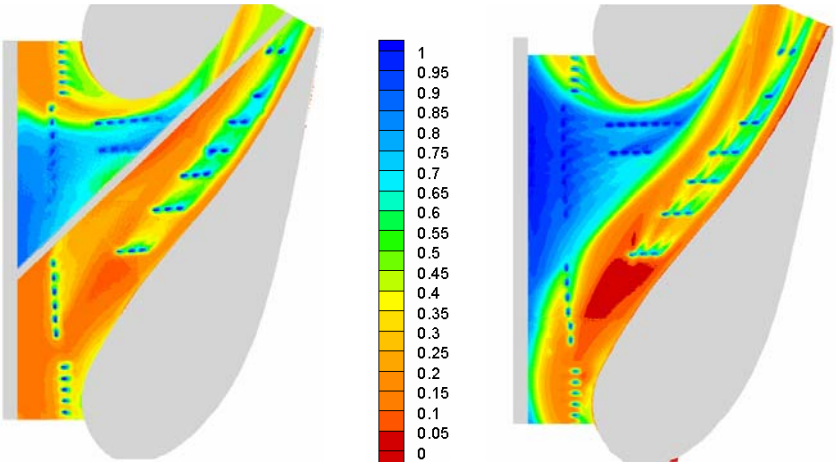

Figure 1.6a-b Contours of adiabatic effectiveness for film-cooling cases (a) rough endwall with mid-passage slot (b) smooth endwall with no mid-passage slot.

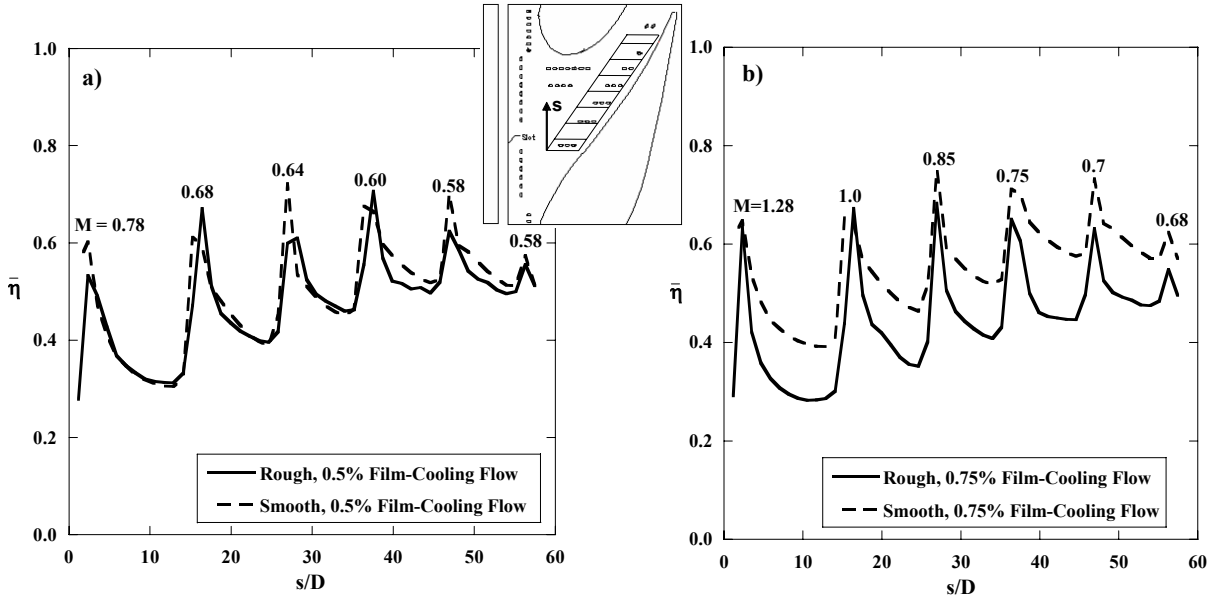

Figure 1.7a-b Plots of laterally averaged adiabatic effectiveness on the film-cooling holes on the pressure side: (a) for 0.75% upstream slot flow and 0.5% film-cooling and (b) 0.75% upstream slot flow and 0.75% film-cooling.

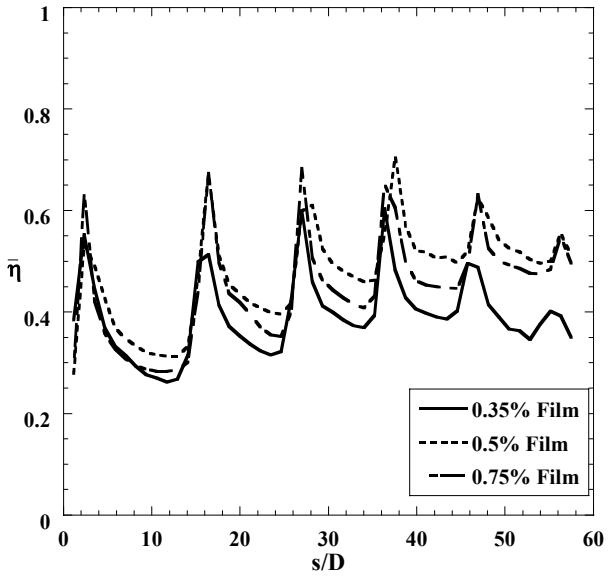

Figure 1.8 Laterally averaged adiabatic effectiveness for 0.35%, 0. 5% and 0.75% film-cooling flows for a rough endwall.

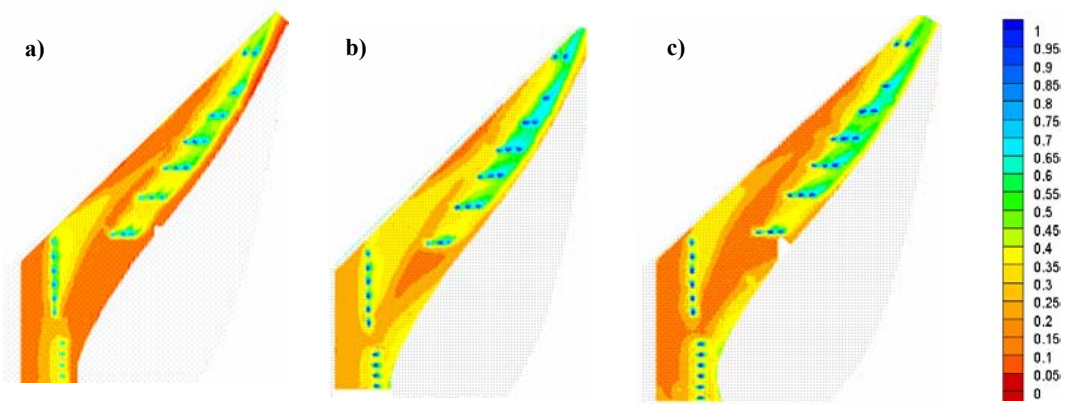

Figure 1.9a-c Contours of adiabatic effectiveness with a rough endwall with 0.75% slot flow for (a) 0.35% film-cooling (b) 0.5% film-cooling (c) 0.75% film-cooling.

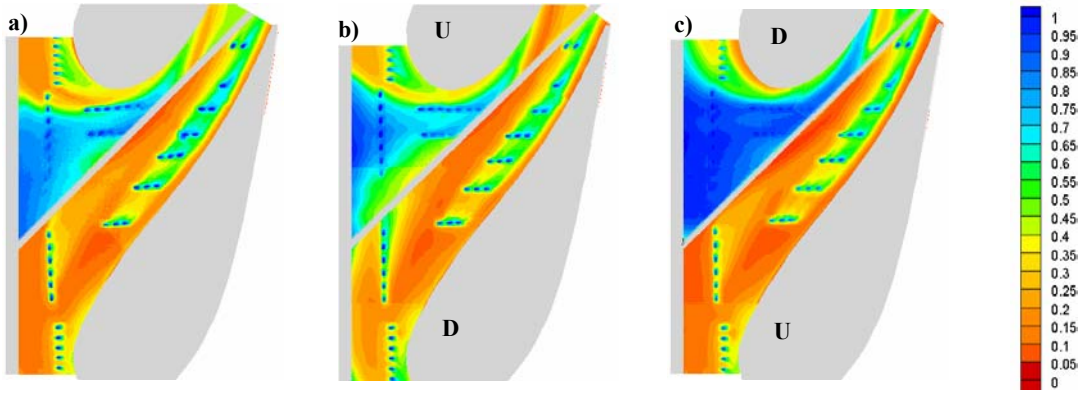

Figure 1.10a-c Contours of adiabatic effectiveness on a rough endwall for the baseline film and slot cooling cases: (a) aligned (b) dam and (c) cascade endwall (note that U refers to raised side and D refers to lowered side).

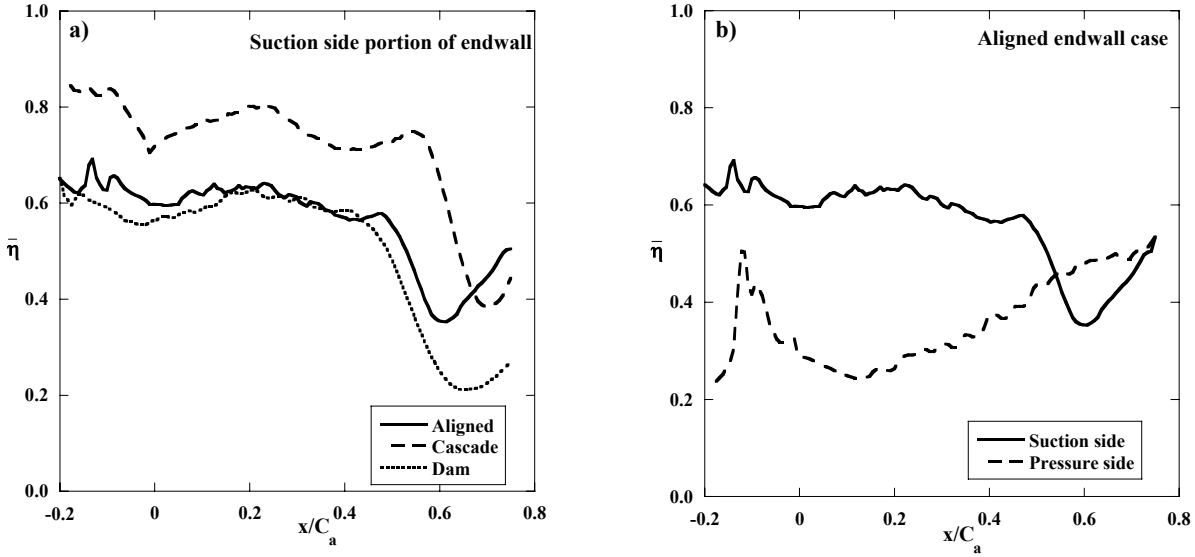

Figure 1.11 Pitch-wise averaged adiabatic effectiveness for the baseline film and slot cooling cases: a) along the suction side for the three endwall settings b) comparison between effectiveness on the suction and pressure side.

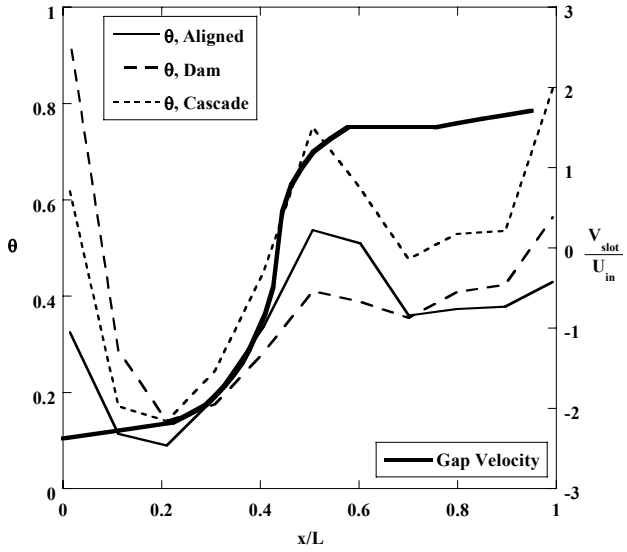

Figure 1.12 Non-dimensional gap temperature profiles for the three endwall alignment modes and the velocity profile for an aligned gap.

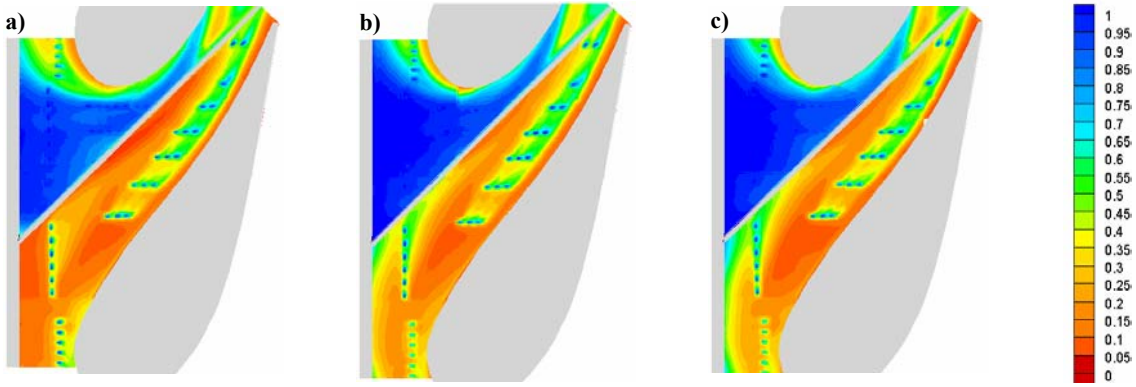

Figure 1.13a-c Contours of adiabatic effectiveness on a rough endwall with cascade setting for different upstream slot flowrate with 0.5% film-cooling: (a) 0.75% (I = 0.08) slot flow, (b) 0.95% (I = 0.12) slot flow, (c) 1.1% (I = 0.16) slot flow.

Paper 2:
THE EFFECTS OF VARYING THE COMBUSTOR-TURBINE GAP

To be presented at the *2006 IGTI Conference**
In review for the *Journal of Turbomachinery**

Abstract

To protect hot turbine components, cooler air is bled from the high pressure section of the compressor and routed around the combustor where it is then injected through the turbine surfaces. Some of this high pressure air also leaks through the mating gaps formed between assembled turbine components where these components experience expansions and contractions as the turbine goes through operational cycles.

This study presents endwall adiabatic effectiveness levels measured using a scaled up, two-passage turbine vane cascade. The focus of this study is evaluating the effects of thermal expansion and contraction for the combustor-turbine interface. Increasing the mass flow rate for the slot leakage between the combustor and turbine showed increased cooling while increasing the momentum flux ratio for the slot leakage dictated the coverage area for the cooling. With the mass flow held constant, decreasing the combustor-turbine interface width resulted in much improved coolant coverage while increasing the slot width resulted in reduced coolant coverage.

*Co-authors: Narayan Sundaram, Mechanical Engineering Department, Virginia Tech
Dr. Karen A. Thole, Mechanical Engineering Department, Virginia Tech

Introduction

Core flow temperatures within the hot section of a gas turbine commonly exceed the metal melting temperature. Cooling techniques are needed to protect the turbine components from the harsh environment. To accomplish the needed cooling, high pressure air is bled from the compressor, bypassed around the combustor, and then routed into the turbine where it is used for internal and external cooling purposes.

Since the entire turbine is not manufactured as a single component, there exist numerous gaps between mating parts allowing leakage of high pressure coolant. Thermal expansion and mechanical stresses within the turbine make it especially difficult to seal these interfaces. One such interface is the slot between the combustor and the first stage of the turbine since the combustor and turbine are not rigidly connected. The gap between adjacent vane sections is another area that allows leakage of high pressure coolant. Leakages result in a significant loss in overall efficiency.

Turbine components are typically cast with high nickel super alloys because of their high strength at elevated temperatures. While the exact materials are proprietary, these alloys are similar in composition to Inconel 625. The average coefficient of thermal expansion for Inconel 625 is equal to 0.138 mm per cm of unrestrained metal over the standard to operating temperature range of 1075°C (www.espimetals.com). If one considers an unrestrained 30 cm combustor, it would result in an expansion of 4 mm. This 4 mm is on the order of the change in slot width we are modeling for this paper.

The work presented in this paper evaluates the effects of expansion and contraction of the combustor-turbine interface on endwall cooling performance. Also compared in this paper is the effect of leakage flowrates from a mid-passage gap between two mating vanes on the overall endwall cooling performance.

Relevant Past Studies

Significant work has been performed documenting the effects of leakage from the slot at the combustor-turbine interface. There have also been studies in the literature analyzing the combined effects of a combustor-turbine slot leakage and film-cooling. Very few studies exist on either the effect of a realistic mid-passage gap or the effect of changes in the combustor-turbine slot width on endwall cooling effectiveness for an actual airfoil passage.

The majority of studies concerned with leakage flow have focused on a slot upstream of the first stage vane meant to simulate the leakage flow that occurs between the combustor and the turbine. One of the earliest works was presented by Blair [1]. Blair's study included a two-dimensional slot upstream of the vane. An enhanced cooling benefit was observed for increases in leakage flow. In a similar study, Burd et al. [2] studied the effects of coolant leaking from an upstream slot. As with Blair, Burd et al. reported better endwall cooling for leakage flows as high as 6% of the total passage flow. Colban et al. [3,4] studied the effects of changing the combustor liner film-cooling and upstream slot leakage flows on endwall effectiveness levels for a first vane cascade. Their results, like others, showed that the upstream slot flow does not evenly distribute along the endwall, with the majority of the cooling benefit along the suction side of the vane. Pasinato et. al [5] studied the effects of injecting air upstream of the vane stagnation through a series of discrete slots. These slots were oriented in the slot in such a manner that the coolant was injected tangentially to the leading edge of their contoured endwall. Pasinato et. al [5] found that this secondary air injection strongly distorted the flowfield upstream of the vane stagnation.

Some studies have combined the effects of upstream slot leakage with endwall film-cooling. The main studies performed are those of Zhang and Jaiswal [6], Kost and Nicklas [7], Nicklas [8], and Knost and Thole [9,10]. Kost and Nicklas [7] and Nicklas [8] reported that coolant ejection from an upstream slot causes radical changes in the near wall flowfield signifying an intensification of the horseshoe vortex, which was observable in their flow angle diagrams. This increase in intensity resulted in the slot coolant being moved off of the endwall surface and heat transfer coefficients that were over three times that measured for no slot flow injection. Endwall studies by Knost and Thole [9,10] investigated endwall effectiveness levels for a vane passage with both film-cooling and upstream slot injection. For increasing slot mass flow, Knost and Thole reported higher local effectiveness levels with the same coolant coverage area on the endwall

Several studies have documented the effect of flow from a gap between two adjacent airfoils. Aunapu et al. [11] showed that blowing through a passage gap could be used to reduce the negative effects of the passage vortex, but with significant aerodynamic losses. Another study done by Ranson and Thole [12] used a mid-passage

gap between two blades for their experimental and computational studies. Their results showed that the flow through the gap was initially directed toward the blade pressure side, due to the incoming velocity vectors, and then convected towards the suction side of the adjacent airfoil. Yamao et al. [13] reported changes in film-cooling effectiveness levels due to leakage air injected from both an upstream slot and mid-passage gap. Their study indicated that film-cooling effectiveness was enhanced with an increase in sealing flow through both leakage interfaces.

Piggush and Simon [14,15] analyzed the effect of leakage flows on aerodynamic losses for a vane cascade. It was concluded that the mid-passage gap blowing caused both an increase in passage losses and the creation of a second smaller passage vortex which was located below the primary passage vortex. Piggush and Simon [14,15] also concluded that the majority of mid-passage gap blowing became entrained in the formation of a second vortex within the passage. Reid et al. [16] studied the effect of interplatform leakage on overall efficiency for an axial flow turbine stage. They determined that the largest drop in efficiency associated with interplatform leakage was 1.5% when compared to the stage efficiency with no slot present. The main difference in interplatform gap geometry between these two studies is that Reid et al. [16] modeled the internal seal strip of the interplatform gap and Piggush and Simon [14,15] did not.

Cardwell et al. [17] analyzed the effect of a mid-passage gap with a seal strip and platform misalignment on endwall cooling effectiveness. They determined that misalignment between adjacent vanes and between the combustor-turbine interface can significantly affect upstream slot coolant trajectory and effectiveness. Cardwell et al. [17] reported that a backward facing step (cascade configuration) between the combustor-turbine interface greatly reduced the need for suction side endwall film-cooling due to an increased utilization of upstream slot leakage.

de la Rosa Blanco et al. [18] determined the effect of a step in hub diameter just ahead of a blade row on aerodynamic blade performance. They also determined that a backward facing step at this location can lead to a reduction in endwall and mixing losses when compared to a flat endwall while a forward facing step produces higher losses than a flat endwall. Piggush and Simon [14,15] also agreed with the pressure loss results of de la Rosa Blanco et al. [18] for a turbine vane indicating increased losses with a forward and decreased losses with a backward facing step upstream of the vane stagnation.

Vane and Endwall Geometry

The flat endwall used in the linear cascade has three cooling features: a combustor-turbine slot, a mid-passage vane-to-vane gap with accompanying seal strip, and discrete film cooling holes. The same film cooling pattern as shown in Figure 2.1, which was originally designed and tested by Knost and Thole [9,10], was used in this study. Figure 2.1 shows the film cooling hole injection angles, the upstream slot, and the mid-passage gap discussed above. All film cooling holes were cylindrical and inclined at an angle of 30° with respect to the endwall surface. Table 2.1 provides a brief description of the turbine vane geometry and operating conditions. Significant studies have been performed in our lab on this particular vane geometry with a more detailed description given in Radomsky and Thole [19].

Figure 2.1 also shows a two-dimensional slot upstream of the vane leading edge, which represents the mating interface of the turbine and combustor. This slot had an injection angle of 45° and was located 30% of the axial chord upstream of the vane stagnation location. This leakage interface will be referred to as the upstream slot. Table 2.2 provides a summary of parameters relevant to the film-cooling holes and upstream slot geometries.

As discussed in the introduction, the primary focus of this work was to analyze the endwall cooling effect of an upstream slot expansion and contraction. For this study the metering slot width was expanded by 50% and contracted by 50%, which will be referred to as double width and half width, respectively. As with the nominal slot, both the double width and half width slots had a 45° surface injection angle. For these studies, the upstream slot was expanded and contracted while keeping the slot centerline fixed relative to the vane stagnation.

The gap between adjacent vane sections will be referred to as the mid-passage gap. A cross-section of the mid-passage gap is shown in Figure 2.2. Unlike the upstream slot, the mid-passage gap had a recessed seal strip as found in many engine designs, which influenced its interaction with the coolant and mainstream flow. To allow flow control, the mid-passage gap had a separate supply plenum which did not open into the upstream slot. The cross section of the mid-passage gap is also shown in Figure 2.2. This gap, which was described in the previous study be Cardwell et al. [17], had a 90°

surface injection angle, a width of 0.635 cm, and a gap flow length to width ratio of 5. For this study, the mid-passage gap width was not varied.

Similar to the previous study reported by Cardwell et al. [17], the endwall surface was covered with a uniform roughness. To simulate a random array of a uniform roughness level, wide-belt industrial sandpaper was used to cover the entire endwall. The sandpaper had a closed coat 36 grit surface and a grade Y cloth backing. A closed coat surface had roughness elements arranged in a random array over 100% of its surface. The 36 grit sandpaper had an average particle size of 538 microns (www.sizes.com/tools/sandpaper.htm) which was roughly twice that observed by Bons et. al. [20] for in service turbine endwalls. A custom construction technique was used to guarantee a uniform and high tolerance fit around each film-cooling hole. This technique ensured a uniform interaction between the rough surface and coolant jets for the entire endwall.

Experimental Methodology

The experimental facility used for this study consisted of a linear cascade test section placed in a closed loop wind tunnel, as shown in Figure 2.3. Flow within the wind tunnel was driven by a 50 hp axial vane fan, which was controlled by a variable frequency inverter. After being accelerated by the fan, the flow turned 90° and then passed through a primary finned-tube heat exchanger. This heat exchanger was used to precool the bulk flow. After passing through the primary heat exchanger, the flow encountered another 90° turn before entering a three way split. This split simulated the primary core flow through the combustor and the bypass flow around the combustor. The flow split was achieved by using a porous plate with a 25% open area to act as a valve thereby directing a portion of the flow into the upper channel. The primary core flow passed through a resistance heater bank where its temperature was increased to 60°C. The secondary flow in the top channel passed through a secondary finned-tube heat exchanger where the flow temperature was lowered to 10°C. The mainstream flow continued through the middle channel into the test section. The cooler bypass flow from the top channel was pulled into a 2 HP blower where it then flowed into the test section for the coolant supplies.

The test section consisted of a vane cascade comprised of two full passages with one center vane and two half vanes, an endwall with film cooling holes, an upstream slot, and mid-passage gap geometries, which were scaled up by a factor of nine. A detailed account of its construction has been previously described by Cardwell et al. [17]. The two main differences between the current test section and the one described by Cardwell et al. [17] were a change in the upstream approach flow and the ability to vary the upstream slot metering width. The previous upstream approach flow had a 15.6° contraction directly upstream of the test section while the upstream flow path used in this study had a 45° contraction that was 2.9 chords upstream of the vane giving a longer constant flow area into the test section. The upstream slot was interchangeable so that the flow metering width could be adjusted. The endwall, which was the main focus of the study, was constructed of low thermal conductivity foam (0.033 W/m.K). The endwall foam was 1.9 cm thick and was mounted on a 1.2 cm thick Lexan plate. The cooling hole pattern was cut using a five-axis water jet machine to ensure proper hole placement and tight dimensional tolerances. The upstream slot, which needed to be stiffer, was constructed of hard wood which also has a low thermal conductivity value (0.16 W/m.K).

Adiabatic endwall temperatures were taken for the different slot geometries and flowrates and also for different gap flowrates. Each coolant path had its own separate plenum for independent control of the flow through the film-cooling holes, upstream slot, and mid-passage gap as shown in Figure 2.4. For the studies reported in this paper, film cooling was not varied so a nominal value was set for all cases. Experiments were conducted for both a sealed and leaking mid-passage gap. Sealing of the mid-passage gap plenum was accomplished by closing the appropriate coolant feed pipe.

Freestream turbulence effects were not simulated as the study was more focused on industrial gas turbines rather than propulsive engines. The inlet turbulence was measured to be 1.3%. The turbulent inlet boundary layer thickness was measured as 22% of span at a location 15 slot widths upstream of the center vane stagnation location.

During steady state operation, a temperature difference of 40 °C was maintained between the mainstream and the coolant. From a room temperature start, the typical time to achieve steady state conditions was 3 hours.

Coolant Flow Settings

As stated earlier, all three coolant plenums were sealed with respect to each other and had independent flow control. CFD studies reported by Knost and Thole [9] were used to set the coolant massflows through the film-cooling holes through the use of a predicted discharge coefficient. The method previously described by Knost and Thole and Cardwell et al. [17] was used whereby a global discharge coefficient was found through CFD analysis. Only one film-cooling flowrate was used for all of these studies, which was 0.5% of the core flow.

A discharge coefficient of 0.6 was chosen for the upstream slot. This is a typically assumed value for a flow through a sharp-edged orifice. No assumed discharge coefficient was needed for the mid-passage gap as the coolant flow rate was measured directly using a laminar flow element placed downstream of the coolant control valve. Feeding this plenum differently was necessary due to the high amounts of ingestion seen in the mid-passage gap, which will be explained later in the paper.

Instrumentation and Measurement Techniques

Spatially-resolved adiabatic endwall temperature contours were recorded using an FLIR P20 infrared camera. The test section had multiple viewing ports on the top end wall through which measurements were taken until the entire endwall surface was mapped. At each viewing location the camera was placed perpendicular to the endwall surface at a distance of 55 cm. Given the camera's viewing angle, each picture covered an area of 24 cm by 18 cm, with the resolution being 320 by 240 pixels. The camera's spatial integration was 0.16 hole diameters (0.71 mm). Post calibration of the images was accomplished using actual temperature values taken by thermocouples placed on the endwall surface. The surface emissivity was assumed to be 0.92, which is a commonly reported value for the material type and surface structure associated with coarse grit sandpaper [21]. During post calibration, the image background temperature was adjusted until the thermocouple data and infrared image data were within 0.01 °C. Typical values of background temperature were 55 °C (note the freestream temperature was typically 60 °C). Six images were taken at each viewing location, of which five were used to obtain an average image using an in-house Matlab program. The same program then scales, rotates, and assembles the averaged images at all locations. This fully assembled contour gives a complete temperature distribution for the endwall surface.

Freestream temperature values were measured at 25%, 50%, and 75% of the vane span at four locations across the passage pitch. Maximum variations along the pitch and span were less than 0.5 °C and 1.0 °C, respectively. Three thermocouples were attached in the upstream slot plenum and two thermocouples were attached in the film cooling plenum to measure the respective coolant temperatures. Differences in temperature between the plenums were typically less than 1 °C. Eleven thermocouples were placed within the mid-passage gap to measure the air temperature profile. These thermocouples were located six seal strip thicknesses beneath the endwall surface (see Figure 2.2). A 32 channel data acquisition module by National Instruments was used with a 12-bit digitizing card to measure and record the thermocouple voltage data. All temperature data was recorded and compiled after the system had reached steady state.

A one-dimensional conduction correction as described by Ethridge et. al. [22] was applied to all adiabatic effectiveness measurements. This correction involved measuring the endwall surface effectiveness with no coolant flow. This was accomplished by blocking off the film-cooling holes within the passage. The resulting η correction was 0.16 at the entrance for a η value of 0.9 and 0.02 at the exit region at a measured η value of 0.5.

An uncertainty analysis was performed on the measurements of adiabatic effectiveness using the partial derivative method described at length by Moffat [23]. The precision uncertainty was determined by taking the standard deviation of six measurement sets of IR camera images with each set consisting of five images. The precision uncertainty of the IR camera measurements was ±0.0143°C and the bias uncertainty was ±1.02°C, based on the calibration of the image. The precision uncertainty and bias uncertainty of the thermocouples was ±0.1°C and ±0.5°C, respectively. The total uncertainty was then calculated as ±1.02°C for the IR images and ±0.51°C for the thermocouples. Uncertainty in effectiveness, η, was found based on the partial derivative of η with respect to each temperature in its definition and the total uncertainty in the measurements. Uncertainties of $\delta\eta = \pm 0.028$ at $\eta = 0.1$ and $\delta\eta = \pm 0.028$ at $\eta = 0.8$ were calculated.

Disussion of Results

A number of tests were conducted for this study with the most representative results being given in this paper, as described in the next section on the test matrix. First, the effect of varying upstream slot width will be discussed for constant mass flow rate and a constant momentum flux ratio. Second, the effect of a fixed slot width for varying upstream slot mass flow rate will be discussed. Last, a mid-passage gap comparison with and without flow width will be discussed.

Derivation of Test Matrix

Significant consideration was given to the creation of a test matrix (shown in Table 2.3), which would be of particular use to the turbine designer. Mass flowrates are reported on a percent basis with respect to the total mass flowrate through the passage. For all cases, the film-cooling mass flow was set at 0.5% and, unless specified, the mid-passage gap was at 0%.

The first comparison done was for a 0.85% matched mass flow for expanding and contracting the slot width by 50%. The mass flow was kept constant by increasing or decreasing the plenum pressure accordingly, which resulted in a matched mass flow but varying momentum flux and mass flux ratios. While a sensible choice from an experimental point of view, this does not necessarily correlate to that of an actual engine.

Within the engine, the pressure difference between the coolant and exit static pressure typically remains constant resulting in a matched momentum flux ratio (given that $\Delta p \sim U2$). The second comparison was for $I = 0.08$ while expanding and contracting the slot width 50%. Total coolant pressure to static gas pressure was held at a constant value, which resulted in nominally the same average slot velocity (and momentum flux ratio) but differing slot mass flows as the slot metering width was contracted or expanded. Next, the effect of varying slot mass flow was analyzed for the nominal slot width. The last effect to be analyzed was the mid-passage gap leakage. The mid-passage gap mass flow was set at 0.1%, 0.2%, and 0.3% of core passage flow.

Matched Mass Flow Rates for Differing Slot Widths

For a nominal slot flow rate of 0.85%, Figure 2.5 compares contours of adiabatic effectiveness for different slot widths. It is important to note that while the slot mass

flow remained constant for all slot widths, the average slot momentum flux ratio changed by a factor of ten between the half and double width slots.

The effect of expanding the slot is shown in Figure 2.5a. No coolant was observed exiting the upstream slot on the pressure side of the mid-passage gap. The hot ring observed on the vane's leading edge was apparent and effectiveness levels on the entire pressure side and suction side had decreased substantially relative to Figure 2.5b. The effect of contracting the slot is shown in Figure 2.5c. Figures 2.5a and 2.5b show the upstream slot coolant had been primarily confined to the suction side surface by the presence of the mid-passage gap. In Figure 2.5c for the half width slot the leakage flow seems evenly distributed over the entire slot pitch with a substantial increase in cooling on the pressure side of the mid-passage gap. Film-cooling holes upstream of the vane stagnation location are redundant and the hot bow wake off the leading edge of the vane is no longer apparent. More even cooling was observed on the mid-passage gap suction side as well in Figure 2.5c, while the locally high values of effectiveness seen using the nominal upstream slot width (Figure 2.5b) were less apparent.

Pitchwise averaged values of effectiveness for the varied slot width with matched mass flow ratios are shown in Figure 2.6. Both expanding and contracting the slot show substantial decreases in averaged effectiveness levels along much of the platform. This can be explained by the contours shown in Figure 2.5 where even though the coverage area was greater in Figure 2.5c, the local levels of effectiveness were lower. The contracted slot shows better coolant coverage than nominal but lower effectiveness levels. This result is expected based on a viewpoint of coolant momentum (see Table 2.3). The higher plenum pressure required to supply 0.85% from the contracted slot has resulted in a substantial increase in slot momentum flux ratio, which explains the increase in coolant coverage area. Since the coolant is exiting the upstream slot in some regions at a higher momentum, it is more likely to separate from the wall and lift off into the passage, thus explaining the locally lower values of adiabatic effectiveness observed in the mid-passage gap suction side. For the expanded slot, lower plenum pressures are required to supply 0.85% mass flow thereby resulting in a much lower local coolant momentum flux across the slot. Through observation of Figure 2.5a it was concluded that a portion of the slot was ingesting hot air since no coolant was observed exiting the slot on the mid-passage gap pressure side. Therefore, the ejected coolant on the suction

side was already premixed with hot main gas within the upstream slot, which explains the strong reduction in averaged effectiveness levels and coolant coverage area for the expanded slot.

Mid-passage gap temperature profiles are shown in Figure 2.7. The non-dimensional gap temperature, θ, was based on the mainstream and the coolant temperatures where θ values of zero and one signify maximum and minimum gap temperatures, respectively. Again, Figure 2.2 illustrates the thermocouple location for the mid-passage gap. Also shown in Figure 2.7 are the calculated inviscid gap velocities based on the local static pressure at the gap exit, which was known from previous studies. Note that this calculation assumed a constant total plenum pressure difference between the mainstream and the gap plenum. An iterative procedure was used to calculate the pressure difference which resulted in zero net mass flow from the slot (ingested flow equals ejected flow). For zero net mass flow through the mid-passage gap, negative velocity values (signifying ingestion) were predicted for $x/L < 0.4$ and positive velocity values (signifying ejection) were predicted for $x/L > 0.4$.

The gap leading edge ingested a substantial amount of coolant from the upstream slot. In the location $0 < x/L < 0.2$, this ingested coolant resulted in cooler temperatures with the amount of coolant being ingested decreasing with increasing x/L. There was also increased ingestion of the hot mainstream flow which caused a rapid increase in the gap air temperature. Temperature in the gap increased dramatically as hot mainstream flow was ingested near $x/L = 0.2$. This mixture of coolant and hot mainstream gas convects inside the mid-passage gap until the exit static pressure is low enough for it to exit the gap. Up to $x/L = 0.5$, the inviscid velocity is indicated to be into the slot (static endwall pressure is higher than the plenum pressure), which is consistent with the fact that flow is ingesting into the gap. Beyond $x/L = 0.5$, Figure 2.7 shows that flow is exiting the mid-passage gap.

All θ profiles for varying slot width in Figure 2.7 are very similar with values slightly lower for both the double and half width upstream slots. Since the coolant exiting the half-width slot has a relatively high momentum compared with the nominal, it is less likely that it will be ingested into the mid-passage gap.

Matched Momentum Flux Ratios for Differing Slot Widths

Upstream slot momentum flux ratios were matched to a nominal value of I = 0.08, which corresponded to a nominal width upstream slot flow of 0.75%. As previously, the upstream slot width was contracted and expanded by 50%. There was 0% flow in the mid-passage gap.

Figure 2.8 shows contours of adiabatic effectiveness and Figure 2.9 shows pitchwise averaged values of adiabatic effectiveness on the endwall for an upstream slot momentum flux ratio of 0.08. The coolant coverage area is very similar for all three slot widths, illustrating that coverage area is a function of the coolant to mainstream momentum flux ratios rather than the coolant mass flow rate. By contracting the slot and keeping the plenum-to-mainstream pressure difference the same, the mass flow of coolant exiting the upstream slot was reduced (see Table 2.3). This reduction in coolant flow explains the observed reduction in effectiveness on the suction side platform and the lower values of averaged effectiveness. By the same reasoning, the coolant mass flow would be higher for the expanded slot, thus explaining the increase in averaged coolant effectiveness on the suction side platform.

Figure 2.8 shows there is also an effect of slot width on the trailing edge of the mid-passage gap. In this region, the mid-passage gap is ejecting a mixture of the coolant and main gas which was ingested in the leading edge region. A slight increase in effectiveness levels for the nominal and double slot cases relative to the half slot width were observed on the suction side of the mid-passage gap trailing edge. The cooler region near the trailing edge indicates different amounts of coolant were being ingested into the mid-passage gap near the leading edge and then ejected near the trailing edge. Upstream slot coolant momentum flux ratios were the same for all cases, but coolant mass flux ratios were higher for the double slot and lower for the half slot.

By examining the mid-passage gap temperature profiles in Figure 2.10, we see that by matching the upstream slot coolant momentum flux ratios the amount of coolant being ingested into the mid-passage gap changed with slot width. Expanding the slot width dramatically decreased gap temperature, sometime by as much as 70% from nominal. The effect of contracting the slot is not observed until x/L = 0.5, where ejecting mid-passage gap temperatures were observed to be 10-20% lower than nominal.

Adiabatic Effectiveness with Varying Slot Leakage Flows

For a constant upstream slot width and a varying difference between the coolant and the mainstream static pressures, the coolant flow rate exiting the slot varies. To determine this effect, tests were conducted, as before, with no mid-passage gap flow and upstream slot mass flow rates were set to 0.75%, 0.85%, and 1.0%. The effect of varying upstream slot flowrate was analyzed for a nominal slot width. Contours of adiabatic effectiveness for the effect of coolant mass flux ratio are shown in Figure 2.11.

The primary result was that for all three cases the coverage area had not changed significantly but the cooling benefit had increased. It is important to note that upstream slot momentum flux ratio increased with slot mass flow by a factor of 1.6 from the lowest to highest slot flowrate studied. This increase was much smaller than the factor of ten discussed in the previous section. For each case, there was very little coolant flow from the upstream slot crossing over the mid-passage gap as shown before by Cardwell et al. [16]. As the coolant convected along the gap until the end of the vane passage where it exited the gap. The effect of film-cooling was also nominally the same for all upstream slot flows. As the slot mass flow rate was increased, the amount of coolant observed on the pressure side of the slot increased slightly. The suction side of the gap, which was well cooled for all flow rates, showed higher adiabatic effectiveness levels when the slot flow rate was increased. Although the coolant mass flow rate through the slot was increased substantially, much of the pressure side endwall continued to show lower values of adiabatic effectiveness. To quantify the effect of increasing slot flow at these levels, the adiabatic effectiveness values were pitchwise averaged for all flow rates, as shown in Figure 2.12. Increasing the upstream slot cooling showed increased values of pitchwise averaged adiabatic effectiveness.

Since there was more coolant on the endwall for increased upstream slot leakage, it was hypothesized that more coolant was being ingested into the mid-passage gap. The measured non-dimensional gap temperature profiles for the above mentioned cases are shown in Figure 2.13. Note that again, no coolant mass flow was provided to the gap. The increase in slot flow rate from 0.75% to 0.85% showed a substantial decrease in gap temperatures. The ratio of ingested coolant to hot gas was higher, thus explaining the decrease in ejected gap temperatures beyond $x/L = 0.5$. In contrast, negligible changes in gap temperatures were recorded for the increase to 1% upstream slot flow. Most likely the gap was saturated with coolant from the upstream slot at the 1% case.

Adiabatic Effectiveness with Varying Mid-Passage Gap Flows

The last comparison completed for this study was for a variation in the mid-passage gap leakage. These experiments were conducted with a nominal upstream slot width, a 0.75% upstream slot mass flow rate (I = 0.08). Mid-passage gap mass flow rates were set to 0.1%, 0.2%, and 0.3%.

The contours of adiabatic effectiveness for the varying gap flows are shown in Figure 2.14. These contours are very similar to each other with no large effect due to varied mid-passage gap flow. As before, the contours were pitchwise averaged, which is shown in Figure 2.15. No effect is observed in the leading edge region of the slot. It appears that the mid-passage gap flow has little to no effect on the endwall surface for the entire passage in this flowrate range. The presence of the gap, however, does affect the overall endwall effectiveness patterns relative to a continuous endwall as previously described by Cardwell et al. [16].

There was a slight effect of the coolant flow rate on the non-dimensional temperature distribution within the gap. Figure 2.16 shows the non-dimensional gap temperature profiles for the three cases as compared to the nominal no-flow case. As compared to the nominal (no gap flow) condition, the gap temperature was equally lower for all values of coolant mass flow between x/L = 0 to x/L = 0.4. As explained previously, the slot transitions from ingesting to ejecting at x/L = 0.4. This was where the effect of increasing gap flow rate was observed. Increasing the mid-passage gap flow rate reduced the temperature measured within the gap for $0.4 < x/L < 1$. For x/L between 0.4 and 1, decreases in gap temperatures were observed for increases in mid-passage gap flow. Note that the ejected fluid was a mixture of ingested upstream slot coolant, ingested main gas, and mid-passage gap coolant.

Figure 2.17 shows thermal field profiles which were taken within the passage for 0% and 0.3% mid-passage gap flow. The measurement plane was located at s/C=0.5, which is illustrated by the red line on Figure 2.1. There was little change in the passage temperature profiles indicating little change in the secondary flows. Again as previously noted when comparing gap temperature profiles, the interaction of the mid-passage gap was only slightly affected by changes in leakage flow and was primarily driven by the endwall static pressure distribution throughout the passage.

Conclusions

Measurements of endwall adiabatic effectiveness and non-dimensional mid-passage gap temperature profiles were presented for a double, nominal, and half-width combustor to turbine interface. Two flow parameters were used to compare the different configurations: mass flow and momentum flux ratios.

When comparing varying slot width while matching mass flow, it was observed that decreasing the slot width caused the coolant to be more evenly distributed on the endwall; however, average effectiveness values for the half slot width decreased slightly. Increasing the slot width while matching mass flow indicated a reduced coverage with no coolant observed on the pressure side of the passage. Moreover, the effectiveness values on the suction side were lower that those observed at the same flow rate for a nominal slot width. This decrease was caused by ingesting hot mainstream gas. Averaged effectiveness values were found to be the lowest for the double slot relative to the nominal and half width.

Matching the slot momentum flux ratios for the three slot widths resulted in endwall contours that looked nominally the same in terms of area coverage. These results indicated that the upstream coolant coverage area was a function of momentum flux ratio, not mass flow rate. The cooling from the upstream slot had a beneficial effect only along the suction side endwall surface. Doubling the slot width resulted in better endwall cooling on the suction side platform and significantly lowered temperatures within the mid-passage gap. Given the same slot momentum flux ratio, halving the slot resulted in less coolant mass flow and higher temperatures within the gap.

With a nominal width, increasing upstream slot cooling resulted in improved endwall adiabatic effectiveness values and lower gap temperatures. Even at 1.0% mass flow, the upstream coolant momentum was still too low to adequately cool the pressure side platform due to the presence of the ingesting mid-passage gap.

Mid-passage gap leakage flows proved to have little effect on endwall adiabatic effectiveness levels, though gap temperatures were lower for increased leakage flows. Since the gap plenum was ingesting, it was at an equilibrium pressure somewhere between the passage inlet static wall pressure, which was higher, and the passage exit static wall pressure, which was lower. By introducing coolant flow to the gap plenum, the temperature of the gap fluid was effectively lowered while the equilibrium pressure

stayed nominally the same. Thus it would require much higher coolant pressure to significantly affect the mid-passage gap velocity distribution.

These results indicate that the leakage through the combustor-turbine interface can provide cooling to the endwall. Since this interface width changes as the turbine and combustor heat up, it is important to account for the associated changes in coolant coverage area and local coolant levels thereby reducing the need for film-cooling on certain areas of the vane-endwall surface.

Acknowledgements

This publication was prepared with the support of the US Department of Energy, Office of Fossil Fuel, and National Energy Technology Laboratory and the South Carolina Institute for Energy Studies (SCIES) University Turbine Systems Research program (UTSR). However, any opinions, findings, conclusions, or recommendations expressed herein are solely those of the authors and do not necessarily reflect the views of the DOE, SCIES, or the UTSR program. The authors would also like to thank Mike Blair (Pratt & Whitney), Ron Bunker (General Electric), and John Weaver (Rolls-Royce) for their input on the modeling of realistic turbine features.

Nomenclature

C true chord of stator vane
Ca axial chord of stator vane
D diameter of film-cooling hole
I average momentum flux ratio, $I = \frac{\rho_c u_c^2}{\rho_\infty U_\infty^2} = \frac{\rho_s (\dot{m}/\rho_s A_s)^2}{\rho_\infty U_\infty^2}$
L length of mid-passage gap
$\dot{m}$ mass flowrate
M average blowing ratio
p static pressure
P vane pitch; hole pitch
Rein Reynolds number,
S span of stator vane
T temperature
X local coordinate along the mid-passage gap
U velocity
s distance along vane from flow stagnation

Greek

η adiabatic effectiveness, $\eta = (T_\infty - T_{aw})/(T_\infty - T_c)$

ρ density
ν kinematic viscosity
θ non-dimensional gap effectiveness, $\theta = (T_\infty - T_G)/(T_\infty - T_c)$

Subscripts
aw adiabatic wall
c coolant conditions
G gap air temperature
in inlet conditions
∞ freestream conditions

References

[1] Blair, M.F., 1974, "An Experimental Study of Heat Transfer and Film-cooling on Large-Scale Turbine Endwall," ASME J of Heat Transfer, vol. 96, pp. 524-529.

[2] Burd, S.W., Satterness, C.J., and Simon, T.W., 2000, "Effects of Slot Bleed Injection Over a Contoured Endwall On Nozzle Guide Vane Cooling Performance: Part II - Thermal Measurements," 2000-GT-200.

[3] Colban, W. F., Thole, K. A., and Zess, G., 2002, "Combustor-Turbine Interface Studies: Part 1: Endwall Measurements," J of Turbomachinery, vol. 125, pp.193- 202.

[4] Colban, W. F., Lethander, A. T., Thole, K. A., and Zess, G., 2002, "Combustor - Turbine Interface Studies: Part 2: Flow and Thermal Field Measurements," J of Turbomachinery, vol. 125, pp.203-209.

[5] Pasinato, H. D., Squires, K. D., and Roy, R. P., 2004, "Measurement and modeling of the flow and heat transfer in a contoured vane-endwall passage," Int. J. of Heat and Mass Transfer, 47 (2004) 5685-5702.

[6] Zhang, L.J., and Jaiswal, R.S., 2001, "Turbine Nozzle Endwall Film-cooling Study Using Pressure Sensitive Paint," J of Turbomachinery, 123, pp. 730-738.

[7] Kost, F. and Nicklas, M., 2001, "Film-Cooled Turbine Endwall in a Transonic Flow Field: Part I – Aerodynamic Measurements," ASME Paper Number 2001-GT-0145.

[8] Nicklas, M., 2001, "Film-Cooled Turbine Endwall in a Transonic Flow Field: Part II–Heat Transfer and Film-Cooling Effectiveness," J. of Turbomachinery, 123, pp.720-729.

[9] Knost, D.G., and Thole, K.A., 2003, "Computational Predictions of Endwall Film-Cooling for a First Stage Vane," GT2003-38252.

[10] Knost, D. G., and Thole, K. A., 2005, "Adiabatic Effectiveness Measurements of Endwall Film- Cooling for a First Stage Vane," Journal of Turbomachinery, vol. 127, pp. 297-305.

[11] Aunapu, N.V., Volino, R.J., Flack, K.A., and Stoddard, R.M., 2000, "Secondary Flow Measurements in a Turbine Passage with Endwall Flow Modification," J of Turbomachinery, 122, pp. 651-658.

[12] Ranson, W., Thole, K. A., and Cunha, F., 2005, "Adiabatic Effectiveness Measurements and Predictions of Leakage Flows along a Blade Endwall," Journal of Turbomachinery, vol. 127, pp. 609-618.

[13] Yamao, H., Aoki, K., Takeishi, K., and Takeda, K., 1987, "An Experimental Study for endwall Cooling Design of Turbine Vanes," IGTC-1987, Tokyo, Japan.

[14] Piggush, J.D., and Simon, T.W., "Flow Measurements in a First Stage Nozzle Cascade having Endwall Contouring, Leakage, and Assembly Features," GT2005-68340.

[15] Piggush, J. D., and Simon, T. W., 2005, "Flow Measurements in a First Stage Nozzle Cascade having Leakage and Assembly Features: Effects of Endwall Steps and Leakage on Aerodynamic Losses," IMCE2005-83032.

[16] Reid, K., Denton, J., Pullan, G., Curtis, E., and Longley, J., "The Interaction of Turbine Inter-Platform Leakage Flow with the Mainstream Flow," GT2005-68151.

[17] Cardwell, N. D., Sundaram, N., and Thole, K. A., "Effects of Mid-Passage Gap, Endwall Misalignment and Roughness on Endwall Film-Cooling," GT2005-68900.

[18] de la Rosa Blanco, E., Hodson, H. P., and Vazquez, R., "Effect of Upstream Platform Geometry on the Endwall Flows of a Turbine Cascade," GT2005-68938.

[19] Radomsky, R. and Thole, K. A., 2002, "Detailed Boundary Layer Measurements on a Turbine Stator Vane at Elevated Freestream Turbulence Levels," Journal of Turbomachinery, vol. 124, pp. 107-118.

[20] Bons, J.P., Taylor, R.P., McClain, S.T., and Rivir, R.B., 2001, "The Many Faces of Turbine Surface Roughness," 2001-GT-0163.

[21] Modest, M. F., 2003, Radiative Heat Transfer, 2nd Edition, pp. 743-758

[22] Ethridge, M. I., Cutbirth, J. M., and Bogard, D. G., 2000, "Scaling of Performance for Varying Density Ratio Coolants on an Airfoil with Strong Curvature and Pressure Gradient Effects," ASME Paper No. 2000-GT-239.

[23] Moffat, R. J., 1988, "Describing the Uncertainties in Experimental Results," Experimental Thermal and Fluid Science, Vol.1, pp. 3-17.

Table 2.1 Geometric and Flow Conditions

Scaling factor	9
Scaled up chord length (C)	59.4 cm
Scaled up axial chord length (C_a)	29.3 cm
Pitch / chord (P/C)	0.77
Span / chord (S/C)	0.93
Re_{in}	2.1×10^5
Inlet and exit angles	0° & 72°
Inlet, exit Mach number	0.017,0.085
Inlet mainstream velocity	6.3 m/s

Table 2.2 Summary of Endwall Geometry

	Parameter	Experimental
Upstream Slot	Nominal slot width	0.024 C
	Double slot flow length to width	0.94
	Nominal slot flow length to width	1.9
	Half slot flow length to width	3.8
	Upstream slot surface angle	45°
Film Cooling	FC hole diameter (cm)	0.46
	FC Hole L/D	8.3
	Film-cooling surface angle	30°

Table 2.3 Upstream Slot Coolant Settings

	% mass flow	M	I
Double Width Slot	0.75%	0.19	0.03
	0.85%	0.22	0.04
	1.00%	0.26	0.06
	1.13%	0.29	0.08
Nominal Slot Width	0.75%	0.29	0.08
	0.85%	0.33	0.10
	1.00%	0.39	0.13
Half Width Slot	0.38%	0.29	0.08
	0.42%	0.32	0.10
	0.75%	0.58	0.30
	0.85%	0.66	0.39

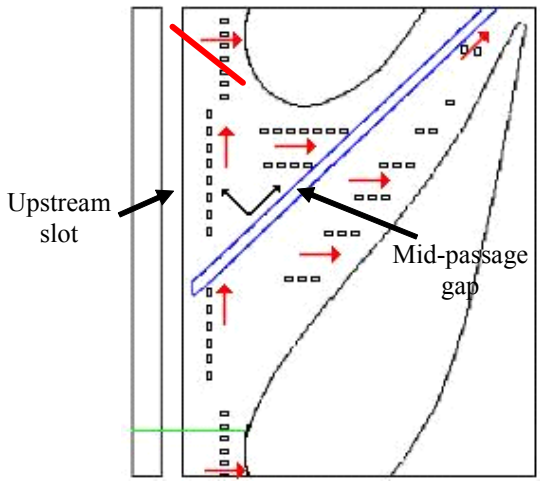

Figure 2.1 Endwall geometry with film-cooling holes, an upstream slot, and a mid-passage gap.

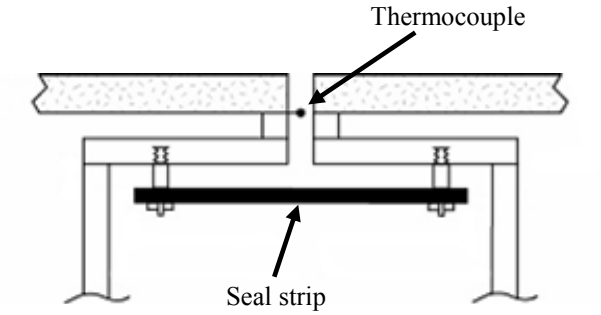

Figure 2.2 Cross section view of the mid-passage gap geometry with accompanying seal strip.

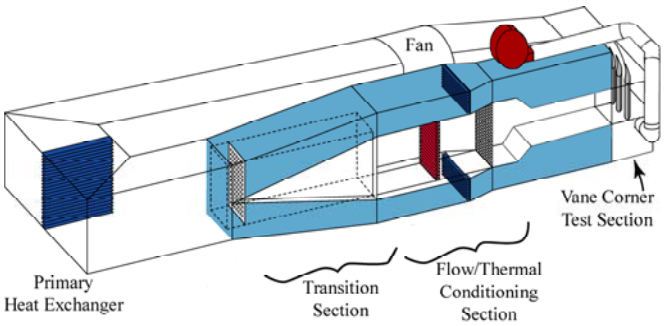

Figure 2.3 Illustration of the wind tunnel facility.

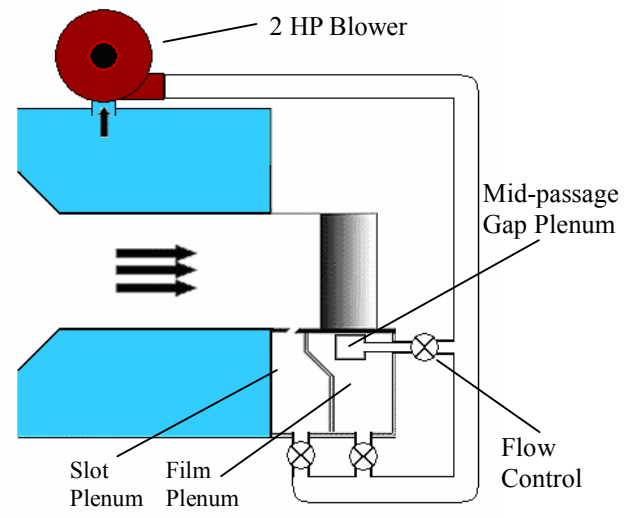

Figure 2.4 Separate plenums for film-cooling, upstream slot, and mid-passage gap provided independent flow control.

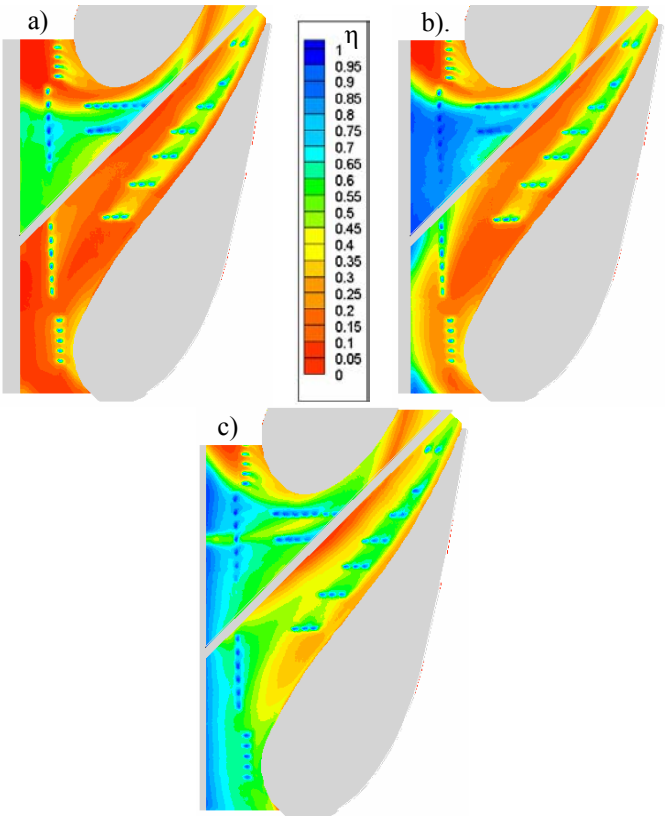

Figure 2.5 Contours of adiabatic effectiveness for a) double, b) nominal c) half width upstream slot with 0.85% slot mass flow ratio.

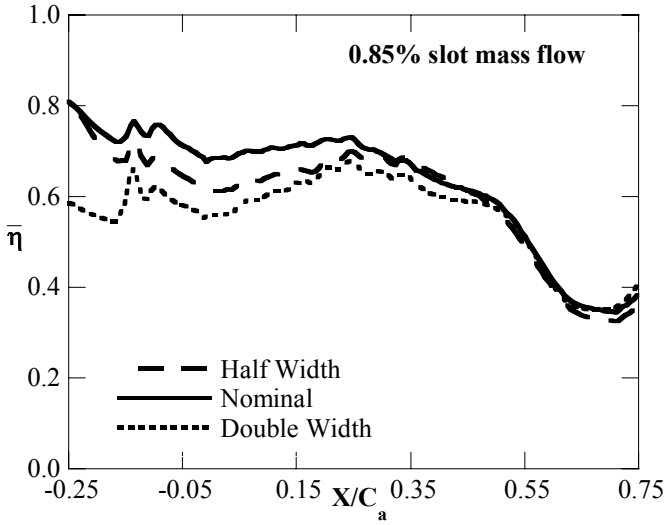

Figure 2.6 Pitchwise averaged adiabatic effectiveness for the entire passage with varied upstream slot widths.

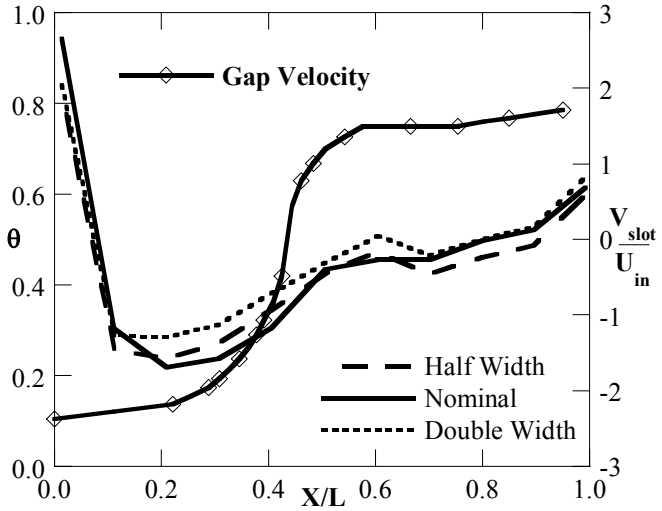

Figure 2.7 Non-dimensionalized mid-passage gap temperature profiles with varied upstream slot widths.

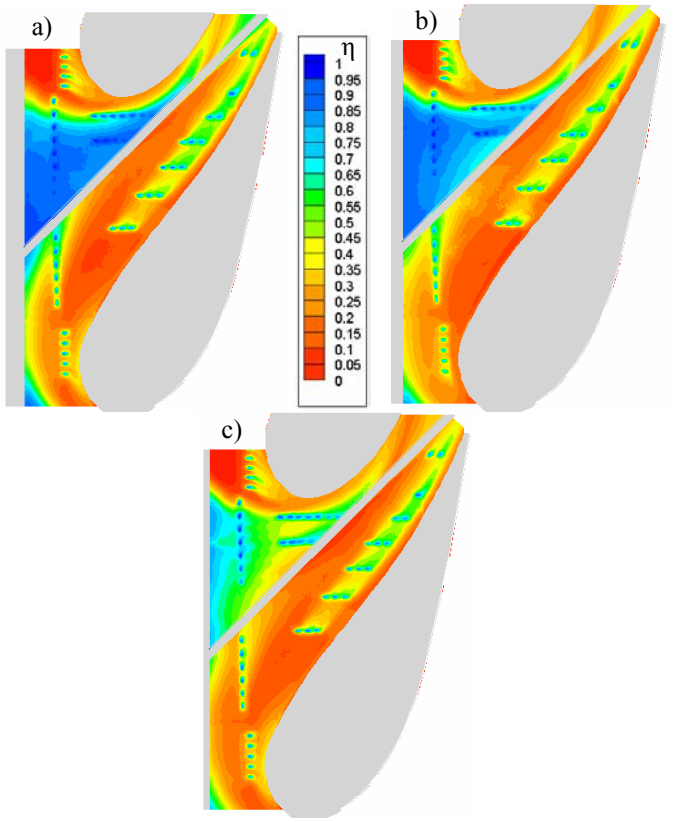

Figure 2.8 Contours of adiabatic effectiveness for a) double, b) nominal c) half-width upstream slot with I = 0.08 average slot momentum flux ratio.

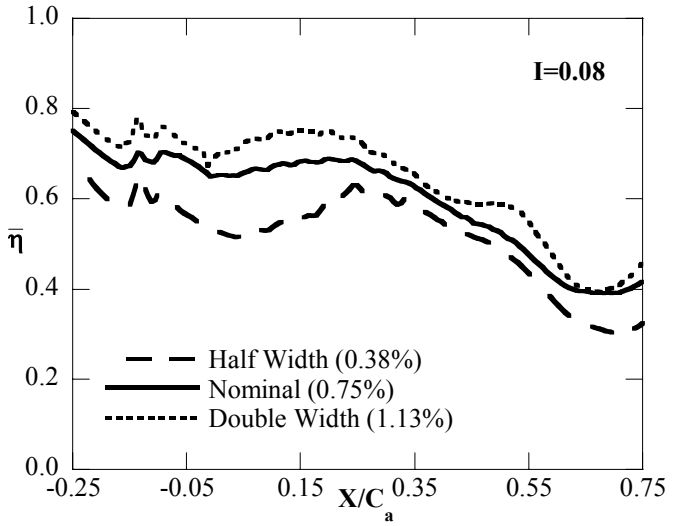

Figure 2.9 Plots of pitchwise averaged adiabatic effectiveness for the entire passage with varied slot widths

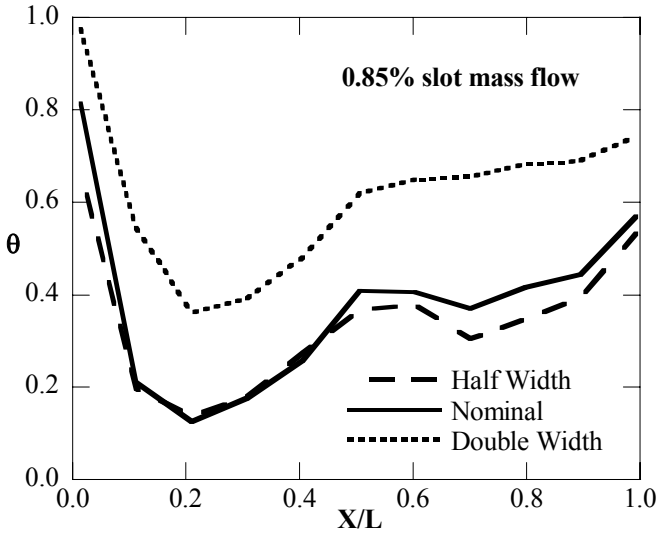

Figure 2.10 Non-dimensionalized mid-passage gap temperature profiles varied upstream slot widths given a nominal slot momentum flux ratio.

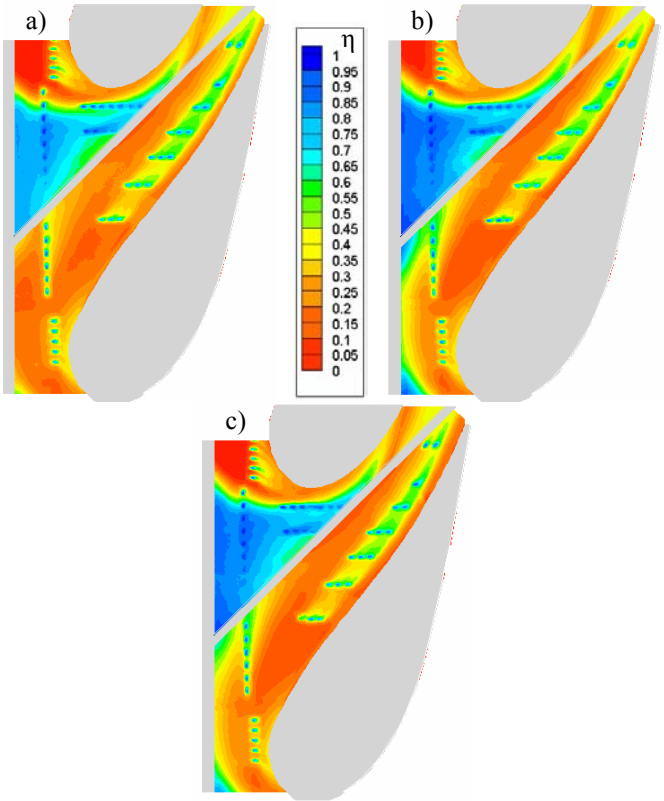

Figure 2.11 Contours of adiabatic effectiveness for a) 0.75%, b) 0.85% c) 1.0% upstream slot mass flow rate for a nominal slot width.

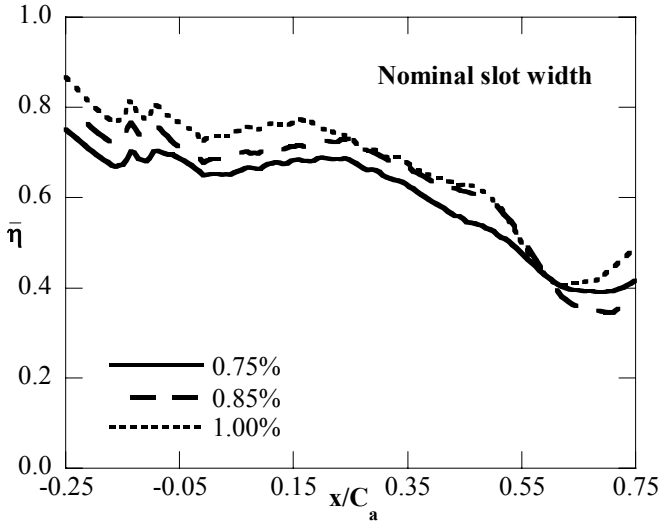

Figure 2.12 Plots of laterally averaged adiabatic effectiveness for the entire passage with varied upstream slot mass flow.

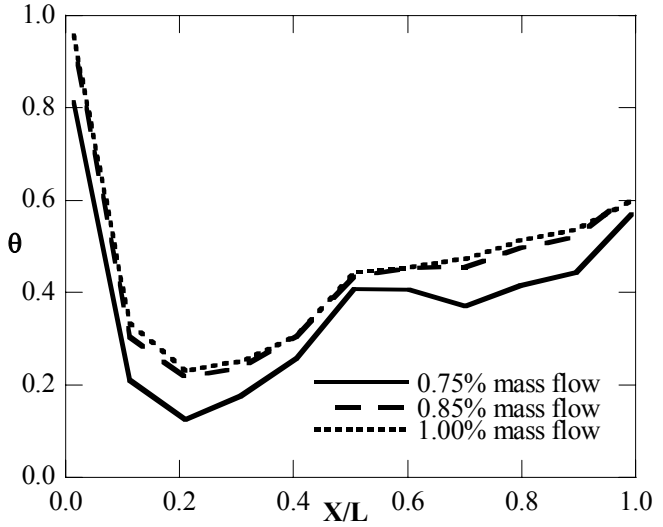

Figure 2.13 Non-dimensionalized mid-passage gap temperature profiles varied upstream slot mass flow.

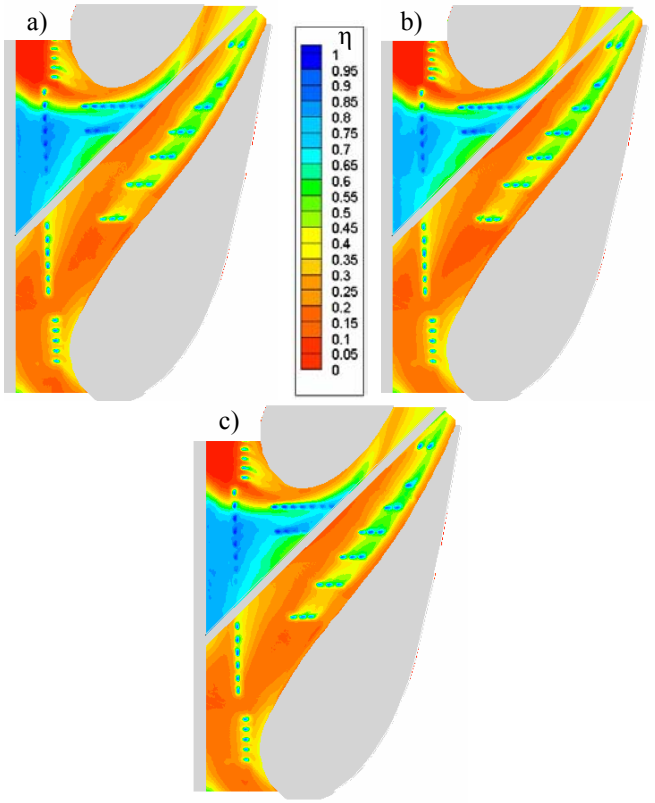

Figure 2.14 Contours of adiabatic effectiveness for a) 0.1%, b) 0.2%, and c) 0.3% mid-passage gap mass flow with nominal upstream slot width.

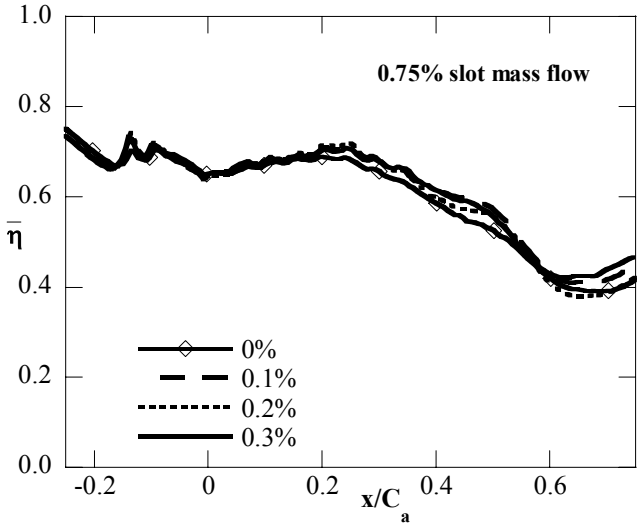

Figure 2.15 Plots of laterally averaged adiabatic effectiveness for the entire passage with varied mid-passage gap cooling.

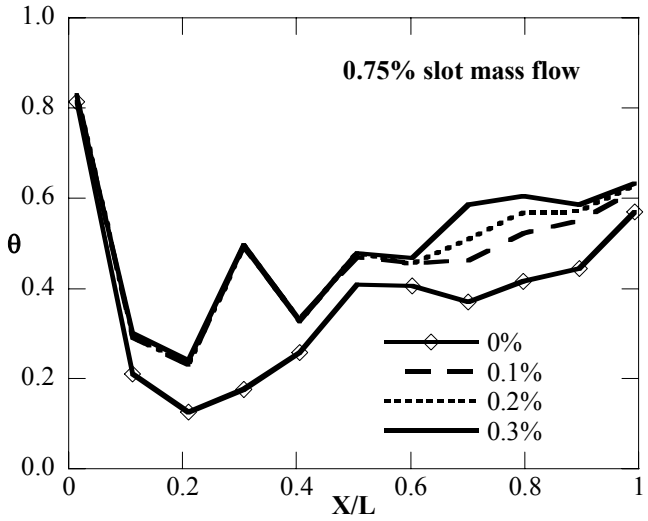

Figure 2.16 Non-dimensionalized mid-passage gap temperature profiles with varied mid-passage gap cooling

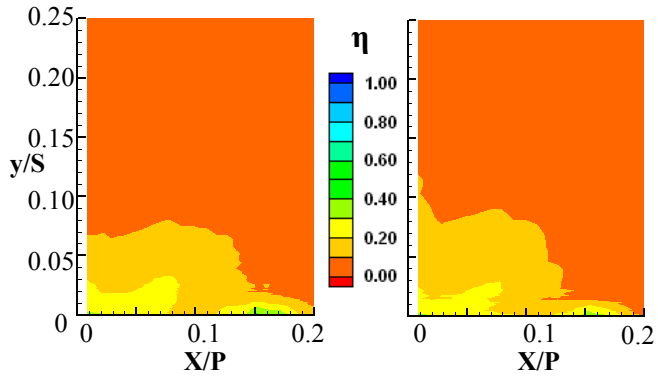

Figure 2.17 Plots of thermal field data for a). 0% flow and b) 0.3% flow within the mid-passage gap.

Appendix A:
Additional Analysis for Paper 1

Given in this appendix is the additional analysis performed for the first paper of this these, entitled *Effects of a Mid-Passage Gap, Endwall Misalignment, and Roughness on Endwall Film-Cooling* [1]. Several of the cases reported in this appendix are repeats of the data already described in the paper, while others are for unique flowrates which were not included due to a space limitation for the paper itself.

A.1 Discussion of Additional Data

Figure A.1a-b shows two identical cases: (a) data presented in the paper without conduction correction (b) the same case analyzed with the conduction correction. For each case taken, a contour plot and lateral average of the endwall is reported (figures A.2 – A.8). The endwall surface was divided along the mid passage gap into two quadrants which correspond to the vane surface of which they are adjacent to the following: pressure side surface (PS) and suction side surface (SS). A complete list of the cases reported in this appendix and their associated flowrates and endwall conditions are shown in Table A.1. It is important to note that the conduction error analysis described in the second paper was applied to all data within the appendices. This is in contrast to the results displayed in Paper 1 which is shown without this analysis due to the fact that it had been submitted to the *Journal of Turbomachinery* before the conduction correction analysis was formulated.

Figure A.9 compares an increase in film-cooling flow given a nominal upstream flowrate which results in a decrease in adiabatic effectiveness for both the SS and PS. As illustrated in the paper, roughness reduces the effectiveness of film-cooling especially at higher coolant mass flowrates. A comparison of varied upstream slot flow for the dam endwall is shown in Figure A.10. Increases of adiabatic effectiveness were observed even when the coolant had to traverse up and over the misaligned endwall surface. For a cascade endwall surface, Figure A.11 shows a greater increase in cooling effectiveness on the suction side surface for roughly the same increase in upstream slot cooling. This is

due to the fact that the coolant exiting the upstream slot can flow unobstructed onto the SS endwall surface. Figure A.12 compares all three alignment modes for nominally the same coolant flowrates. The best performing alignment mode for the SS surface is the cascade setting, and the worst performing is the dam setting.

References

[1] Cardwell, N. D., Sundaram, N., and Thole, K. A., "Effects of Mid-Passage Gap, Endwall Misalignment and Roughness on Endwall Film-Cooling," GT2005-68900. (to appear in the Journal of Turbomachinery)

Table A.1 Endwall and Flow Conditions

Case #	Platform	Upstream Slot	Film-Cooling	Roughness Level
1	Aligned	0.75%	0.5%	36 grit
2	Aligned	0.75%	0.75%	36 grit
3	Dam	0.75%	0.5%	36 grit
4	Dam	0.95%	0.5%	36 grit
5	Dam	1.0%	0.5%	36 grit
6	Cascade	0.75%	0.5%	36 grit
7	Cascade	1.1%	0.50%	36 grit

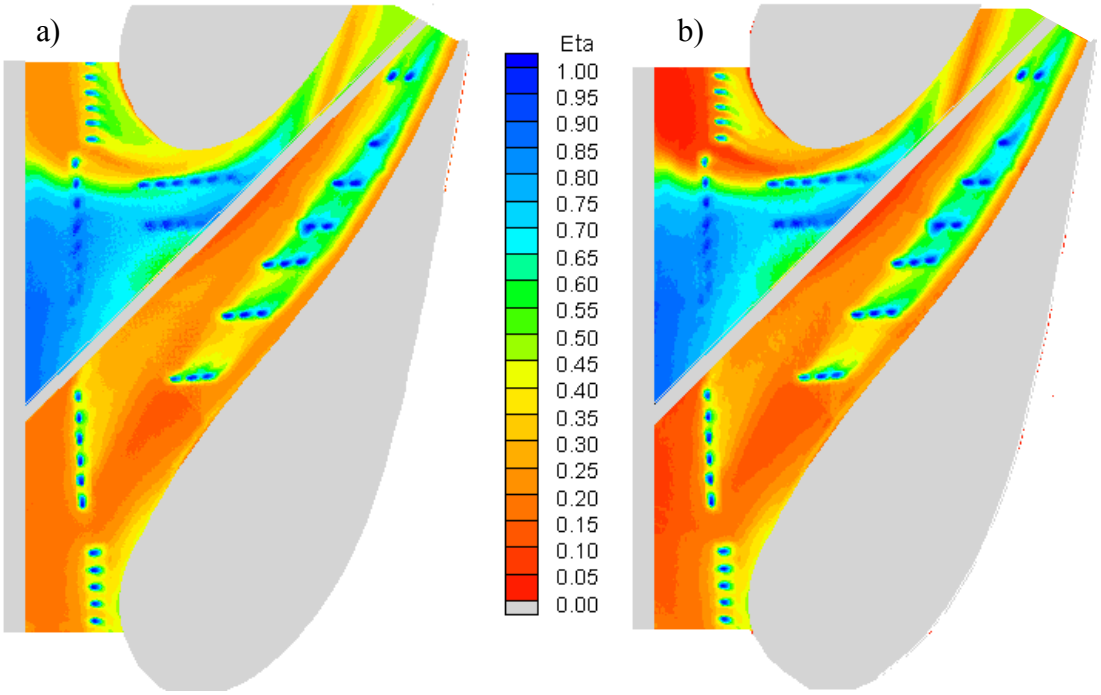

Figure A.1a-b Comparison (a) without conduction correction (b) with conduction correction for an aligned platform with 0.75% upstream slot, 0.5% film-cooling, a rough endwall surface. (Case #1)

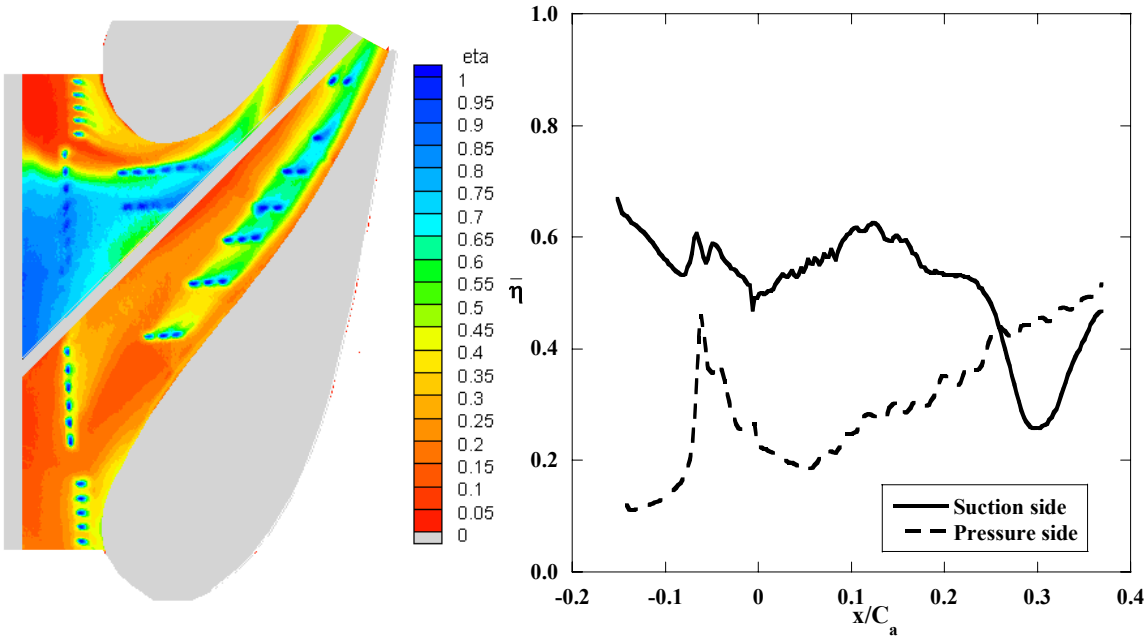

Figure A.2a-b Contour plot and pitchwise averaged plot of adiabatic effectiveness for an aligned platform with 0.75% upstream slot, 0.5% film-cooling, a rough endwall surface. (Case#1)

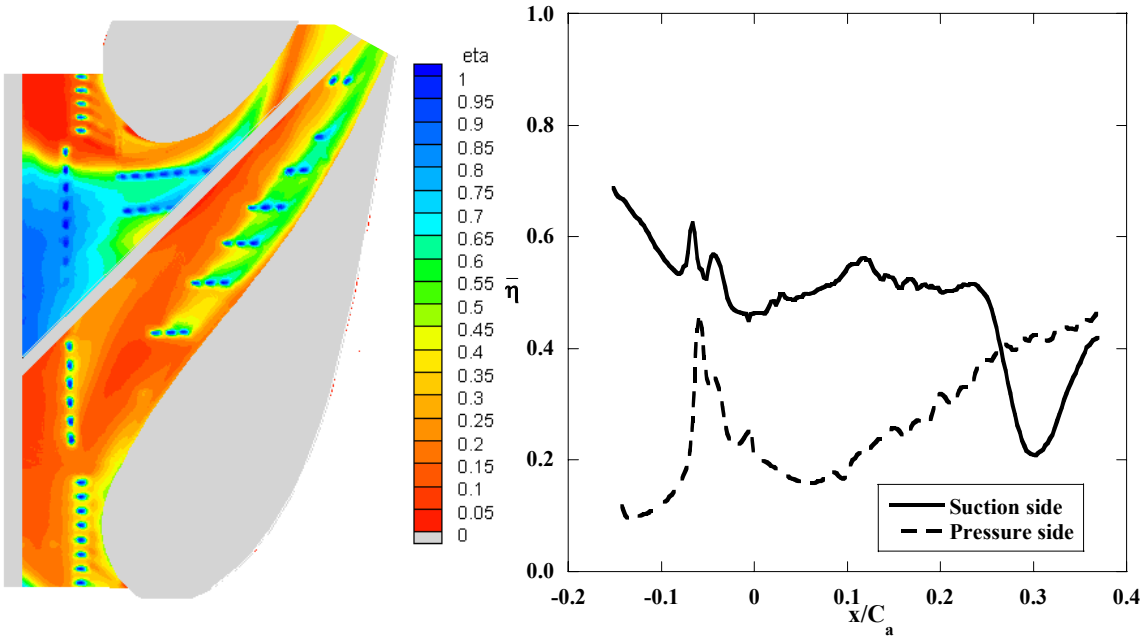

Figure A.3a-b Contour plot and pitchwise averaged plot of adiabatic effectiveness for an aligned platform with 0.75% upstream slot, 0.75% film-cooling, a rough endwall surface. (Case#2)

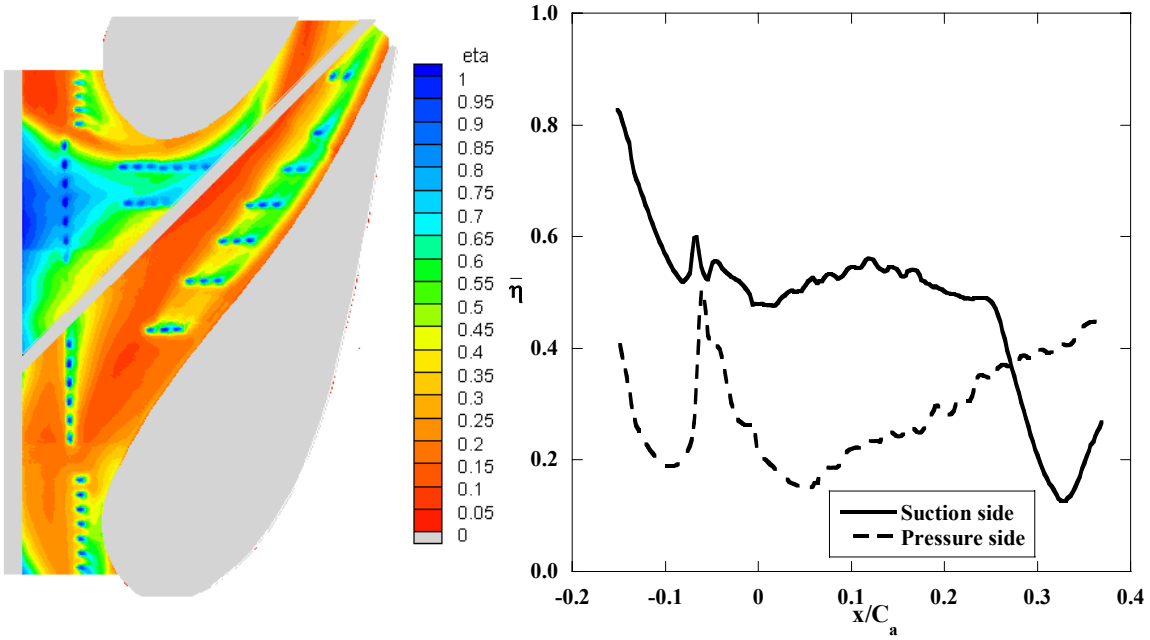

Figure A.4a-b Contour plot and pitchwise averaged plot of adiabatic effectiveness for a dam platform with 0.75% upstream slot, 0.5% film-cooling, a rough endwall surface. (Case#3)

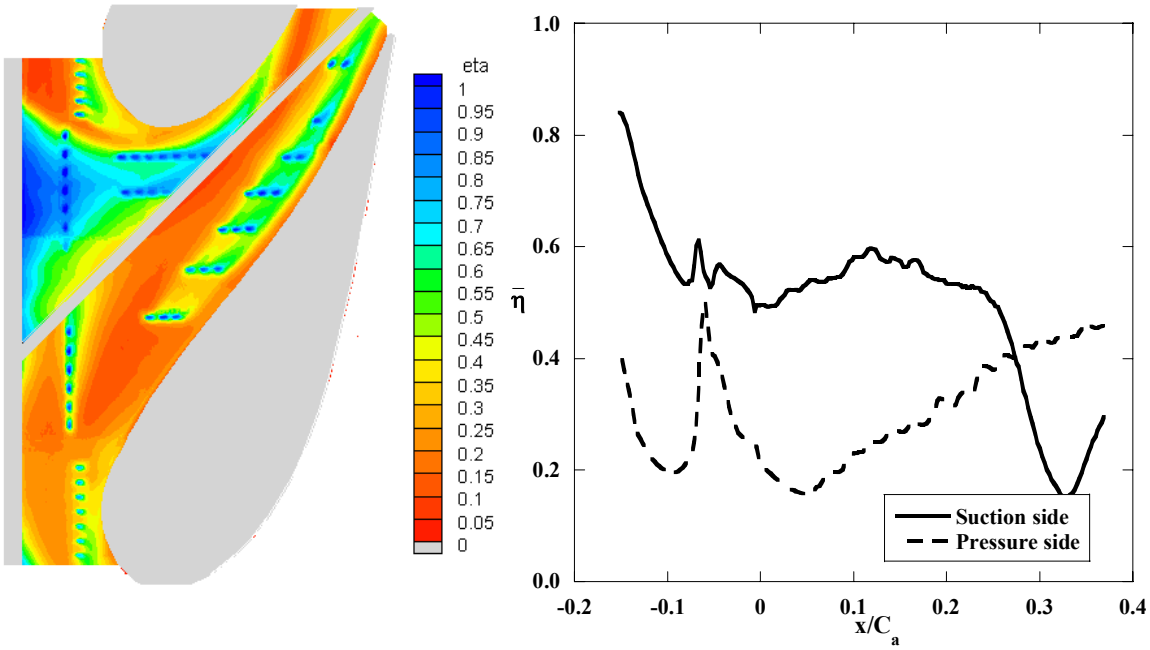

Figure A.5a-b Contour plot and pitchwise averaged plot of adiabatic effectiveness for a dam platform with 0.95% upstream slot, 0.5% film-cooling, a rough endwall surface. (Case#4)

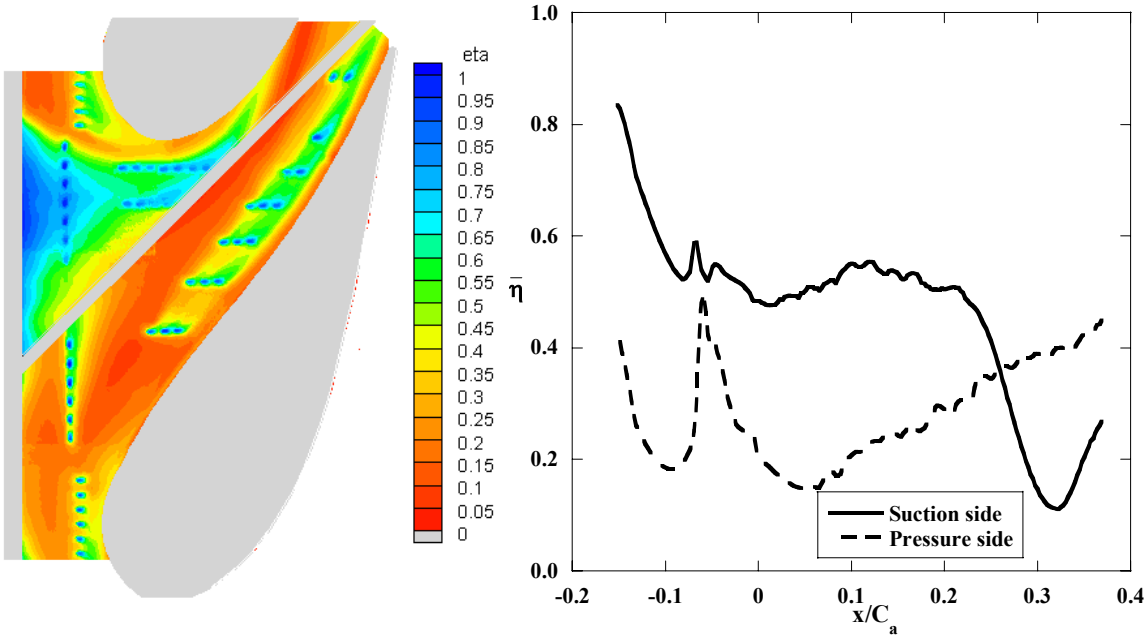

Figure A.6a-b Contour plot and pitchwise averaged plot of adiabatic effectiveness for a dam platform with 1.0% upstream slot, 0.5% film-cooling, a rough endwall surface. (Case#5)

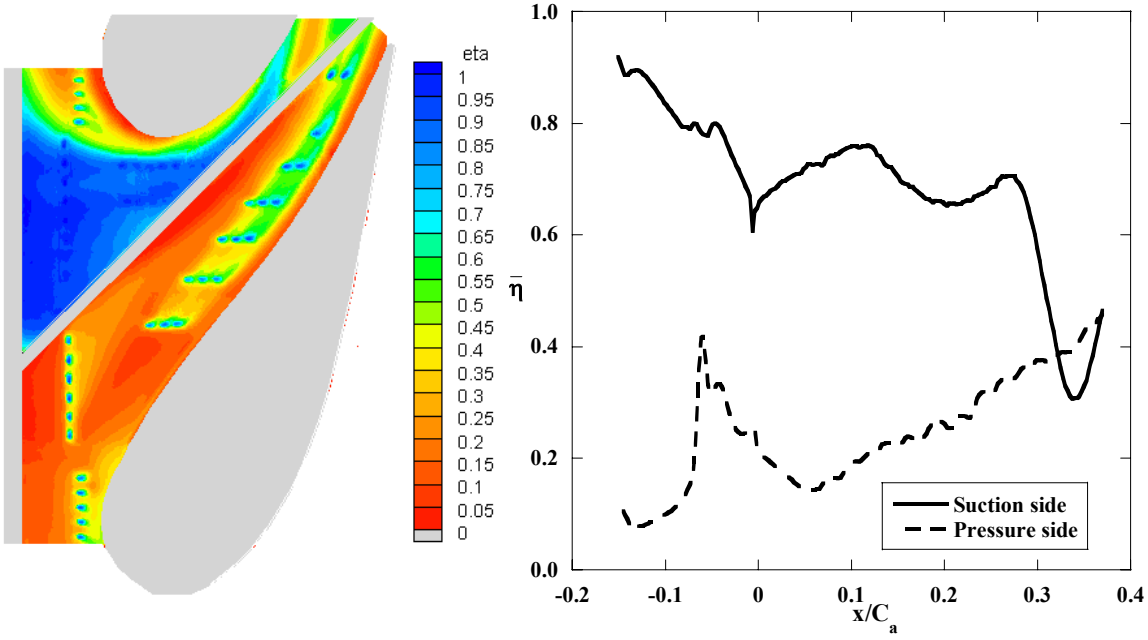

Figure A.7a-b Contour plot and pitchwise averaged plot of adiabatic effectiveness for a cascade platform with 0.75% upstream slot, 0.5% film-cooling, a rough endwall surface. (Case#6)

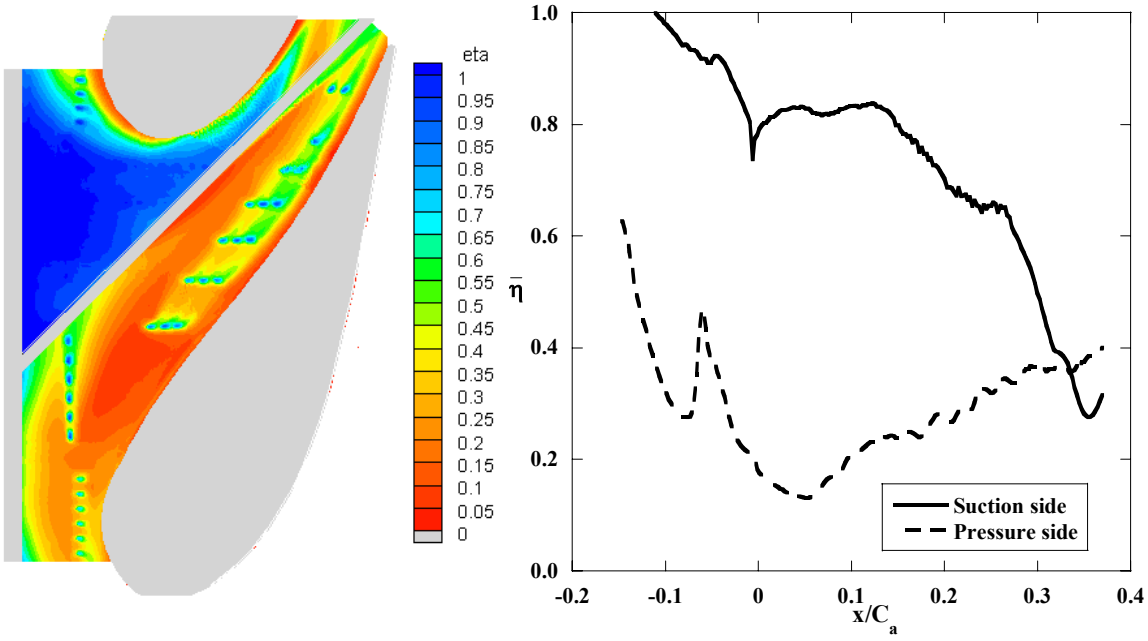

Figure A.8a-b Contour plot and pitchwise averaged plot of adiabatic effectiveness for a cascade platform with 1.1% upstream slot, 0.5% film-cooling, a rough endwall surface. (Case#7)

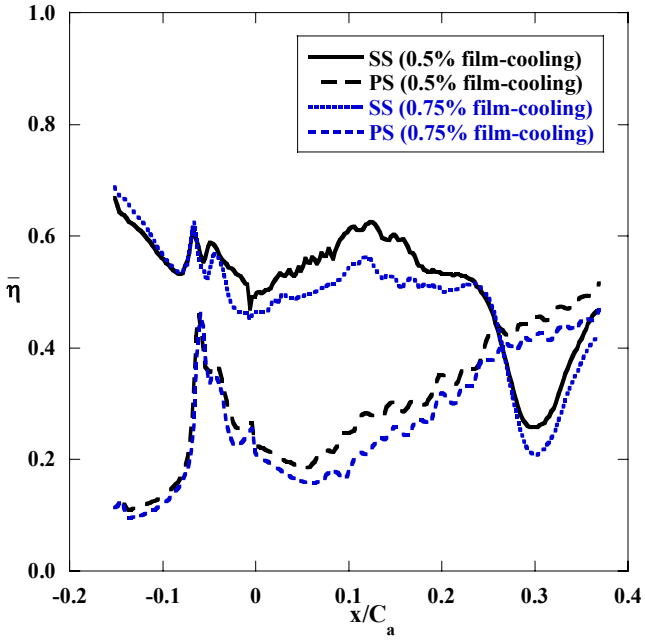

Figure A.9 Comparison of pitchwise averaged adiabatic effectiveness for an aligned platform with 0.75% upstream slot, 0.5% & 0.75% film-cooling, a rough endwall surface. (Cases#1, 2)

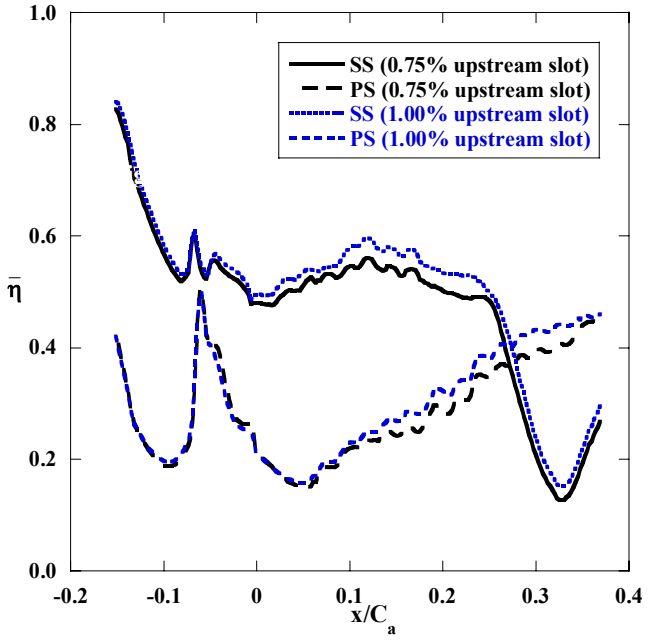

Figure A.10 Comparison of pitchwise averaged adiabatic effectiveness for a dam platform with 0.75% & 1.0% upstream slot, 0.5% film-cooling, a rough endwall surface. (Cases#3, 4, 5)

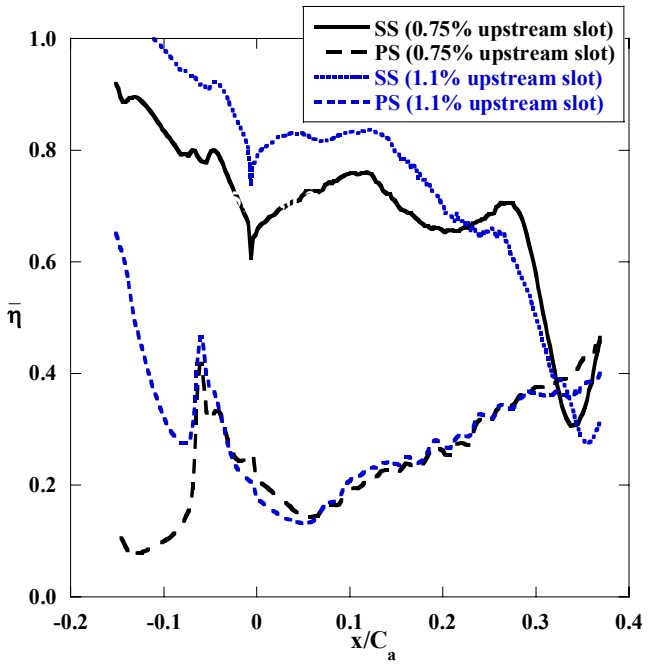

Figure A.11 Comparison of pitchwise averaged adiabatic effectiveness for a cascade platform with 0.75% & 1.1% upstream slot, 0.5% film-cooling, a rough endwall surface. (Cases#6, 7)

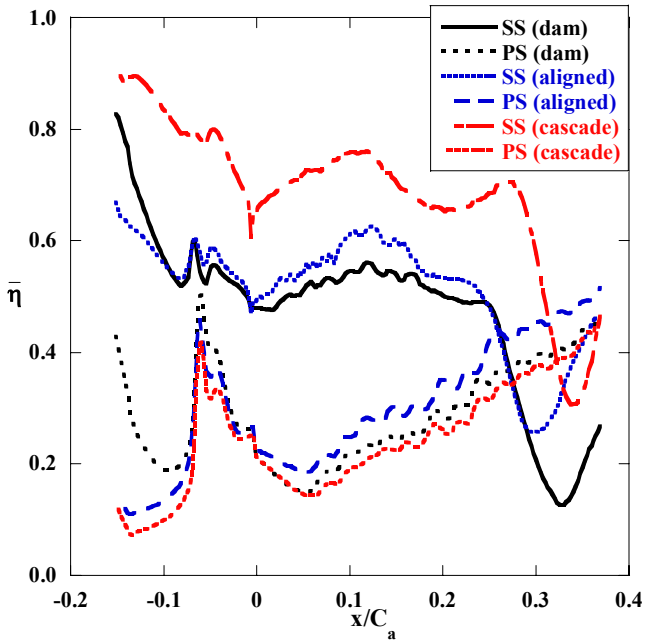

Figure A.12 Comparison of pitchwise averaged adiabatic effectiveness for a dam, aligned and cascade platform with 0.75% upstream slot, 0.5% film-cooling, a rough endwall surface. (Cases#1, 3, 6)

Appendix B:
Additional Analysis for Paper 2

Given in this appendix is the additional analysis performed for the second paper of this these, entitled *The Effects of Varying the Combustor-Turbine Gap* [1]. Several of the cases reported in this appendix are repeats of the data already described in the paper, while others are for unique flowrates which were not included due to a space limitation for the paper itself.

B.1 Discussion of Additional Data

For each case taken, a contour plot and lateral average of the endwall is reported (Figures B.1 – B.17). The endwall surface was divided along the mid passage gap into two quadrants which correspond to the vane surface of which they are adjacent to the following: pressure side surface (PS) and suction side surface (SS). A complete list of the cases reported in this appendix and their associated flowrates and endwall conditions are shown in Table B.1. It is important to note that the conduction error analysis described in the second paper was applied to all data within the appendices.

Figures B.18a-b and B.19a-b show that, for a nominal upstream slot mass flowrate, averaged adiabatic effectiveness levels on the PS surface increase dramatically when the slot width is halved, especially at the highest mass flowrate of 1%. Matching momentum flux ratio of I=0.10 for the upstream slot is shown in Figure B.20a-b. As reported in the paper for I=0.08, this results in a matched coolant velocity profile with mass flowrate varying with slot metering width, thus explaining the increase in averaged adiabatic effectiveness levels for the double width slot. Figures B.21a-b and B.22a-b compare average effectiveness levels for varying upstream slot mass flowrate given a half and double slot width, respectively. As with the nominal slot width, increasing upstream slot mass flowrate results in higher averaged effectiveness levels on both the PS and SS endwall surfaces.

References

[1] Cardwell, N. D., Sundaram, N., and Thole, K. A., "The Effects of Varying the Combustor-Turbine Gap", GT2005-90089.

Table B.1 Endwall and Flow Conditions

Case #	Upstream Slot Width	Upstream Slot Mass Flowrate	Upstream Slot Momentum Flux (I)	Film-Cooling
1	Nominal	0.75%	0.08	0.50%
2	Nominal	0.75%	0.08	0.75%
3	Nominal	0.85%	0.10	0.50%
4	Nominal	1.00%	0.13	0.50%
5	Nominal	0.75%	0.08	0.50%
6	Nominal	0.75%	0.08	0.50%
7	Nominal	0.75%	0.08	0.50%
8	Half	0.38%	0.08	0.50%
9	Half	0.43%	0.10	0.50%
10	Half	0.75%	0.30	0.50%
11	Half	0.85%	0.39	0.50%
12	Half	1.00%	0.54	0.50%
13	Double	0.75%	0.03	0.50%
14	Double	0.85%	0.04	0.50%
15	Double	1.00%	0.06	0.50%
16	Double	1.13%	0.08	0.50%
17	Double	1.25%	0.10	0.50%

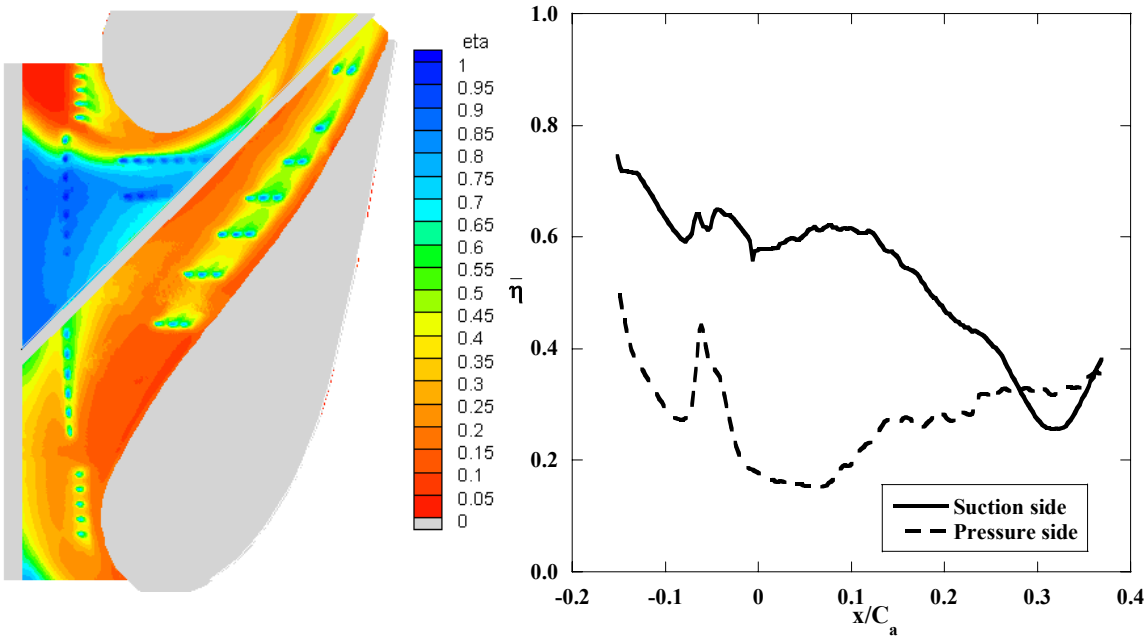

Figure B.1a-b Contour plot and pitchwise averaged plot of adiabatic effectiveness for nominal slot width with 0.75% upstream slot, 0.5% film-cooling, and no net mid-passage gap flow (Case #1).

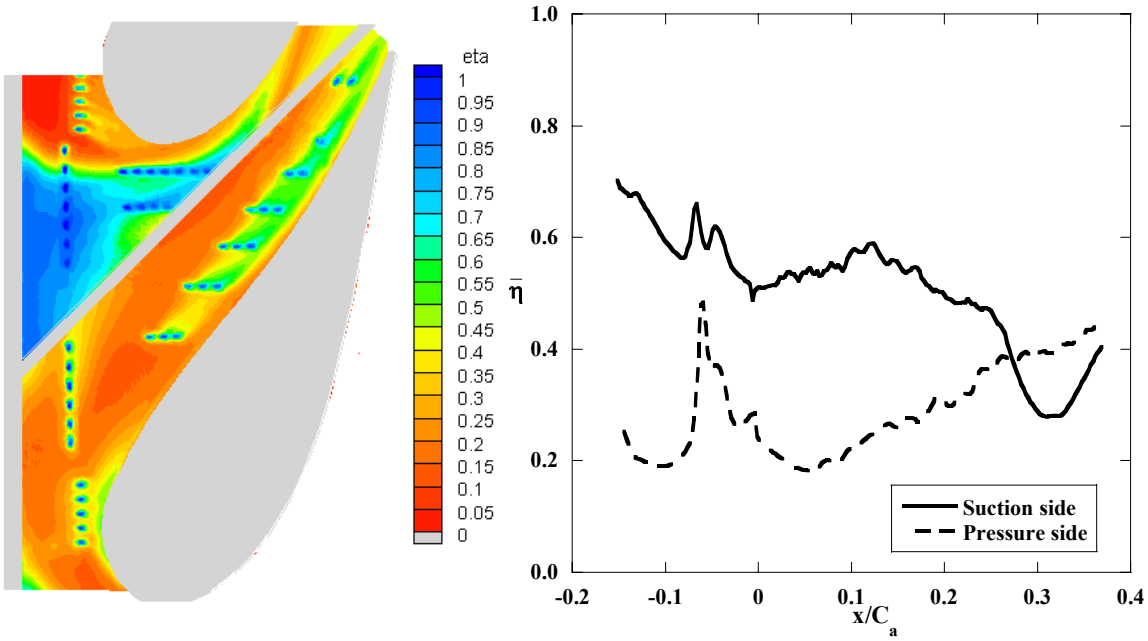

Figure B.2a-b Contour plot and pitchwise averaged plot of adiabatic effectiveness for nominal slot width with 0.75% upstream slot, 0.75% film-cooling, and no net mid-passage gap flow (Case #2).

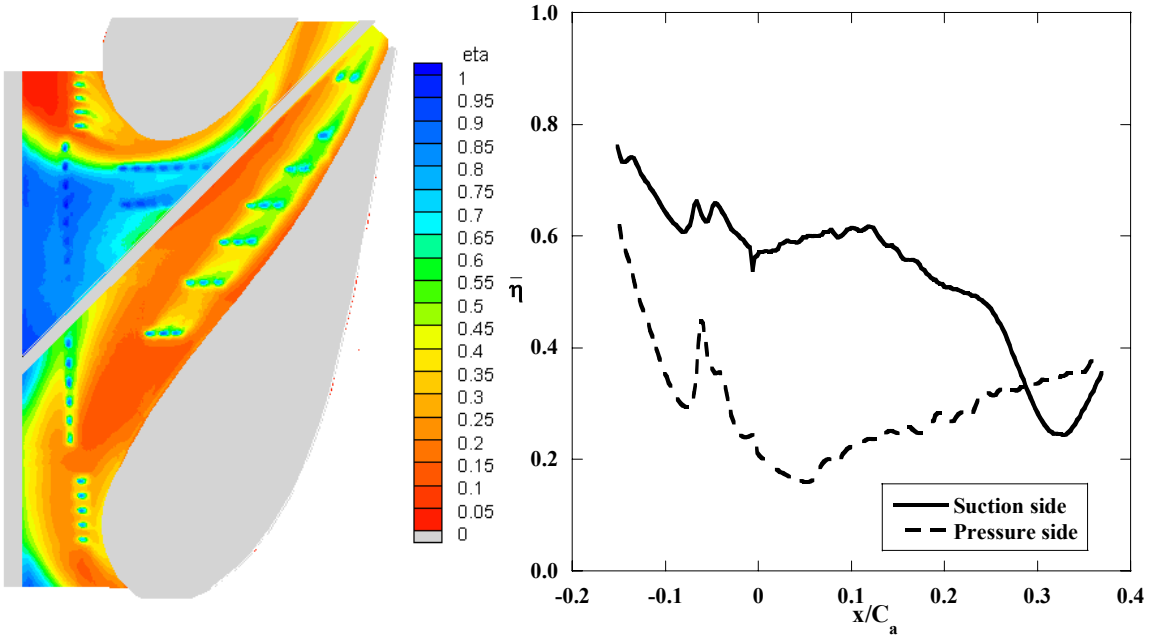

Figure B.3a-b Contour plot and pitchwise averaged plot of adiabatic effectiveness for nominal slot width with 0.85% upstream slot, 0.5% film-cooling, and no net mid-passage gap flow (Case #3).

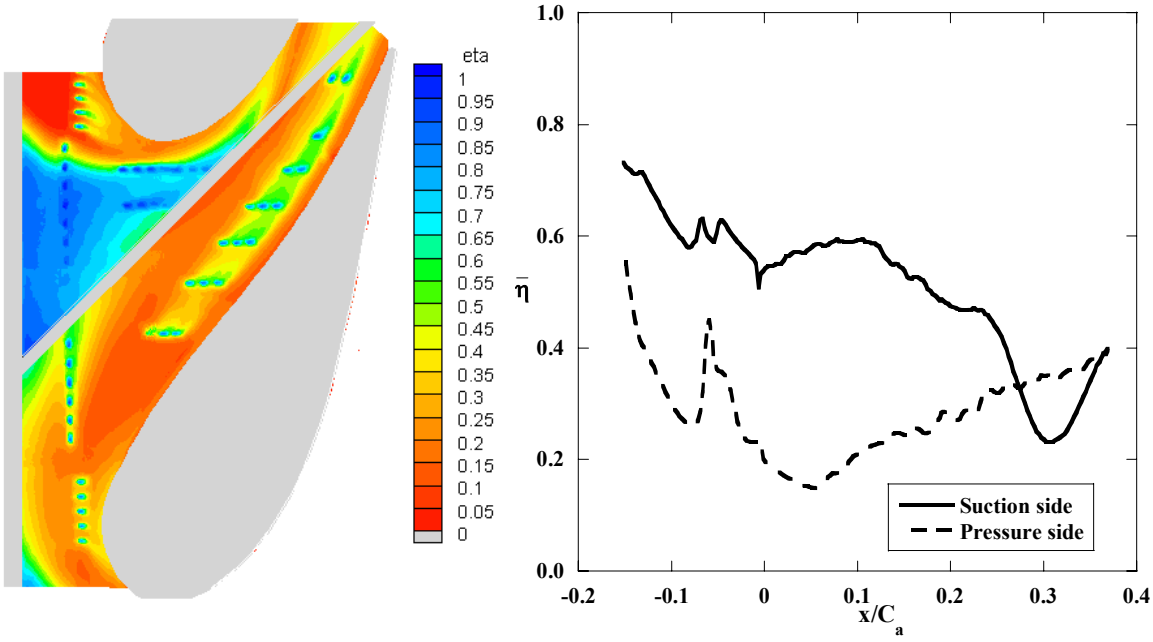

Figure B.4a-b Contour plot and pitchwise averaged plot of adiabatic effectiveness for nominal slot width with 1.0% upstream slot, 0.5% film-cooling, and no net mid-passage gap flow (Case #4).

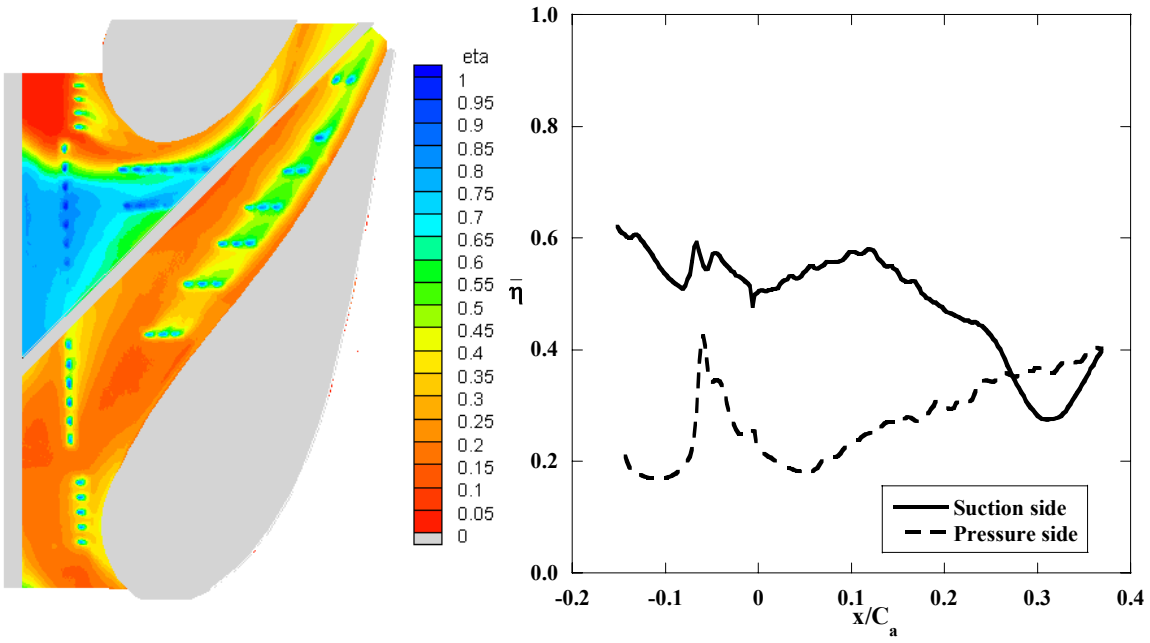

Figure B.5a-b Contour plot and pitchwise averaged plot of adiabatic effectiveness for nominal slot width with 0.75% upstream slot, 0.5% film-cooling, and 0.1% net mid-passage gap flow (Case #5).

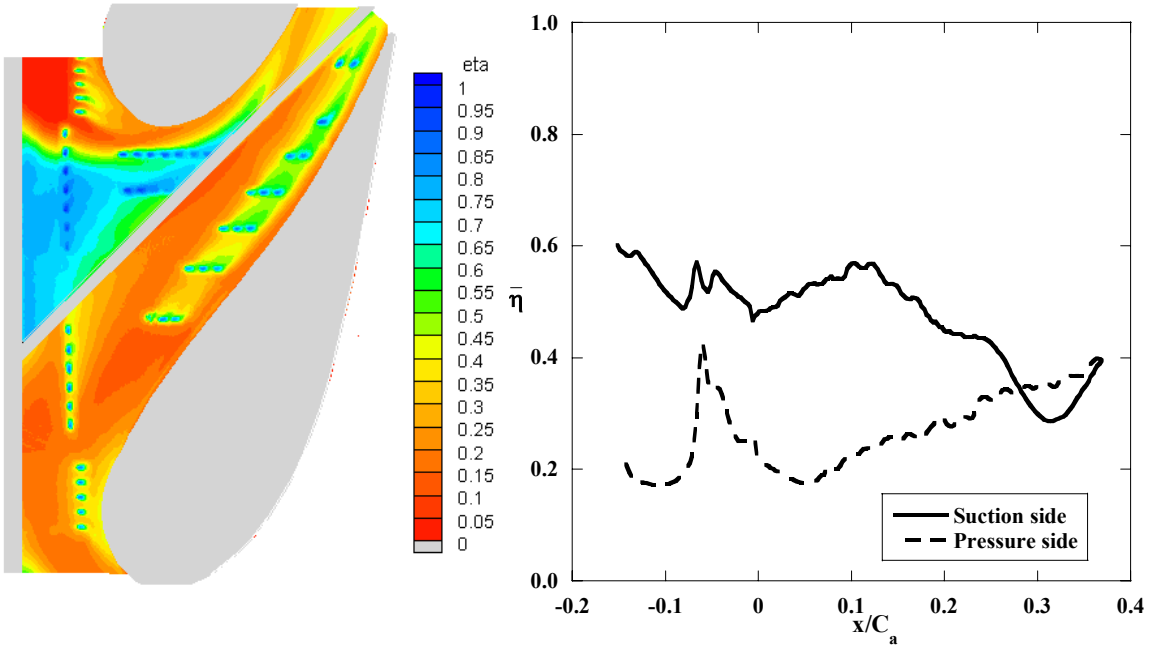

Figure B.6a-b Contour plot and pitchwise averaged plot of adiabatic effectiveness for nominal slot width with 0.75% upstream slot, 0.5% film-cooling, and 0.2% net mid-passage gap flow (Case #6).

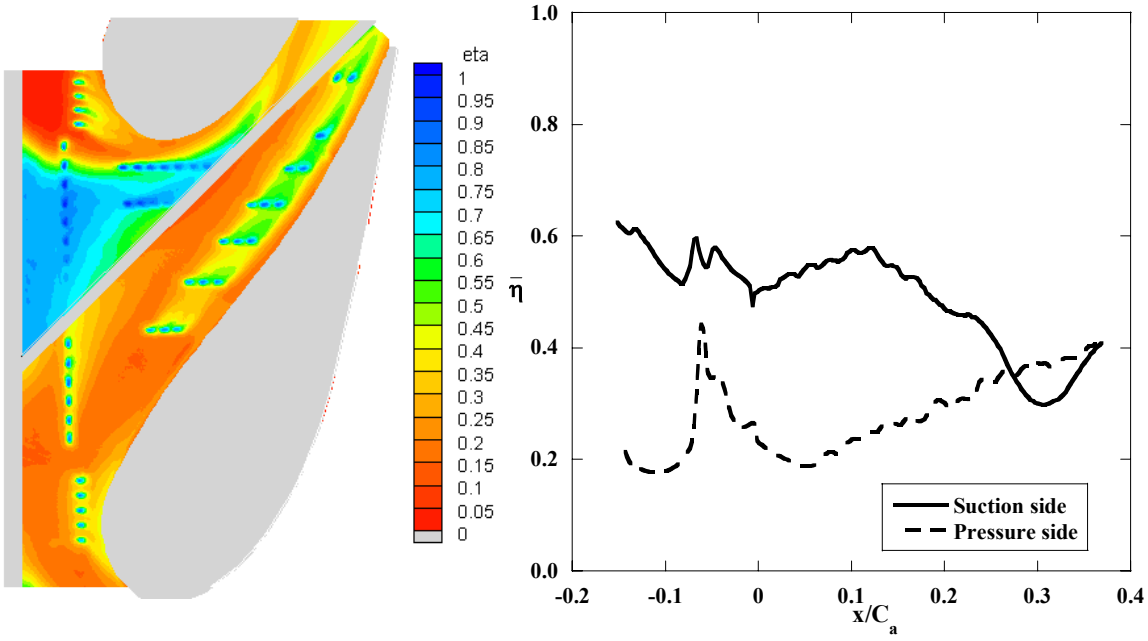

Figure B.7a-b Contour plot and pitchwise averaged plot of adiabatic effectiveness for nominal slot width with 0.75% upstream slot, 0.5% film-cooling, and 0.3% net mid-passage gap flow (Case #7).

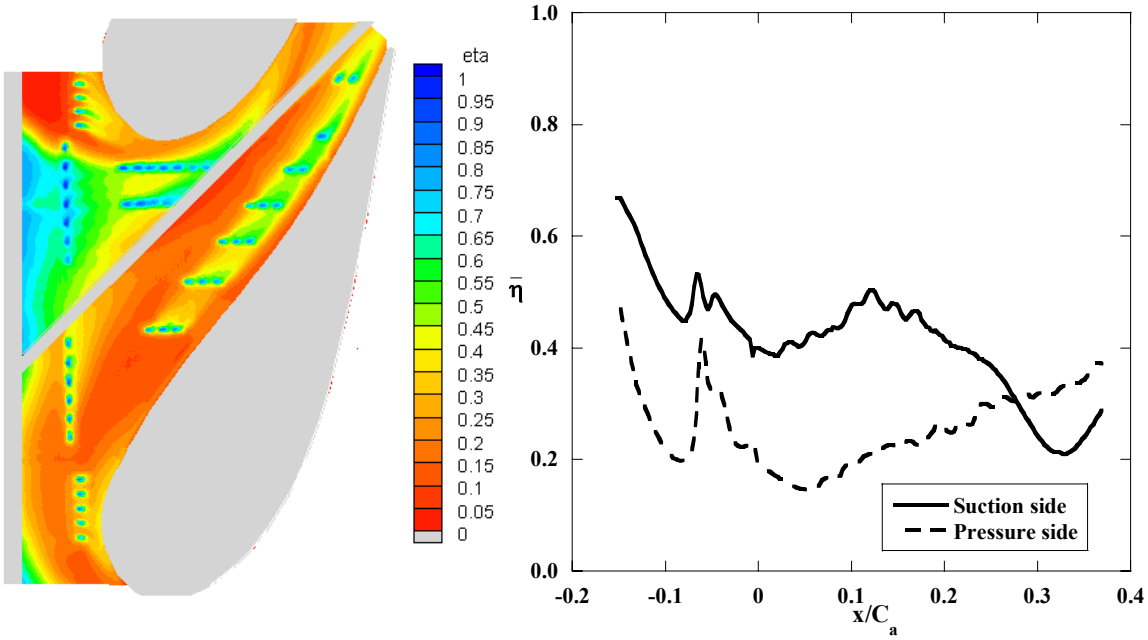

Figure B.8a-b Contour plot and pitchwise averaged plot of adiabatic effectiveness for a half-width slot with 0.38% upstream slot (I=0.08), 0.5% film-cooling, and no net mid-passage gap flow (Case #8).

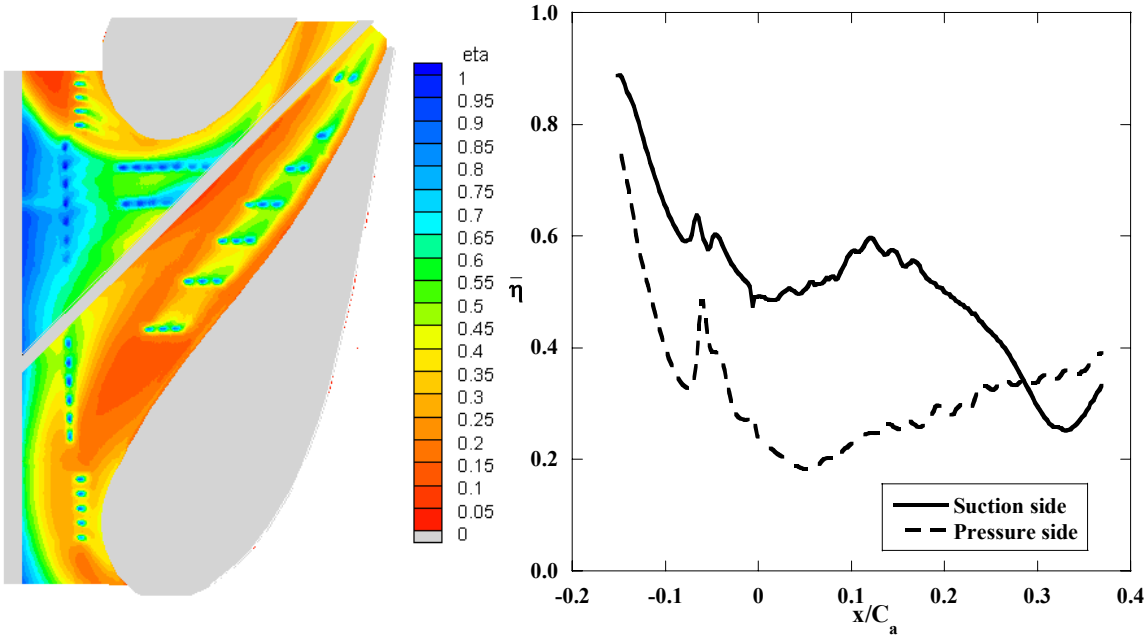

Figure B.9a-b Contour plot and pitchwise averaged plot of adiabatic effectiveness for a half-width slot with 0.43% upstream slot (I=0.10), 0.5% film-cooling, and no net mid-passage gap flow (Case #9).

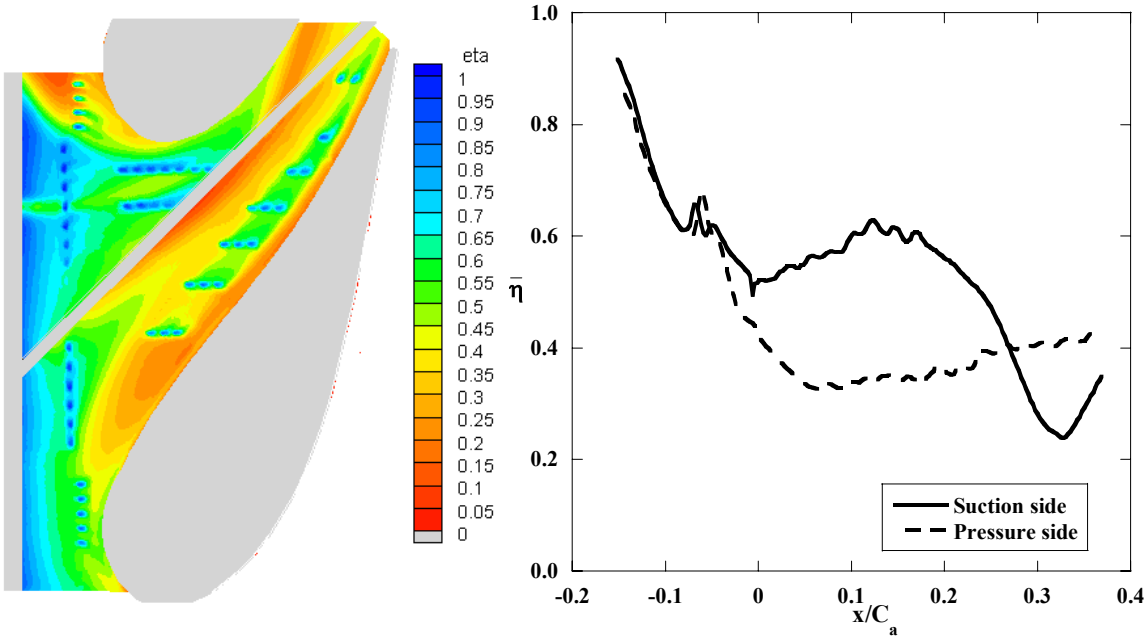

Figure B.10a-b Contour plot and pitchwise averaged plot of adiabatic effectiveness for a half-width slot with 0.75% upstream slot, 0.5% film-cooling, and no net mid-passage gap flow (Case #10).

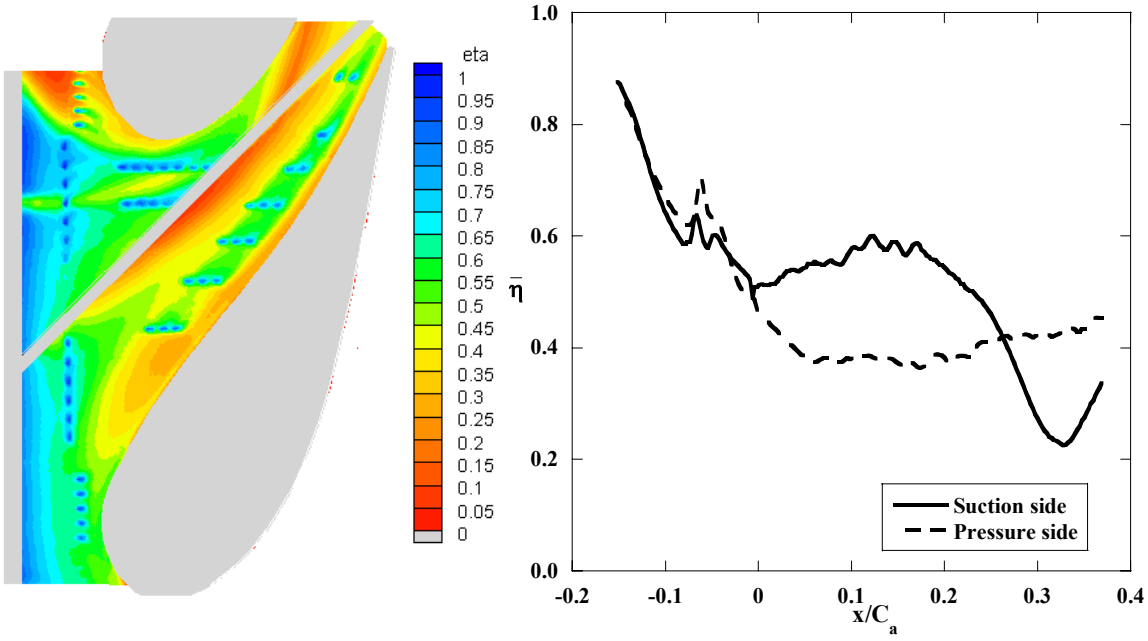

Figure B.11a-b Contour plot and pitchwise averaged plot of adiabatic effectiveness for a half-width slot with 0.85% upstream slot, 0.5% film-cooling, and no net mid-passage gap flow (Case #11).

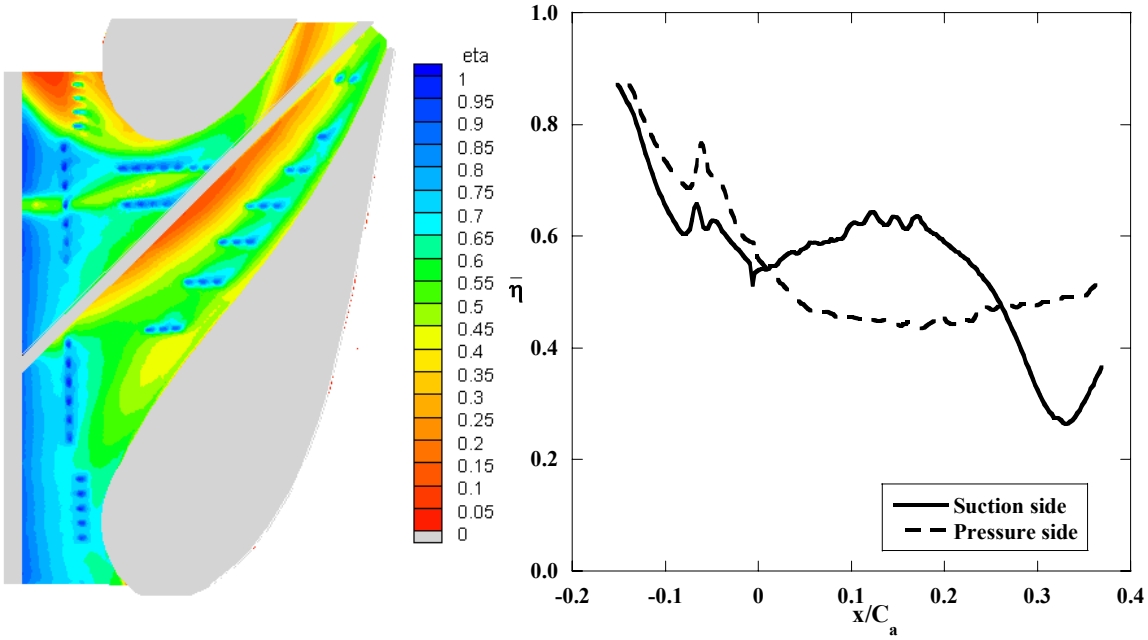

Figure B.12a-b Contour plot and pitchwise averaged plot of adiabatic effectiveness for a half-width slot with 1.0% upstream slot, 0.5% film-cooling, and no net mid-passage gap flow (Case #12).

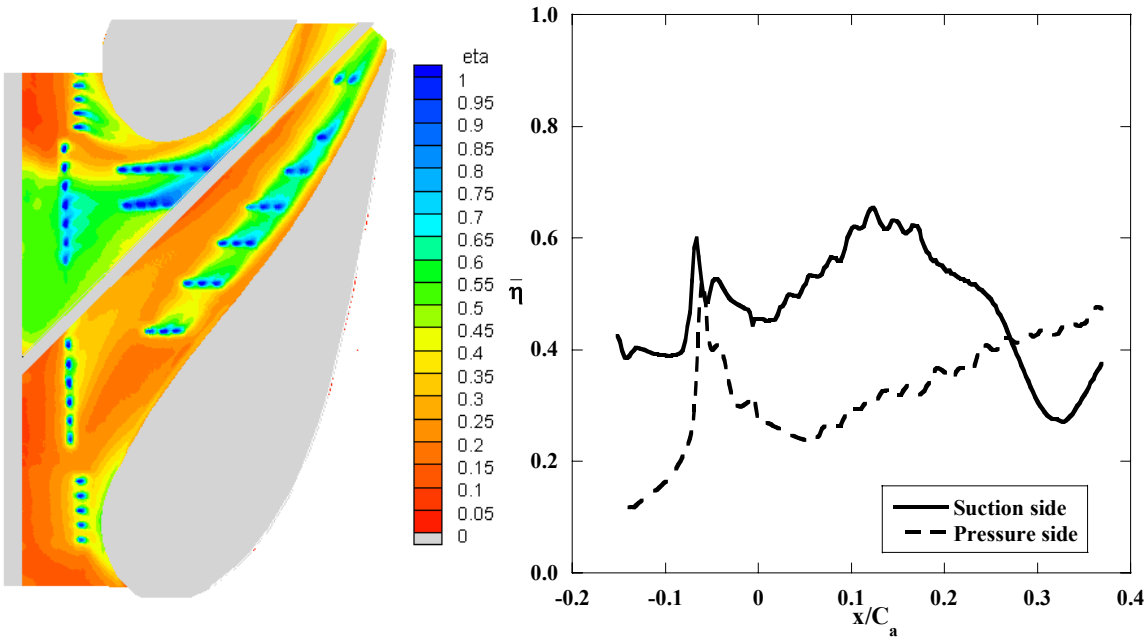

Figure B.13a-b Contour plot and pitchwise averaged plot of adiabatic effectiveness for a double-width slot with 0.75% upstream slot, 0.5% film-cooling, and no net mid-passage gap flow (Case #13).

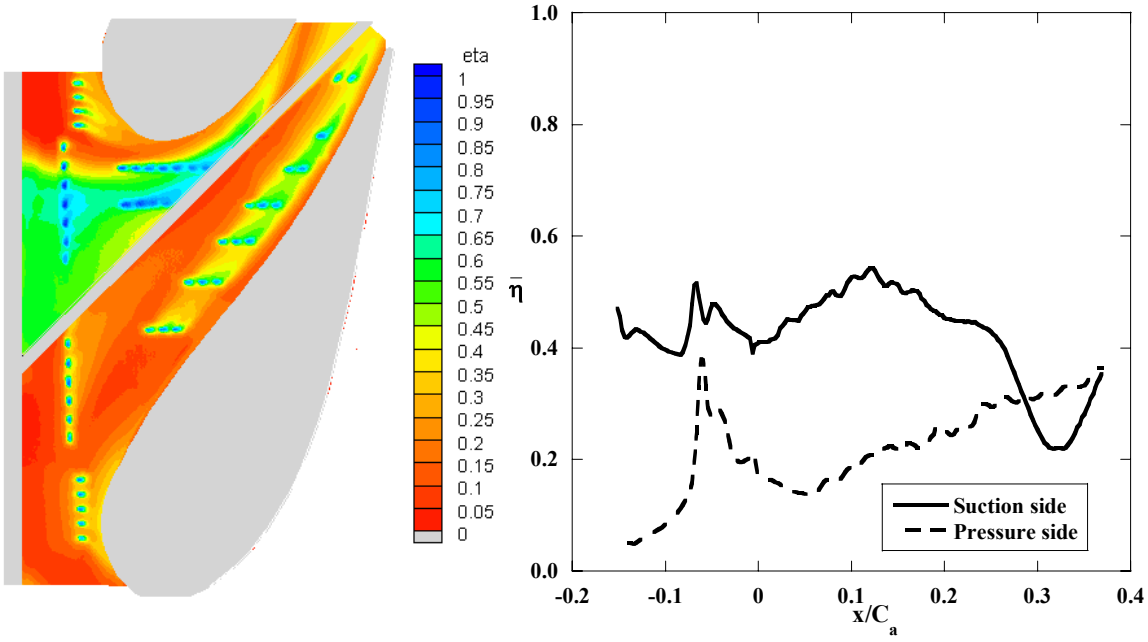

Figure B.14a-b Contour plot and pitchwise averaged plot of adiabatic effectiveness for a double-width slot with 0.85% upstream slot, 0.5% film-cooling, and no net mid-passage gap flow (Case #14).

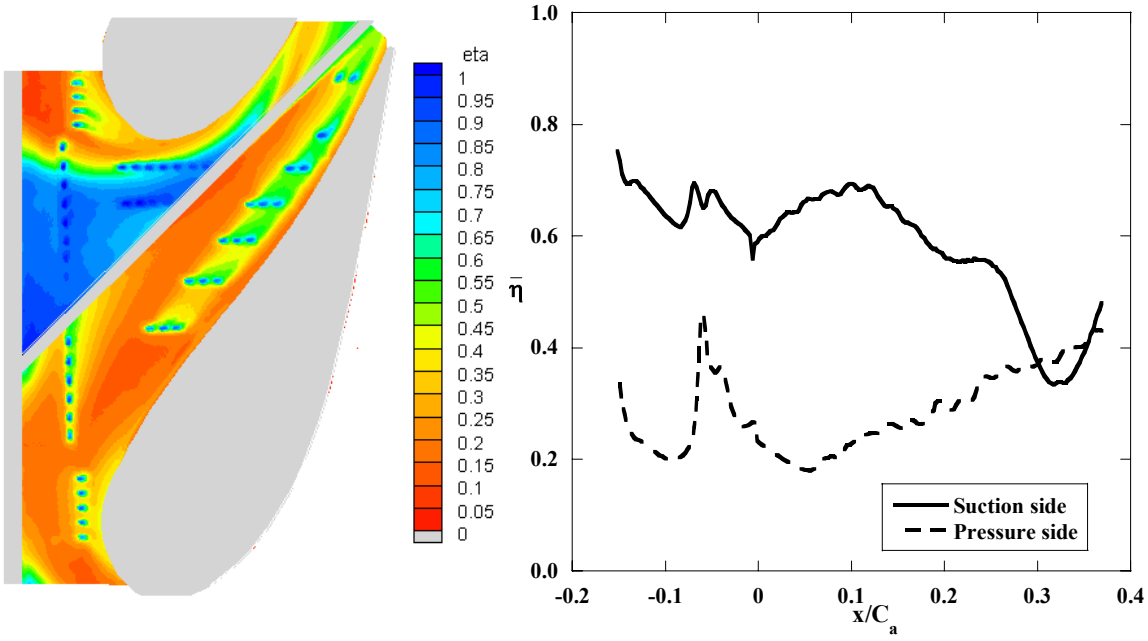

Figure B.15a-b Contour plot and pitchwise averaged plot of adiabatic effectiveness for a double-width slot with 1.0% upstream slot, 0.5% film-cooling, and no net mid-passage gap flow (Case #15).

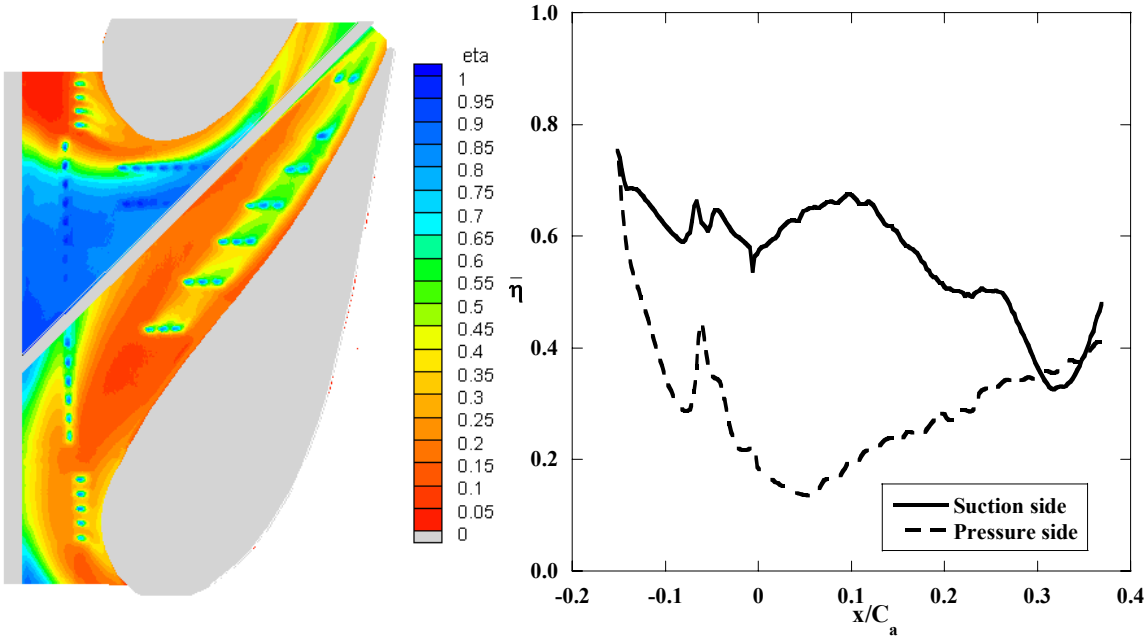

Figure B.16a-b Contour plot and pitchwise averaged plot of adiabatic effectiveness for a double-width slot with 1.13% upstream slot, 0.5% film-cooling, and no net mid-passage gap flow (Case #16).

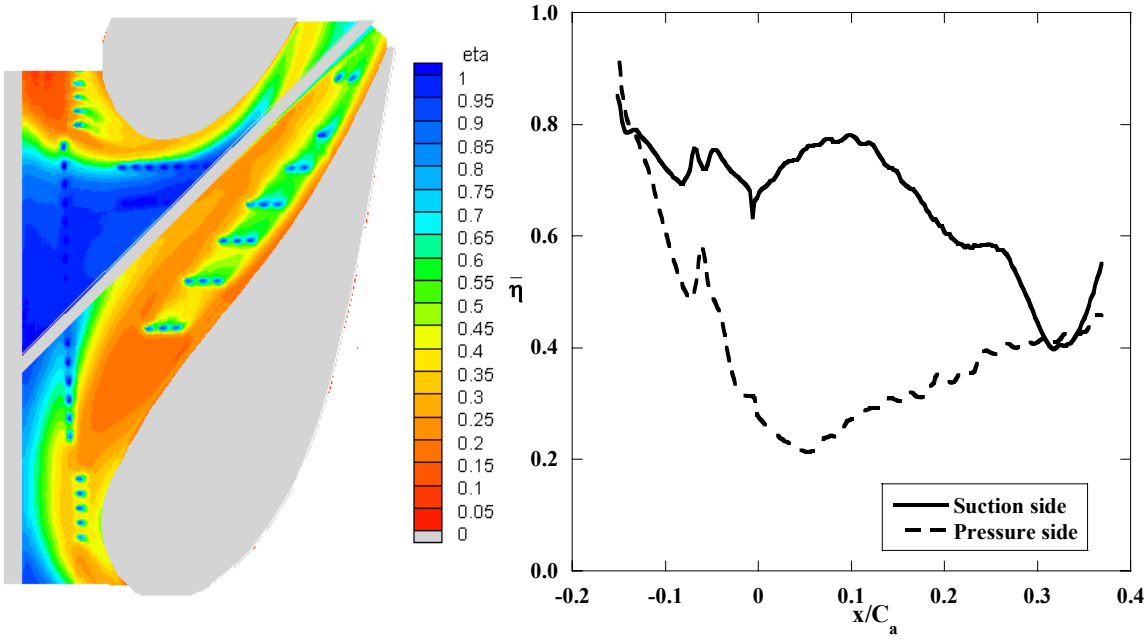

Figure B.17a-b Contour plot and pitchwise averaged plot of adiabatic effectiveness for a double-width slot with 1.25% upstream slot, 0.5% film-cooling, and no net mid-passage gap flow (Case #17).

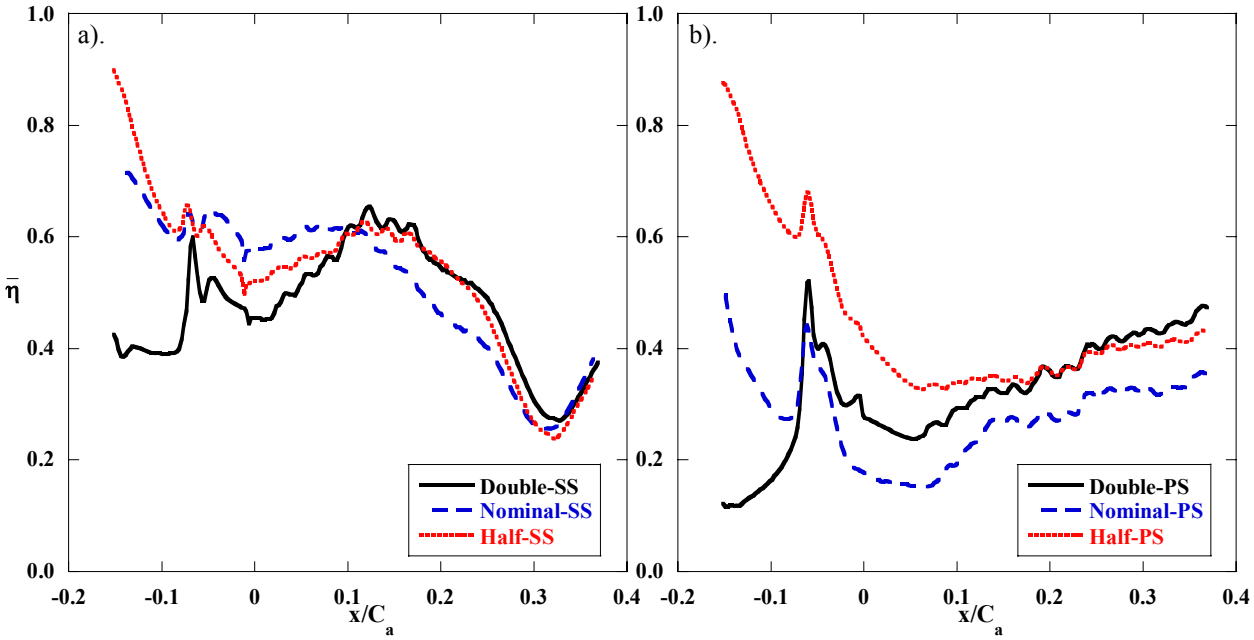

Figure B.18a-b Pitchwise averaged plots of adiabatic effectiveness for a). SS b). PS platform given a double, nominal, and half-width slot with 0.75% upstream slot, 0.5% film-cooling, and no net mid-passage gap flow (Cases #1, 10, 13).

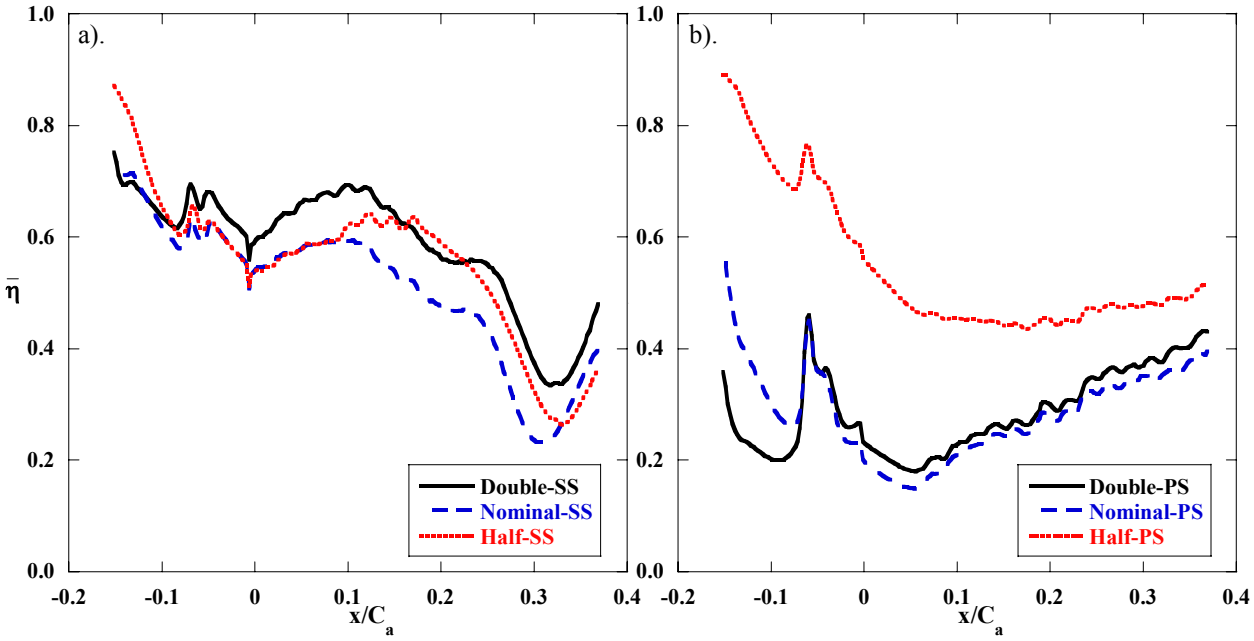

Figure B.19a-b Pitchwise averaged plots of adiabatic effectiveness for a). SS b). PS platform given a double, nominal, and half-width slot with 1.00% upstream slot, 0.5% film-cooling, and no net mid-passage gap flow (Cases #4, 12, 15).

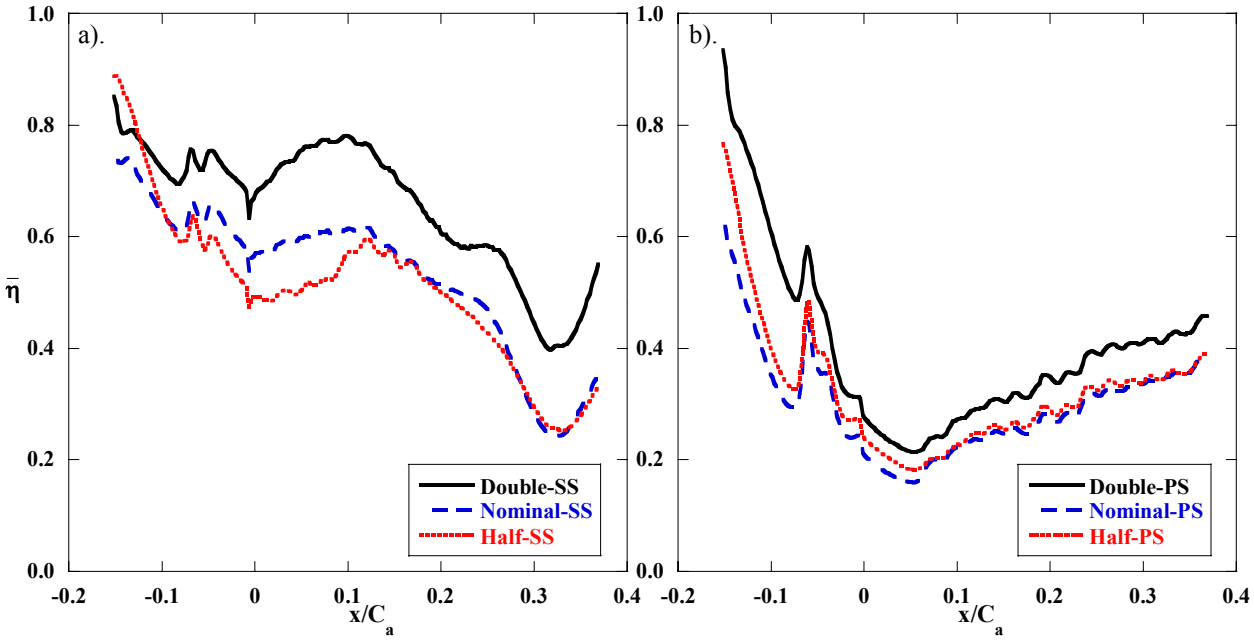

Figure B.20a-b Pitchwise averaged plots of adiabatic effectiveness for a). SS b). PS platform given a double, nominal, and half-width slot with I=0.10 upstream slot, 0.5% film-cooling, and no net mid-passage gap flow (Cases #3, 9, 17).

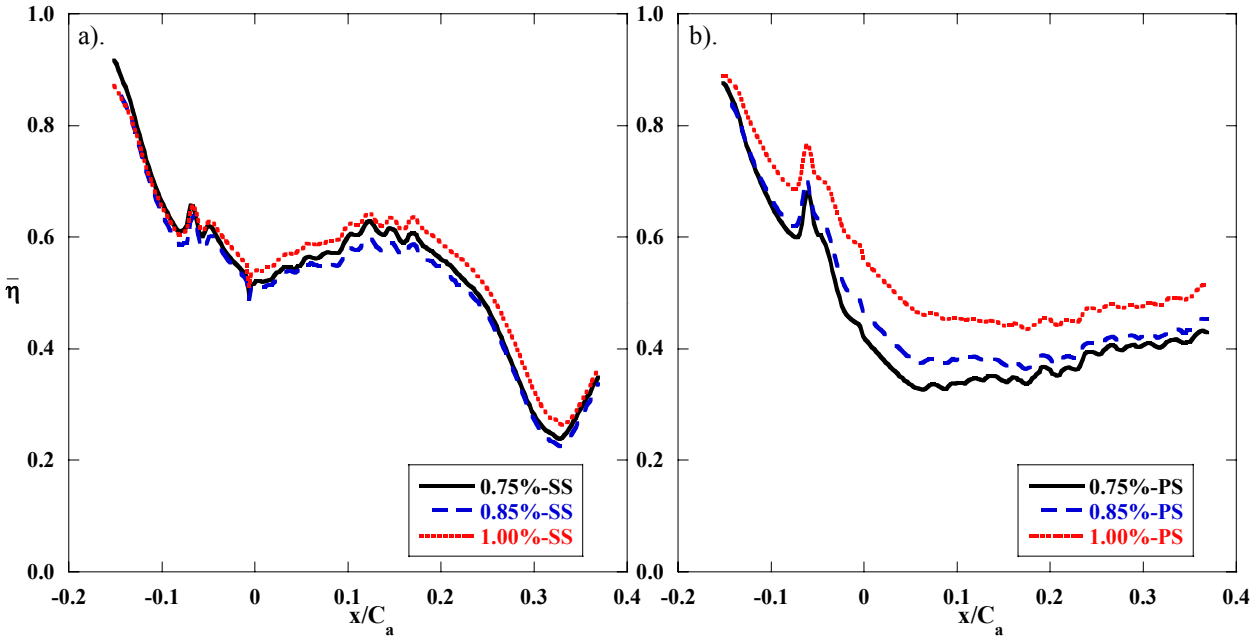

Figure B.21a-b Pitchwise averaged plots of adiabatic effectiveness for a). SS b). PS platform given a half-width slot with 0.75% 0.85% and 1.00% upstream slot, 0.5% film-cooling, and no net mid-passage gap flow (Cases #10, 11, 12).

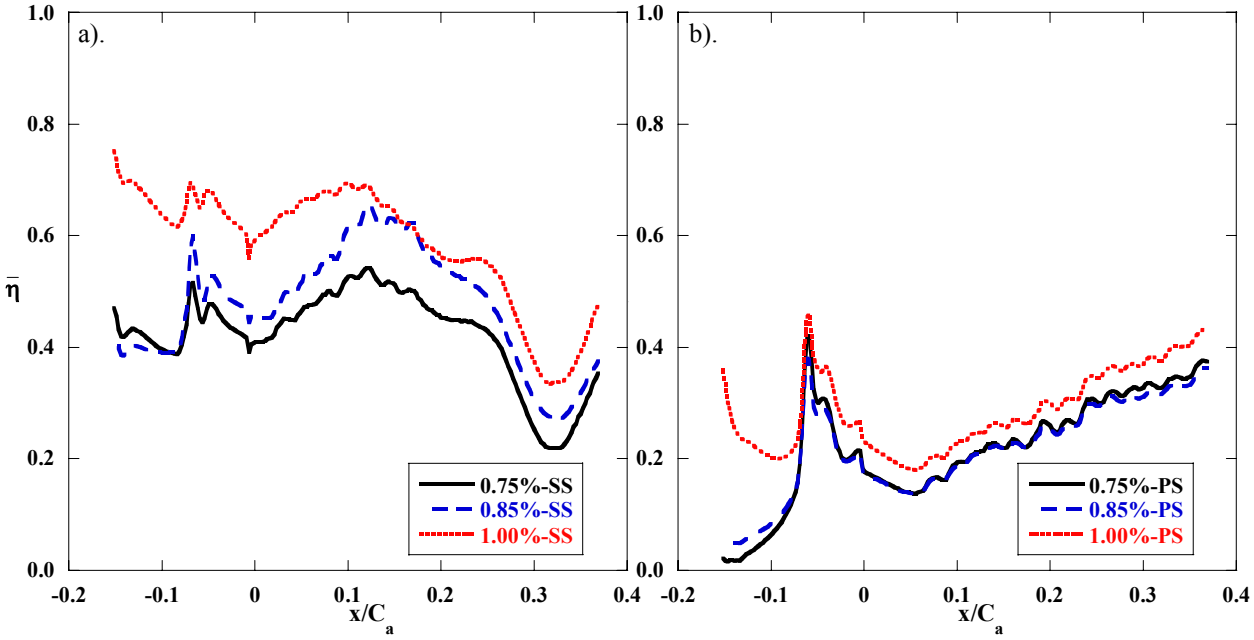

Figure B.22a-b Pitchwise averaged plots of adiabatic effectiveness for a). SS b). PS platform given a double-width slot with 0.75% 0.85% and 1.00% upstream slot, 0.5% film-cooling, and no net mid-passage gap flow (Cases #13, 14, 15).

Appendix C:
Relevance of Experimental Results

This appendix describes the method used to apply the experimental results presented in this thesis for predicting turbine blade temperatures. In a highly competitive international field, such as gas turbine design, the best product is one which satisfies all design criterions while providing the lowest lifetime cost. Therefore, any changes made to the existing product, for the purpose of improving the design criterions, must also not increase the manufacturing or operational costs in such a manner as to reduce the viability of the design. It is of vital importance that the experimentalist understands this relationship so that the quality of a design change can be properly assessed.

C.1 Problem Description

For a modern gas turbine, the main gas temperature operates above the incipient metal melting temperature, as shown in Figure C.1. To protect the turbine, colder high pressure air is bled from the compressor, bypassed around the combustor, and then routed into the turbine. Figure C.2 illustrates how this bypassed air is then used for internal and external cooling. Internal cooling schemes remove heat from the metal and also set up a lower temperature internal boundary condition. External cooling schemes typically employ holes or slots machined into the metal surface which allow internal cooling air to inject out these holes and form a protective film over the metals surface, as shown in Figure C.3. Along with new high temperature alloys, the combination of these techniques ensures that the turbine is capable of operating well above the metals melting temperature.

As the complication of these cooling schemes increases, so does the difficulty in calculating turbine metal temperature. Thus the difficulty for the turbine designer, how does one evaluate the viability of one particular design over another? Due to their extreme complexity, it would be both cost and time prohibitive to build each design and physically test them against one another. Therefore a combination of computational and scaled experimentation must be employed to ultimately determine if the design changes are worth their associated cost. For this appendix a typical turbine vane geometry with

internal and external cooling was used to illustrate the process of calculating metal temperature.

C.2 Problem Solution

Shown in Figure C.4 is a sketch of the problem domain. From knowledge of the problem and experimentation, the following parameters in Figure C.4 are known: T_∞, η, St_o, T_c, St_i, k, and t. Experimentally derived parameters, such as adiabatic effectiveness and Stanton number, are nondimensional and therefore may be applied to the actual engine to calculate heat flux into and out of the metal surfaces.

$$\eta = \frac{T_\infty - T_{aw}}{T_\infty - T_c} \tag{1}$$

$$St_o = \frac{h_o}{\rho_\infty c_{p,\infty} U_\infty} \tag{2}$$

$$Q_o = h_o (T_{aw} - T_o) \tag{3}$$

First the external adiabatic wall temperature, which is the temperature the wall would be assuming no heat transfer through the metal surface, is calculated using the experimentally verified adiabatic effectiveness. T_{aw} is representative of the mixed coolant and mainstream fluid temperatures which is adjacent to the wall for the actual turbine vane. Next the associated external heat transfer coefficient, h_o, is calculated using the experimentally verified Stanton number with film-cooling since its injection onto the surface affects the boundary layer. Now all variables associated with calculating external heat flux, except for T_o, are known.

Next the heat flux from the internal metal surface to the cooling fluid is calculated using the following equations.

$$Q_i = h_c (T_c - T_i) \tag{4}$$

$$Nu_i = \frac{h_i D_H}{k_c} \tag{5}$$

Now that the internal and external boundary conditions for the vane metal have been set, a full three-dimensional computational conduction analysis is performed. The turbine designer can now compare the new cooling design to existing or alternative

designs. Assuming the turbine wall thickness is small, a simple 1-D calculation using Fourier's Law can be performed to produce quicker results, as illustrated in Figure B.5.

Given the manufacturing and life-cycle costs of the cooling improvements and the associated benefits in turbine life and efficiency, the designer can now truly evaluate the viability of the new design.

C.3 Nomenclature

h_i = internal heat transfer coefficient
h_o = external heat transfer coefficient
k = thermal conductivity of the vane metal
Nu_i = internal Nusselt number
Q_i = internal heat flux
Q_o = external heat flux
St_o = external surface Stanton number
t = vane metal thickness
T_c = coolant temperature within the internal passage
T_∞ = main gas temperature
U = flow velocity

Subscripts
aw = adiabatic wall temperatures
c = coolant conditions within the internal passage
i = vane internal surface conditions
o = vane external surface conditions
∞ = inviscid conditions at the edge of the boundary layer

Greek
η = adiabatic effectiveness

C.4 References

[1] Han J. C., Dutta S., Ekkad S. V.. 2000. *"Gas turbine heat transfer and cooling technology,"* Taylor & Francis, Inc.

[2] Prausa, J. N., 2004. *"Heat Transfer Coefficient and Adiabatic Effectiveness Measurements for an Internal Turbine Vane Cooling Feature,"* (Blacksburg, VA: Virginia Tech, 2004).

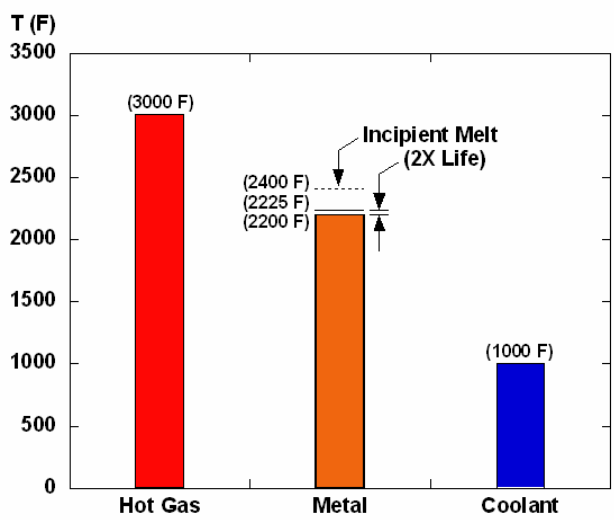

Figure C.1 Comparison of typical turbine metal, coolant, and main gas temperatures.

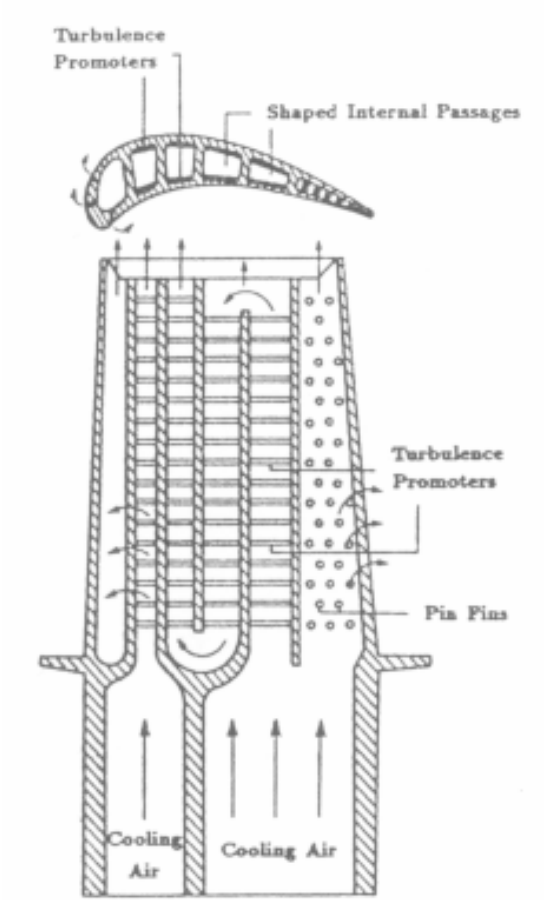

Figure C.2 Illustration of internal and external cooling for a turbine blade [1].

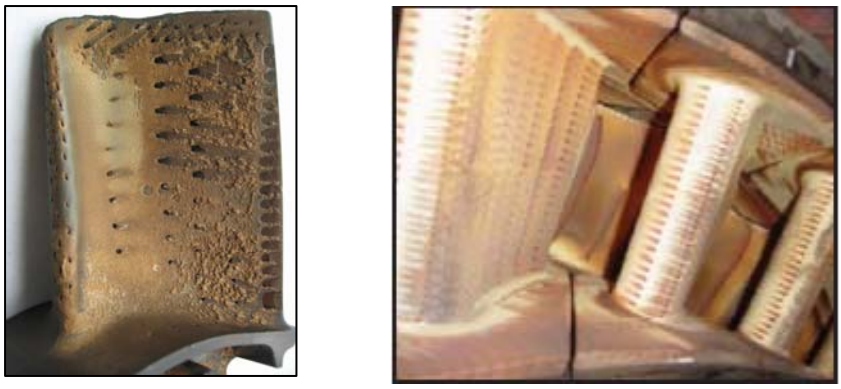

Figure C.3 Turbine blade and vane with film-cooling.

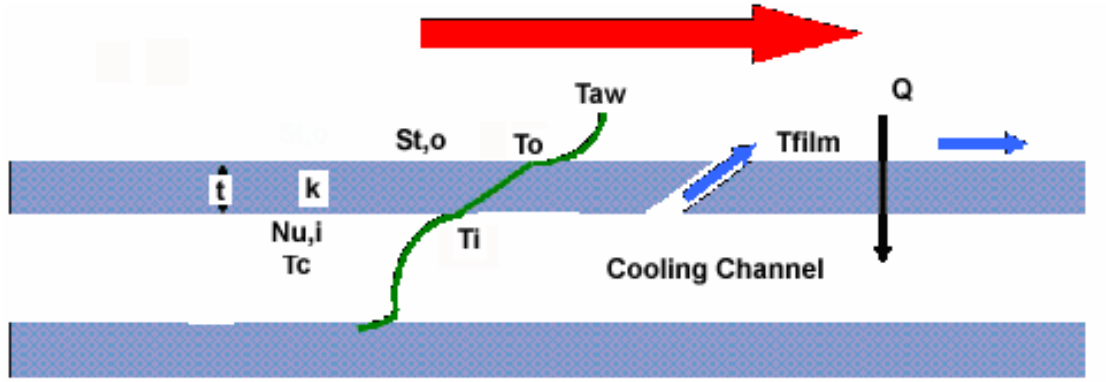

Figure C.4 Visualization of the problem statement: a turbine passage with internal and external cooling. [2]

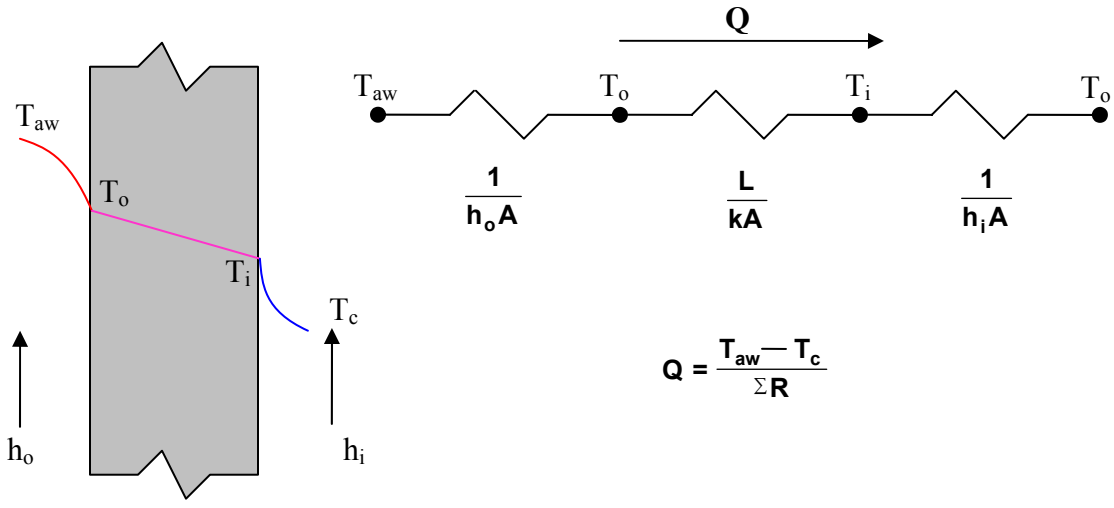

Figure C.5 Electrical resistance analogy representing the 1-D conduction calculation of metal temperature.